TECHNISCHE UNIVERSITÄT MÜNCHEN

TUM School of Life Sciences

Lehrstuhl für Molekulare Ernährungsmedizin

Recruitment of brown adipocytes in visceral white adipose tissue by fibroblast growth factor 8b

Thomas Uwe Robin Gantert

Vollständiger Abdruck der von der TUM School of Life Sciences der Technischen Universität München zur Erlangung des akademischen Grades eines

Doktors der Naturwissenschaften

(Dr. rer. nat.)

genehmigten Dissertation.

Vorsitzende: Prof. Dr. Henriette Uhlenhaut

Prüfende der Dissertation:

1. Prof. Dr. Martin Klingenspor
2. Prof. Dr. Stephan Herzig

Die Dissertation wurde am 25.01.2021 bei der Technischen Universität München eingereicht und durch die TUM School of Life Sciences am 21.06.2021 angenommen.

TABLE OF CONTENTS

LIST OF ABBREVIATIONS

2-DG	2-deoxy-D-glucose
ACTB	Beta-actin
ANOVA	Analysis of variance
ARID5A	AT-Rich interaction domain 5A
ATF2	Activating transcription factor 2
ATF5	Activating transcription factor 5
ATP	Adenosine triphosphate
BCA	Bicinchoninic acid
BMI	Body mass index
BNC1	Basonuclin 1
BSA	Bovine serum albumin
cAMP	Cyclic adenosine monophosphate
CD137	TNF receptor superfamily member 9
cDNA	complementary deoxyribonucleic acid
CDS	Coding sequence
CEBP	CCAAT enhancer binding protein
ChIP	Chromatin immunoprecipitation
CIDEA	Cell death inducing DFFA like effector A
CONC.	Concentration
COX7A1	Cytochrome C oxidase subunit VIIa polypeptide 1
CREB	cAMP-response element binding protein
DMEM	Dulbecco’s modified Eagle’s medium
DMSO	Dimethyl sulfoxide
DNA	Deoxyribonucleic acid
DsiRNA	Dicer-substrate, short-interfering RNA
EDTA	Ethylenediaminetetra-acetic acid
EGF	Epidermal growth factor
EGFR	Epidermal growth factor receptor
EGFP	Enhanced green fluorescent protein
enChIP	engineered DNA-binding molecule-mediated ChIP
ERK1/2	Mitogen-activated protein kinase 1/2
ESRRA	Estrogen related receptor alpha
ETV1	ETS variant transcription factor 1
Ex/Em	Excitation/Emission
FABP4	Fatty acid binding protein 4
FAD	Flavine adenine dinucleotide
FASN	Fatty acid synthase
FBS	Fetal bovine serum
FCCP	Carbonylcyanide p-trifluoromethoxyphenylhydrazone
FFA	Free fatty acid
FGF	Fibroblast growth factor

FGFR	Fibroblast growth factor receptor
FLII	Protein flightless-1 homolog
H^+	Proton
HBSS	Hank’s buffered salt solution
HES1	Hairy and enhancer of split 1
HK2	Hexokinase 2
HOXC9	Homeobox C9
HPLC	High performance liquid chromatography
HSL	Hormone-sensitive lipase
HSPG	Heparan sulfate proteoglycans
IRDye	Infrared Dye
kDa	Kilodalton
KLB	Beta-klotho
LC-MS/MS	Liquid chromatography tandem mass spectrometry
LDH	Lactate dehydrogenase
LLOQ	Lower limit of quantitation
LOD	Limit of detection
LRRFIP1	Leucine rich repeat (In FLII) interacting protein 1
MAPK	Mitogen-activated protein kinase
MCT1	Monocarboxylate transporter 1
MEK1/2	Mitogen-activated protein kinase kinase 1/2
mRNA	messenger ribonucleic acid
$NADH/NAD^+$	Nicotinamide adenine dinucleotide (reduced/oxidized)
NR2F2	Nuclear receptor subfamily 2 group F member 2
NRF1	Nuclear respiratory factor 1
NST	Non-shivering thermogenesis
NUPR1	Nuclear transcriptional regulator protein 1
ORO	Oil red O
P38 MAPK	Mitogen-activated protein kinase P38 α
PBS	Phosphate buffered saline
PDGF	Platelet-derived growth factor
PGC1A	PPARG coactivator 1 α
PGE_2	Prostaglandin E_2
PGI_2	Prostaglandin I_2
$PGF_{2\alpha}$	Prostaglandin $F_{2\alpha}$
PI3K	Phosphatidylinositol 3-kinase
PKC	Protein kinase C
PLA2G4A	Phospholipase A2 group IV A
PLCγ	Phospholipase C gamma
PLN1	Perilipin 1
PPARs	Peroxisome proliferator-activated receptors
PRDM16	PR/SET domain 16
PREF-1	Preadipocyte factor 1
PTGER	Prostaglandin E_2 receptor

PTGES1	Prostaglandin E_2 synthase 1
PTGIR	Prostaglandin I_2 receptor
PTGIS	Prostaglandin I_2 synthase
PTGS1/2	Prostaglandin-endoperoxide synthase 1 and 2
RIN	RNA integrity number
RIPA	Radioimmunoprecipitation assay (buffer)
RLU	Relative light units
ROSI	Rosiglitazone
RT-qPCR	Real-time quantitative polymerase chain reaction
SDS	Sodium dodecyl sulphate
SHOXC2	Short stature homeobox 2
SLC27A1	Solute carrier family 27 member 1
SLC2A1	Glucose transporter 1
SLCO2A1	Prostaglandin transporter
SNS	Sympathetic nervous system
STAT	Signal transducer and activator of transcription
SVF	Stromal-vascular fraction
SV40 LT	*Simian virus* 40 large T-antigen
T3	3,3,5-triiodo-L-thyronine
TBS	Tris buffered saline
TBX1	T-Box transcription factor 1
TFAM	Mitochondrial transcription factor 1
TFIIB	General transcription factor IIB
TMEM26	Transmembrane protein 26
UCP1	Uncoupling protein 1
UCP1-LUC	Luciferase activity linked *Ucp1* expression

LIST OF FIGURES

LIST OF TABLES

ZUSAMMENFASSUNG

Kontrolle über den Rekrutierungsprozess thermogener Adipozyten in weißem Fettgewebe auszuüben, auch als Bräunung bekannt, hat in den letzten Jahren viel Interesse erzeugt aufgrund seines Potentials für die Therapie von Stoffwechselerkrankungen. Thermogene Adipozyten, darunter braune und beige Adipozyten, zeichnen sich durch einen hohen Gehalt an Entkopplungsprotein 1 (*Ucp1*) aus, einem mitochondrialen Protein, das Energie aus der Substratoxidation in Form von Wärme abgibt. In vorangegangenen Arbeiten unserer Arbeitsgruppe konnte FGF8b in einem Screening aller parakriner Fibroblastenwachstumsfaktoren als stärkster Faktor identifiziert werden, der die *Ucp1* Expression in weißen Adipozyten erhöht.

Die vorliegende Arbeit charakterisiert das Bräunungspotential von FGF8b in weißen Adipozyten und Präadipozyten und deckt den molekularen Wirkmechanismus auf. Genexpressionsanalysen zeigten, dass FGF8b die *Ucp1*-Expression induzierte, ohne eine koordinierte thermogene Induktion oder Veränderungen der thermogenen Aktivität hervorzurufen. FGF8b hatte stattdessen eine anti-adipogene, mitogene und pro-glykolytische Wirkung auf Adipozyten, erhöhte allerdings auch die *Ucp1*-Expression unabhängig von Differenzierungssignalen in Präadipozyten. Die Effekte von FGF8b und anderer parakriner FGFs auf die präadipozyten-spezifische *Ucp1*-Expression wurde darauffolgend intensiv validiert. Die *Ucp1*-Expression stieg durch FGF8b, FGF6 und FGF9 stark an. Der FGF-Signalweg wurde mithilfe von Inhibitoren untersucht und zeigte, dass für die Induktion von *Ucp1* die Aktivierung einer FGFR1-MEK1/2-ERK1/2-Achse nötig war. Eine Transkriptomanalyse deckte die koordinierte Hochregulierung von zwei Stoffwechselwegen durch FGF8b auf, der Prostaglandin E_2-Biosynthese und Glykolyse. Die LC-MS/MS basierende Analyse von Lipidmediatoren in FGF8b-konditioniertem Medium bestätigte, dass Prostaglandin E_2 auf FGF8b-Behandlung reagierte. Genetische und pharmakologische Experimente bestätigten die kausale Rolle einer PTGS2-PTGES1-PGE_2-Achse für die FGF8b vermittelte *Ucp1*-Expression. Für die FGF8b vermittelte *Ucp1*-Expression war allerdings auch ein hoher glykolytischer Flux nötig, selbst dann wenn die Reaktion auf PGE_2-Ebene intakt war. Knockdown-Experimente potentieller Transkriptionsfaktoren zeigten, dass FGF8b die *Ucp1*-Expression in *Hes1*-Abhängigkeit regulierte. Zusammenfassend, parakrine FGFs regulieren die PGE_2-Biosynthese und Glykolyse, um die *Ucp1*-Expression zu erhöhen. Damit wurde eine neue Art der *Ucp1*-Regulation, in einem vormals wenig beachteten Zelltyp, der undifferenzierten Präadipozyte, aufgedeckt.

ABSTRACT

Control over the recruitment process of thermogenic adipocytes within white adipose tissue (WAT), known as WAT browning, has garnered a lot of interest in recent years due to its therapeutic implications for metabolic diseases. Thermogenic adipocytes such as brown and brite adipocytes are characterized by high levels of Uncoupling protein 1 (*Ucp1*) expression, a mitochondrial protein capable of dissipating energy from substrate oxidation as heat. In work previously performed in our group, all paracrine Fibroblast growth factors (FGFs) were screened for their capacity to induce *Ucp1* expression in white adipocytes, and FGF8b was identified as the strongest inducer.

The present work aimed to comprehensively characterize the potential browning capacity of FGF8b in cultured white adipocytes and preadipocytes and unravel its molecular mode of action. Gene expression analyses demonstrated that FGF8b strongly induced *Ucp1* expression in the absence of any coordinated thermogenic induction, and thermogenic activity remained unchanged. Instead FGF8b exhibited an anti-adipogenic, mitogenic and pro-glycolytic effect on adipocytes. In contrast, FGF8b strongly induced *Ucp1* expression in preadipocytes, independent of any differentiation cues. The effects of FGF8b and other paracrine FGFs on preadipocyte-specific *Ucp1* expression were extensively validated. *Ucp1* expression strongly increased upon treatment with FGF8b and other FGFs such as FGF6 and FGF9. The FGF signaling pathway was probed with small molecule inhibitors, revealing that the induction of *Ucp1* required the activation of a FGFR1-MEK1/2-ERK1/2 axis. A transcriptomic analysis uncovered a coordinated FGF8b induced upregulation of two metabolic pathways, i.e. the prostaglandin E_2 biosynthesis and glycolysis. Lipid mediator analysis in FGF8b conditioned media by LC-MS/MS confirmed prostaglandin E_2 to be responsive to FGF8b treatment. Genetic and pharmacological loss-of-function experiments corroborated the causal role of a PTGS2-PTGES1-PGE_2 axis for FGF8b induced *Ucp1* expression. Notably, high glycolytic flux was required to induce *Ucp1* expression by FGF8b, even in the presence of an intact PGE_2 response. Knockdown experiments of putative transcriptional regulators revealed that FGF8b induced *Ucp1* expression required the transcription factor *Hes1*. Thus, paracrine FGFs regulate PGE_2 biosynthesis and glycolysis to upregulate *Ucp1* expression, revealing a novel regulatory network in control of *Ucp1* expression in a formerly not widely recognized cell type, the undifferentiated preadipocyte.

INTRODUCTION

1. White, brite and brown adipocytes in metabolic health.

Obesity is a condition defined as a pathological accumulation of body fat, and it represents one of the most pressing public health concerns globally with wide ranging negative societal and economic implications. For decades the primary function of adipose tissue was thought of as a site for excess energy storage only, but it is being increasingly recognized for its remarkable cellular plasticity and its function as a secretory organ (Pellegrinelli *et al*, 2016; Villarroya *et al*, 2017a).

The dominant cell type in adipose tissue is the adipocyte, which can be classified into two distinct types, the white and the brown adipocyte (Wang & Seale, 2016). The white adipocyte is characterized by a singular lipid droplet, which accounts for most of the volume of the cell. White adipocytes also have relatively few mitochondria and its main task is to store and release fatty acids in response to hormonal cues evoked by changes in the energy status of the organism. Brown adipocytes, on the other hand, contain multiple small lipid droplets, are rich in mitochondria and oxidize substrates such as fatty acids and glucose to generate heat in a process known as non-shivering thermogenesis (NST). In mice, white adipocytes reside in visceral and subcutaneous white adipose tissue (WAT) depots such as the gonadal (epididymal ♂, periovarian ♀) and inguinal fat depot, respectively. Brown adipocytes reside in brown adipose tissue (BAT) depots, which are located, for instance, in the interscapular region (de Jong *et al*, 2015). Upon cold exposure and other stimuli, WAT is able to undergo a browning process, which involves both the transition of white to brown adipocytes known as brite or beige adipocytes and the differentiation from mesenchymal precursor cell populations known as preadipocytes (Bartelt & Heeren, 2014). Hence, brite adipocytes are found in interspersed locations of WAT. The different capacities of white, brite and brown adipocytes to engage in thermogenesis is, on the molecular level, linked to the abundance of Uncoupling protein 1 (UCP1), a 32 kDa protein, which constitutes 15-20 % of the total protein mass within the inner membrane of rodent mitochondria (Lin & Klingenberg, 1980). As a consequence, classical white fat depots are practically devoid of any meaningful *Ucp1* expression, whereas *Ucp1* expression is very high in brown fat depots (Kalinovich *et al*, 2017). Notably, white fat depots prone to browning such as inguinal WAT are able to markedly induce *Ucp1* expression in response to cold and other stimuli, albeit not to levels seen in BAT. Thermogenic function relies on UCP1

activity, which diminishes the proton motive force as protons (H^+) are translocated from the intermembrane space back into the mitochondrial matrix by the action of UCP1, which in turn, increases respiratory chain activity and dissipates energy from substrate oxidation as heat. Thus, UCP1 uncouples oxygen consumption from ATP production, which would be the main driver of respiratory chain activity in the absence of active UCP1. BAT activation has been shown to improve glucose tolerance and insulin sensitivity, and contributed to triglyceride clearance in mice (Stanford *et al*, 2013; Bartelt *et al*, 2011a). Moreover, transplantation of BAT has been demonstrated to prevent and reverse diet-induced obesity in mice, and controlled whole-body energy metabolism (Liu *et al*, 2013). Given these profound metabolic implications, recruitment of brown adipocytes in BAT and WAT via adipogenic and thermogenic differentiation represents a promising therapeutic avenue for metabolic diseases.

2. The classical pathway in control of thermogenic differentiation.

The general adipogenic program is a highly ordered and complex process, but two events are pivotal, sustained growth arrest and the induction of adipogenic master regulators Peroxisome proliferator activated receptor gamma (*Pparγ*) and CCAAT/ enhancer-binding proteins (*Cebpa*, *Cebpb* and *Cebpd*) (Rosen *et al*, 2000). Terminally differentiated adipocytes are characterized by gene expression of adipocyte marker genes such as Hormone-sensitive lipase (*Hsl*), Fatty-acid binding protein 4 (*Fabp4*), Fatty acid synthase (*Fasn*) and many other genes related to lipid and glucose metabolism. Thermogenic differentiation towards a brown phenotype is regulated by an additional set of transcription factors and co-regulators, which most prominently include PPARγ coactivator 1 alpha (*Pgc1a*) and PR/SET Domain 16 (*Prdm16*). Brown adipocyte identity is commonly validated by *Ucp1* expression as UCP1 protein abundance is one of the most reliable indicators of thermogenic activity (Nedergaard & Cannon, 2013). Its transcription is regulated by a multitude of transcription factors and co-regulators, mostly exerting their influence on two main regulatory regions, the distal enhancer and proximal promoter of the *Ucp1* gene (Villarroya *et al*, 2017b). Besides *Ucp1*, other BAT markers exist such as Cell death-inducing DFFA-like effector A (*Cidea*) and cytochrome C oxidase subunit VIIa polypeptide 1 (*Cox7a1*), and many more putative markers for brite adipocytes have been discussed in the literature (Perdikari *et al*, 2018; Waldén *et al*, 2012; Wu *et al*, 2012a).

The classical pathway leading to the activation of the thermogenic transcriptional cascade is initiated by the sympathetic nervous system (SNS) in response to cold exposure (Cannon & Nedergaard, 2004). A sustained cold-induced release of the SNS-neurotransmitter norepinephrine causes an induction of thermogenic gene expression in brite adipocytes and activates BAT thermogenesis. This involves activation of adrenergic receptors by norepinephrine, leading to elevated intracellular cyclic adenosine monophosphate (cAMP) levels, ultimately triggering both fatty acid induced UCP1 activation as a result of lipolysis, and *Ucp1* expression by protein kinase A mediated phosphorylation of cAMP-response element binding protein (CREB) and p38-MAPK mediated phosphorylation of activating transcription factor 2 (ATF2) (Cao *et al*, 2004). In cultured adipocytes, this process can be mimicked with the β-adrenergic agonist isoproterenol, but in human subjects adrenergic activation of BAT is linked to unfavorable cardiovascular outcomes, thus is not a viable and safe therapeutic option for long term clinical use (Arch, 2002; Cypess *et al*, 2015). Multiple secreted factors have been proposed to regulate the browning of WAT via autocrine/paracrine mechanisms and activation of thermogenesis by alternative pathways has been extensively studied (Villarroya et al, 2017a).

3. Prostaglandin-dependent regulation of WAT browning.

Arachidonic acid belongs to the group of ω-6 polyunsaturated fatty acids and once released from its esterified form within phospholipids by the action of phospholipases, it gives rises to a plethora of bioactive lipid mediators (Hanna & Hafez, 2018). Three major enzymatic pathways metabolize free arachidonic acid via the action of cyclooxygenases, also known as prostaglandin endoperoxidase synthases (*Ptgs*), lipoxygenases and cytochrome P450s. The pathway most frequently associated with WAT browning has been the PTGS regulated prostaglandin biosynthetic pathway.

Recruitment of brown adipocytes in WAT has been demonstrated to depend on norepinephrine-induced PTGS2 activity, and to mechanistically rely on a prostaglandin I_2 (PGI_2)-prostaglandin I_2 receptor (*Ptgir*)-PPARγ axis (Vegiopoulos *et al*, 2010). In the same study, overexpression of PTGS2 was shown to protect mice from diet-induced obesity by elevating energy expenditure via brown fat recruitment. Subsequent reports corroborated the involvement of PTGS2 in WAT browning, even though evidence for a different downstream mechanism was obtained involving a prostaglandin E_2 (PGE_2)-prostaglandin E_2 receptor 3/4 (*Ptger3/4*) axis (Madsen *et al*, 2010). Notably, the same

study showed that inhibition of PTGS2 activity increased adiposity in mice, which provided evidence that prostaglandin mediated WAT browning affects systemic energy metabolism (Madsen *et al*, 2010). Following these early studies, the role of PTGS2 and downstream PGE_2 biosynthesis in regulating browning of WAT and BAT thermogenesis was independently confirmed by others (García-Alonso *et al*, 2013; García-Alonso & Clária, 2014; Shamsi *et al*, 2020).

Taken together, these studies established a role for a PTGS and prostaglandin-dependent mechanism in WAT browning with profound implications for whole-body energy homeostasis in mice. Contrarily, arachidonic acid, the precursor for all prostaglandins, strongly inhibited *Ucp1* expression in differentiated human adipose derived stem cells, potentially via $PGF_{2\alpha}$ and PGE_2, adding some uncertainty to the already complex regulation of WAT browning by prostaglandins (Pisani *et al*, 2014). Other prostaglandin synthases such as Prostaglandin D_2 synthase have been implicated in controlling nutrient partitioning in BAT as well, albeit in their role as lipid binding proteins known as lipocalins, and independent of prostaglandin production (Virtue *et al*, 2012).

In conclusion, the prostaglandin-dependent pathway represents one of the earliest studied alternative pathways in control of brown adipocyte recruitment, stimulated BAT research and offered interesting therapeutic options due to access to selective and well-studied drugs. However, a lack of reproducibility, possibly attributable to the very unstable nature of compounds of the eicosanoid family constituted a significant challenge to the advancement of the field, illustrated by futile efforts to identify prostaglandins as brite adipocyte markers (Dieckmann *et al*, 2020).

4. Fibroblast growth factor-dependent regulation of WAT browning.

Fibroblast growth factors (FGFs) are peptide hormones belonging to the FGF protein family consisting of 22 structurally related members, classified according to their mode of action into intracrine, paracrine and endocrine factors (Ornitz & Itoh, 2015). Due to their N-terminal signal peptide most FGFs are secreted, except a small group of intracrine FGFs, and signal via cell surface tyrosine kinase receptors, which are encoded by four FGF-receptor genes (*Fgfr1-4*). FGFs exhibit a wide range of biological activities, particularly related to cell fate decisions during embryogenesis including proliferation, migration and differentiation. Thus, germline disruption of FGF function in

mice lead to developmental abnormalities (Itoh & Ornitz, 2011). In adult physiology, FGFs have been implicated in the control over regenerative processes, tissue repair and metabolism (Maddaluno *et al*, 2017; Degirolamo *et al*, 2016). While paracrine FGFs bind to heparin/heparan sulfate proteoglycans (HSPGs) to initiate FGF signaling, endocrine FGFs require cofactors of the Klotho family (Ornitz & Itoh, 2015). Formation of the ternary FGF-FGFR-cofactor complex induces receptor dimerization and autophosphorylation, followed by an activation of various signaling cascades including RAS-MAPK, PI3K-AKT, STAT and PLCγ-PKC (Ornitz & Itoh, 2015).

The most well studied FGF in the context of BAT physiology is FGF21, an endocrine member of the FGF protein family. FGF21 is strongly induced in BAT upon cold exposure and β3-adrenergic stimulation (Hondares *et al*, 2011; Chartoumpekis *et al*, 2011), and promotes browning of WAT (Fisher *et al*, 2012; Kim *et al*, 2013; Emanuelli *et al*, 2014), while mice deficient in FGF21 show an impaired recruitment of beige adipocytes in WAT in response to cold (Fisher *et al*, 2012). Mechanistically, the cold-induced expression of FGF21 has been linked to a cAMP-dependent activation of p38 MAPK (Hondares *et al*, 2011), while its effect on BAT thermogenesis and WAT browning required the interaction of either PPARα or PPARγ, respectively (Hondares *et al*, 2010; Dutchak *et al*, 2012). In early studies the metabolic improvements mediated by FGF21 were attributed to BAT activation or the browning phenotype of WAT, but later studies questioned the dependence of important metabolic outcomes such as weight loss and the amelioration of systemic glucose and lipid metabolism on UCP1-dependent thermogenesis (Véniant *et al*, 2015; Samms *et al*, 2015).

The role of paracrine FGFs in controlling thermogenic differentiation and activity is less well known. The corresponding literature is therefore much more fragmented and heterogeneous in its employed methodology. Initial research efforts focused on exploiting the mitogenic activity of paracrine FGFs to expand brown precursor cell populations to improve differentiation of brown adipocytes. For instance, low doses of FGF1 and FGF2 (1-5 ng/ml) retained their proliferative activity in cultured brown preadipocytes, while permitting brown adipocyte differentiation at the same time (García & Obregón, 2002). The browning activity of FGF1 was shown in an endothelial-specific FGF1 overexpression mouse model, which was characterized by multilocular and densely clustered adipocytes, and increased *Ucp1* expression in the visceral fat depot (Keeley *et al*, 2019). However, the same authors reported suppressed adipogenesis upon FGF1 treatment in visceral adipocytes differentiated from the

stromal-vascular fraction (SVF). Another study reported an autocrine pathway involving a FGF10-FGFR2-AKT axis in control of *de novo* recruitment of brown adipocytes in WAT, inhibitable via the action of miR-327 (Fischer *et al*, 2017). Furthermore, the same authors showed that FGF10 treatment of 3T3-L1 preadipocytes increased lipid accumulation during differentiation, contrasting the observations made with FGF1. Adenovirus mediated overexpression of FGF16 revealed an induction of browning in inguinal WAT of diet-induced obese mice and a massive upregulation of *Ucp1* expression in this depot (Rulifson *et al*, 2017). Although FGF16 gain-of-function promoted massive weight loss in mice, there was no difference in oxygen consumption or thermogenesis between control and FGF16 overexpressing mice, questioning the contribution of the browning phenotype to any observed metabolic improvement in this mouse model. FGF9 expression in white adipose tissue was demonstrated to be downregulated in response to cold and β3-agonism, and treatment of white adipocytes with FGF9 dose-dependently suppressed *Ucp1* expression and adipogenesis (Sun *et al*, 2019). Contrarily, a recent report demonstrated an induction of *Fgf9* expression in WAT upon cold exposure in mice, and a positive regulation of *Ucp1* expression in white and brown adipocytes by FGF6 and FGF9, despite suppressed adipogenesis (Shamsi *et al*, 2020). The same authors deciphered that FGF6 and FGF9 induced *Ucp1* expression occurred in the undifferentiated preadipocyte and required a PTGES-PGE_2-prostaglandin E_2 receptor 2/4 (*Ptger2/4*) axis, independent of PPAR signaling. Moreover, using a combination of CRISPR-based chromatin immunoprecipitation (ChIP) and quantitative proteomics, the authors elegantly demonstrated that FGF9 dependent BAT thermogenesis relied on the interaction of the *Ucp1* promoter region with a ternary transcriptional complex consisting of estrogen-related receptor α, flightless protein II and leucine-rich-repeat-(in FLII)- interacting-protein-1 (ERRA-FLII-LRRFIP1) complex (Shamsi *et al*, 2020).

In summary, research on paracrine FGFs did provide some important insights into how paracrine members of the FGF protein family regulate BAT activity, browning of WAT and adipogenesis. It is important to note, however, that most findings on the *in vivo* capacity of paracrine FGFs to induce browning were based on correlation rather than on causation. General statements about the effects of paracrine FGFs on adipocyte biology are difficult to derive from the available data in the face of heterogenous research methodology and a lack of replication. The distinction between preadipocytes and adipocytes as a source of *Ucp1* expression, as illustrated by Shamsi *et al.* (2020), certainly was a step forward to an improved understanding of FGF regulated *Ucp1*

expression in cultured cells. More research was needed to reproduce these findings in order to clarify discrepancies between studies, particularly by employing a more mechanistic approach in a well controlled cell culture setting.

5. Fibroblast growth factor 8b induced *Ucp1* expression.

Controlling the browning process and UCP1-dependent thermogenesis to improve metabolic health in obesity and related morbidities has emerged as a promising therapeutic tool in recent decades. It has been estimated that a ten-fold increase in *Ucp1* transcript abundance in WAT is sufficient to elicit a meaningful metabolic benefit in obese subjects (Maurer *et al*, 2020). Unfortunately, no drug has been approved yet, whose mode of action relies on browning of WAT and offers the efficacy and safety needed for long term clinical use. Many important physiological and pharmacological regulators of WAT browning have been identified so far and they range from lipid derived prostaglandins to endocrine and paracrine FGFs.

The present work evolved from our own data obtained by screening all paracrine FGFs with respect to their capacity to induce *Ucp1* expression in white epididymal adipocytes, and identified FGF8b as the most promising candidate (Westphal *et al*, 2019).

FGF8b was originally identified as a growth factor in response to androgen treatment of the mouse mammary cancer line SC-3 (Tanaka *et al*, 1992), and unlike most other FGFs, is subject to alternative splicing, which produces eight murine (FGFa-h) and four human (FGFa, b, e, f) FGF8 isoforms (MacArthur *et al*, 1995b; Gemel *et al*, 1996). Notably, mouse and human FGF8b protein sequences share 100 % identity, which illustrates its essential function in both species based on their conserved sequences (Ghosh *et al*, 1996). Evidence from loss-of function experiments during embryogenesis suggest that FGF8b may be the most dominant FGF8 isoform (Sunmonu *et al*, 2011), e.g. illustrated by the fact that FGF8b possesses the highest transforming potential of NIH-3T3 cells from all FGF8 isoforms (MacArthur *et al*, 1995a). The primary function of FGF8b in physiology is to regulate multiple patterning and outgrowth events during early and late embryogenesis (Crossley & Martin, 1995; Meyersl *et al*, 1998; Sunmonu *et al*, 2011). Whereas in adult pathophysiology, FGF8 has been linked to the growth and progression of hormonal cancers based on its action as an oncogene (Mattila & Härkönen, 2007). The effect of FGF8b on rat mesenchymal stem cells and muscle

progenitors has been reported very recently showing that FGF8b induces cell proliferation, enhances chondrogenic and myogenic differentiation, while suppressing adipogenic and tenogenic differentiation (Otsuka *et al*, 2021).

6. Research objectives

The present work aims to comprehensively characterize the potential browning capacity of FGF8b, a paracrine member of the FGF protein family, in cultured white adipocytes and preadipocytes, thereby unraveling its molecular mode of action.

The first half of the results section employed immortalized white adipocyte cultures of murine epididymal and inguinal origin with the aim to extensively validate the impact of recombinant FGF8b on thermogenic and adipogenic differentiation. These data in combination with the functional assessment of UCP1-dependent thermogenesis sought to evaluate the browning capacity of FGF8b in cultured white adipocytes. The absence of any meaningful activation of thermogenic activity in white adipocytes by FGF8b coincided with an emerging glycolytic phenotype. The relevance of the metabolic shift towards a more pro-glycolytic profile induced by FGF8b was then hypothesized to be related to the previously established anti-adipogenic and non thermogenic effects of FGF8b. Experiments on undifferentiated preadipocytes revealed that FGF8b was able to strongly induce *Ucp1* expression in this cell type, concomitantly increasing glycolytic flux, possibly in order to sustain high rates of proliferation in preadipocytes. Thus, strong evidence accumulated that the observed induction of *Ucp1* by FGF8b in white adipocyte cultures emanated from the preadipocyte fraction.

The second half of the results section sought to address three questions to delineate the nature of preadipocyte-specific *Ucp1* expression. Firstly, was the biological activity of FGF8b and other paracrine FGFs towards preadipocytes retained in preadipocytes derived from different cell models, mouse strains and independent of the delivery mode (recombinant FGF8b vs. lentiviral delivery)? Secondly, which receptor and signaling components were required to initiate, transmit and mediate the effect of FGF8b on *Ucp1* expression on the molecular level? And thirdly, which metabolic and transcriptional regulators were involved to orchestrate the unexpected induction of *Ucp1* in preadipocytes, a cell type formerly not widely recognized for *Ucp1* transcription?

The present work clearly demonstrated that FGF8b did not classify as a *bona fide* browning agent in WAT due to its anti-adipogenic and non-thermogenic profile, providing a theoretical framework as to why FGF8b failed to induce thermogenesis *in vivo* (Westphal *et al*, 2019). An unexpected role for preadipocyte-specific *Ucp1* expression upon FGF8b treatment was uncovered, which helped to resolve some aspects of the conflicting literature on paracrine FGFs, as outlined above. Lastly, a FGFR1-MEK1/2-ERK1/2 axis was identified to induce changes in both the PGE_2 biosynthetic and glycolytic pathway, which co-regulate and mediate the effect of FGF8b on *Ucp1* expression in preadipocytes, confirming a non-canonical mechanism in control of *Ucp1* expression. Taken together, the present work was able to substantially contribute to the mechanistic understanding of paracrine FGF mediated *Ucp1* expression, and opened up new avenues to potentially manipulate *Ucp1* expression via non-canonical regulators in preadipocytes and other non-adipocyte cell models.

MATERIAL AND METHODS

1. Cell Culture

Primary and immortalized murine preadipocytes, derived from the stromal-vascular fraction (SVF) of brown and white adipose tissue, NIH/3T3 fibroblasts and the viral packaging cell lines BOSC-23 and HEK-293T were cultured in Dulbecco's modified Eagle's medium containing 4.5 g/l glucose, supplemented with 10 % fetal bovine serum (FBS, Biochrom) and antibiotics (40 IU/ml penicillin, 40 µg/ml streptomycin, 40 µg/ml gentamycin) at 37 °C in a humidified atmosphere. Primary cells of the SVF were cultured in cell culture media containing 20 % FBS and 0.5 µg/ml of the antimycotic fungizone.

Adipocyte differentiation

Preadipocytes were subjected to one of two differentiation protocols designated differentiation protocol A and B, when cell confluence reached approximately 90 %.

Differentiation protocol A: Preadipocyte differentiation into mature adipocytes was induced by supplementing cell culture media with 20 % FBS, 250 µM indomethacin, 500 µM 3-isobutyl-1-methylxanthine, 1 µg/ml dexamethasone, 1 nM T_3 and 20 nM insulin. Induction media was exchanged after 24 h with differentiation media containing 1 nM T_3 and 20 nM insulin. Differentiation media was changed every other day for a total of six days. This protocol was mostly applied to immortalized white inguinal and epididymal SVF of FVB/N mice, provided by our collaborator Dr. Sören Westphal (Department of Internal Medicine II, University of Ulm, Ulm, Germany)

Differentiation protocol B: Preadipocyte differentiation into mature adipocytes was induced by supplementing cell culture media with 10 % FBS, 125 µM indomethacin, 500 µM 3-isobutyl-1-methylxanthine, 1 µM dexamethasone, 1 nM T_3 and 850 nM insulin. Induction media was exchanged after 48 h with differentiation media containing 1 nM T_3 and 850 nM insulin. Differentiation media was changed every other day for a total of six days.

Isolation of primary cells

Primary cells were isolated from fat depots of seven week-old male *Ucp1*-reporter mice (C57BL/6N), a transgenic mouse model in which endogenous *Ucp1* expression is coupled to a luciferase reporter (Wang *et al*, 2019), *Ucp1*-wild-type and *Ucp1*-knock-out mice (129S6Sv/Ev Tac). Mice were euthanized by CO_2 asphyxiation in a small

sealed container and white inguinal and brown interscapular adipose tissue was dissected. Tissue was thoroughly minced and incubated in isolation medium (1x Hank's balanced salt solution, w/o Mg and Ca, 3.5 % (w/v) bovine serum albumin (BSA), 0.55 mM glucose, 1 mg/ml collagenase (Biochrom)) at 37 °C under vigorous shaking for 60 min. Digested tissue was passed through a 250 µm nylon mesh and centrifuged at 250 x g for 5 min. The resulting pellet was disrupted by manual shaking in order to release entrapped mature adipocytes and the suspension was centrifuged again at 250 x g for 5 min. The supernatant including the lipid layer was aspirated, discarded and the pellet was resuspended in washing buffer (1x Hank's balanced salt solution, w/o Mg and Ca, 3.5% (w/v) BSA) before the final centrifugation of the sample at 500 x g for 5 min. The supernatant was discarded and isolated cells were resuspended in primary cell culture media. After being passed through a 40 µm cell strainer, cells were seeded out with the desired cell density.

Immortalization of primary cells

Primary murine cells isolated from the SVF of brown and white adipose tissue were immortalized by retroviral transduction with the *Simian virus 40* large T antigen (SV40 LT). For the production of retrovirus particles, calcium phosphate transfection of the packaging cell line BOSC-23 was performed with the vector pBABE-puro SV40 LT, containing the coding sequence (CDS) for SV40 LT. Briefly, for transfection in a 6-well plate format, 5 µg of plasmid DNA was prepared in 100 µl Hepes buffer (250 mM $CaCl_2$, 10 mM Hepes, pH 7.2), which was added dropwise into the same volume of 2x Hank's balanced salt saline (2 g/l dextrose, 10 g/l Hepes, 0.74 g/l KCl, 16 g/l NaCl, 0.27 g/l Na_2HPO_4, pH 7.05 -7.10) under vigorous vortexing. After 5 minutes of incubation the solution was evenly distributed across the well of 60 % confluent BOSC-23 cells. The media was collected on three consecutive days, was sterile filtered each time and diluted with fresh culture media in a 1:1 ratio. The diluted supernatant, containing retrovirus particles and 2 µg/ml polybrene, was added to preconfluent primary cells from the SVF on the same day. Cells were expanded on a 15 cm dish over a week before being selected with 2 µg/ml puromycin for 2 weeks. Aliquots of the immortalized cell lines were stored in liquid nitrogen until use.

2. Fibroblast growth factors

Recombinant human/murine FGF8b (100-25) and mouse FGF1 (450-33A) were purchased from PeproTech, except for white adipocytes differentiated with differentiation protocol A, then human/murine FGF8b (423-F8-025) and murine FGF1 (4686-FA-025) from R&D Systems were used. Recombinant murine FGF6 (5750-F6-025/CF), murine FGF9 (7399-F9-025/CF) and murine FGF21 (8409-FG-025) were purchased from R&D Systems. For paracrine FGFs, 1 µg/ml heparin (H3149-10KU, Sigma) was used as a cofactor, while endocrine FGF21 was co-treated with 1 µg/ml recombinant murine KLB (2619-KB-050, R&D Systems). Other growth factors such as epidermal growth factor (315-09) and platelet-derived growth factor (315-18) were purchased from PeproTech. Lyophilized growth factors were reconstituted either in sterile ultrapure water or PBS as instructed by the supplier.

3. Lipid staining

The degree of differentiation and lipid accumulation of adipocyte cultures was determined using established staining methods for intracellular neutral lipids (lipid droplets) with either Oil Red O (Sigma) or the fluorescent dye BODIPY 493/503 (Invitrogen):

Oil Red O staining (ORO)

A 3 mg/ml ORO stock solution was prepared in isopropanol and passed through a 0.45 µm filter. The ORO staining solution was prepared freshly on the day of lipid staining by mixing the stock solution in a 3 to 2 ratio with water. It was then passed through a 0.45 µm filter again. In the meantime, adipocyte cell culture media was aspirated, washed with phosphate buffered saline (PBS) and cells were fixated with a 4 % paraformaldehyde solution for 1 h. Fixated cells were washed with isopropanaol twice and then incubated with the ORO staining solution for 30 min at room temperature. ORO staining solution was aspirated and cells were washed several times with ultrapure water. Brightfield images of ORO stained lipid droplets were subsequently acquired on a light microscope.

BODIPY 493/503 staining

Adipocyte cell culture media was aspirated and washed with PBS. Cells were incubated with a 3 µg/ml BODPIY 493/503 staining solution for 20 min at 37 °C in the cell incubator. The staining solution was then discarded and cells were washed twice with PBS. A small layer of PBS was added to the cell cultures to prevent the cells from

drying out prior to imaging. Fluorescence images of BODIPY stained lipid droplets were subsequently acquired on a fluorescence microscope (Ex/Em: 488–503/515–545 nm, Leica DMI6000B).

4. Lipid droplet size and number

Representative brightfield microscopy images (10X) of fully differentiated adipocyte cultures were taken and automatically analyzed with a validated pattern recognition module for lipid droplets (WimLipid) on the image analysis platform Wimasis (Onimagin Technologies). Lipid droplet size, number and distribution were obtained as readouts.

5. RNA isolation, cDNA synthesis and RT-qPCR

RNA was isolated using the 'single-step' method, originally described by Chomczynski and Sacchi (Chomczynski & Sacchi, 1987). The principle of the 'single-step' method is based on the separation of RNA from DNA and protein in an acidic solution containing the strong protein denaturant guanidinium thiocyanate, phenol and chloroform. The acidic aqueous upper phase, which is formed after centrifugation, mostly contains RNA, which can be used for downstream applications such as RT-qPCR.

Cells were lysed in TRIsure™ (BIO-38033, Bioline) and mixed with chloroform (1/5 of total volume used for lysis). For a 6-well plate, 400 µl of TRIsure™ were used per well. Samples were centrifuged at 12,000 x g for 15 min at 4 °C. The upper aqueous phase was used as input for the column elution step afetrwards and was performed according to the instructions provided by the manufacturer (SV Total RNA Isolation System, Promega). RNA was eluted from the column with 30-50 µl nuclease free water and RNA concentrations were determined on a spectrophotometer (Nanodrop-1000). 500-100 ng of total RNA was reverse transcribed into cDNA and diluted with 40 µl nuclease free water (SensiFast cDNA Synthesis Kit, Bioline).

The real-time quantitative polymerase chain reaction (RT-qPCR) was set up in a 12.5 µl reaction volume consisting of 1x SensiMix™ SYBR® No-ROX Kit (Bioline), 250 nM of each primer and 1 µl of diluted cDNA in a 384-well plate format. The PCR cycling parameters were: 420 s at 95 °C for initial denaturation and 45 cycles of recurring 10 s at 95 °C for denaturation, 15 s for annealing at 53 °C and 20 s for elongation at 72 °C. The RT-qPCR was run on a LightCycler®480 Real-Time PCR System (Roche). Standard samples were measured in duplicates, and target samples were measured in triplicates. Transcript abundances were calculated based on the relative standard

curve method from pooled cDNA samples. Expression values were normalized to the reference gene general transcription factor IIB (*TfIIb*).

Table 1. Forward and reverse primer sequences used for RT-qPCR.

Target gene	5' - 3' forward primer	5' - 3' reverse primer
Cd137	*CGTGCAGAACTCCTGTGATAAC*	*GTCCACCTATGCTGGAGAAGG*
Cidea	*TGCTCTTCTGTATCGCCCAGT*	*GCCGTGTTAAGGAATCTGCTG*
Cidea	*TGCTCTTCTGTATCGCCCAGT*	*GCCGTGTTAAGGAATCTGCTG*
Cs	*CTGAGGAAGACTGACCCTCG*	*TTCATCTCCGTCATGCCATA*
Esrra	*GCAGGGCAGTGGGAAGCTA*	*CCTCTTGAAGAAGGCTTTGCA*
Fabp4	*GATGGTGACAAGCTGGTGGT*	*TTTATTTAATCAACATAACCATATCCA*
Fasn	*GCATTCAGAATCGTGGCATA*	*TTGCTGGCACTACAGAATGC*
Fgf8b	*TGAGGGAGCAGAGCCTGGTGAC*	*GAAGTGGACCTCACGCTGGTGC*
Fgfr1	*GGTTCGCTATGCCACCTGGAGC*	*GTCGGTGCGGAGATCGTTCCAC*
Fgfr2	*CAAACCCAAGGAGGCGGTCACC*	*GCAGGCCCCCAGGAGGTTGATA*
Flii	*CTGCTACATTGTGCTCAAGACC*	*CCTCCCCACCAATCCAGTA*
Hes1	*ACACCGGACAAACCAAAGAC*	*AATGCCGGGAGCTATCTTTC*
Hk2	*GTCAACTCCGGATGGGACAG*	*CAATGTGGTCAAACAGCTGGG*
Hoxc9	*GCAGCAAGCACAAAGAGGAGAAG*	*GCGTCTGGTACTTGGTGTAGGG*
Lrrfip1	*AGGACATGCTGCTGGAGCTGGA*	*CGCAGGGCCTCTTTCACTTCGG*
Mc4	*AGTGCCATTGGTCTCGTG*	*CATACTTGTAAACTTTGGTTGCATC*
Mct1	*GAGGTTCTCCAGTGCTGTG*	*TCCATACATGTCATTGAGGCG*
Pdk1	*GGACTTCGGGTCAGTGAATGC*	*TCCTGAGAAGATT GTCGGGGA*
Pgc1a	*GGACGGAAGCAATTTTTCAA*	*GAGTCTTGGGAAAGGACACG*
Pla2g4a	*AACCCCGTGTGGAATGAGAC*	*GAACCCAAAATGGCCACCAC*
Pparg	*TCAGCTCTGTGGACCTCTCC*	*ACCCTTGCATCCTTCACAAG*
Prdm16	*CTGTTAGCTTTGGAGCCGAC*	*GACGAGGGTCCTGTGATGTT*
Pref-1	*GGAGGCTGGTGATGAGGAGATC*	*AGAGCTCTAAGGAACCCCGGTA*
Ptges1	*ATGAGTACACGAAGCCGAGG*	*CCAGTATTACAGGAGTGACCCAG*
Ptgs1 (Cox1)	*AGAGGTGACAACTGGAGGGA*	*GCGAGAGACTCCTTCGACTC*
Ptgs2 (Cox2)	*GGGCCATGGAGTGGACTTAAA*	*ACTCTGTTGTGCTCCCGAAG*
Shox2	*TGGAACAACTCAACGAGCTGGAGA*	*TTCAAACTGGCTAGCGGCTCCTAT*
Slc27a1	*CTGGGACTTCCGTGGACCT*	*TCTTGCAGACGATACGCAGAA*
Slc2a1 (Glut1)	*CGGCCTGACTACTGGCTTTG*	*GCCAAACACCTGGGCAATAAG*
Slco2a1	*ATGGTCCTACGTGTGGTGAAC*	*AGGTACCTGTTTCGAAGAGC*
Tbx1	*GGCAGGCAGACGAATGTTC*	*TTGTCATCTACGGGCACAAAG*
TfIIb	*TGGAGATTTGTCCACCATGA*	*GAATTGCCAAACTCATCAAAACT*
Tmem26	*ACCCTGTCATCCCACAGAG*	*TGTTTGGTGGAGTCCTAAGGTC*
Ucp1	*TCTCTGCCAGGACAGTACCC*	*AGAAGCCCAATGATGTTCAG*

6. Lentiviral overexpression

Lentivirus mediated overexpression was used to study the role of *Fgf8b* in controlling *Ucp1* expression in cultured brown preadipocytes. The lentiviral vector pLenti c-MYC-DDK-Puro-GFP (gift from Giovanni Tonon from the San Raffaele Scientific Institute in Milan, Italy, Addgene #123299) was used to evaluate transduction efficiency and for cloning of pLenti c-MYC-DDK-Puro-Fgf8b. The cloning strategy was based on a double digest of the lentiviral backbone and the donor vector pCMV6-FGF8b (RC214620, Origene) with XhoI and AsiSI at 37 °C for 90 min. The cut backbone and inserts were separated on an agarose gel, purified (Wizard® SV Gel and PCR Clean-Up System) and ligated with T4 ligase at 16 °C overnight. NEB® Stable competent *E.coli* were transformed with the ligated constructs using a heat-shock protocol and streaked out on agar plates containing the antibiotic chloramphenicol. After overnight incubation at 37 °C single colonies were picked for several liquid cultures in chloramphenicol. Plasmids were purified (PureYield™ Plasmid Miniprep System) and sent for DNA sequencing to confirm successful cloning.

For lentivirus production, HEK-293T cells were co-transfected with one of the lentiviral constructs and second generation packaging plasmids (psPAX2 + pMD2.G) in a 10 cm dish using a calcium phosphate transfection protocol. On three consecutive days, lentivirus containing cell culture supernatant was collected, passed through a 0.45 µm polyether-sulfone membrane filter and was subsequently precipitated overnight (PEG-it Virus Precipitation Solution, Biocat). Virus precipitate was centrifuged at 4 °C and 16,000 x g for 30 min and the pellet was resuspended in 150 µl ice cold PBS. The physical titer was calculated based on the quantitative assessment of the viral capsid protein p24 in the virus stock solution (One-Wash Lentivirus Titer Kit, HIV-1 p24 ELISA, Origene). Brown preadipocytes (5 x 10^4 cells) were incubated with lentivirus (multiplicity of infection: 500-1000) and 8 µg/ml polybrene for 16-24 h.

7. RNA interference by Dicer-substrate RNAs

Gene silencing by Dicer-substrate, short-interfering RNAs (DsiRNA, Integrated DNA Technologies) was used to study the role of several target genes in mediating FGF8b induced *Ucp1* expression in cultured brown preadipocytes. For DsiRNA delivery, transfection reagent Lipofectamine® RNAiMAX (Thermo Fisher Scientific) and DsiRNA were diluted in Opti-MEM reduced serum medium (Gibco) and incubated for 20 min at room temperature. This amounted to 200 µl Opti-MEM, 3 µl transfection reagent and 2 µl of a 10 µM DsiRNA stock for a single well in a 12-well format. A preconfluent subculture of preadipocyes was trypsinized, centrifuged at 500 x g for 5 min and resuspended in cell culture media. Cells were then added to the transfection mixture up to a final volume of 1 ml. A scrambled, non-targeting DsiRNA control was used to control for the transfection procedure (51-01-19-09, Integrated DNA Technologies). Efficiency of DsiRNA mediated knockdown was evaluated 48 h post-transfection by RT-qPCR. Knockdown of FGFR1 was additionally evaluated 72 h post-transfection by immunoblotting. The effect of target gene knockdown on FGF8b mediated *Ucp1* expression was assessed 48 h after FGF8b treatment corresponding to a time point 96 h post-transfection.

Table 2. Forward and reverse DsiRNA sequences used for gene silencing studies.

Target gene	5' - 3' forward DsiRNA	5' - 3' reverse DsiRNA
anti-Fgfr1	*CAUCCGUUGCUAUAUAUUAAAAACA*	*UGUUUUUAAUAUAUAGCAACGGAUGCU*
anti-Fgfr2	*GGAAGACUGUUUCCUGAUAAGUGGA*	*UCCACUUAUCAGGAAACAGUCUUCCUU*
anti-Ptges1	*UUACUCUACAGUCAGGACAACCUTG*	*CAAGGUUGUCCUGACUGUAGAGUAAGU*
anti-Lrrfip1 #1	*ACAUGGAAUAAUCCUAAAUUCAGAA*	*UUCUGAAUUUAGGAUUAUUCCAUGUUU*
anti-Lrrfip1 #2	*CAGUAAAUGACGUUGGGUAUCAAGC*	*GCUUGAUACCCAACGUCAUUUACUGUG*
anti-Esrra #1	*CUGUGACCUUUUUGAUCGAGAGATA*	*UAUCUCUCGAUCAAAAAGGUCACAGAG*
anti-Esrra #2	*AUUCUGACUCUGUGCACAUUGAAGA*	*UCUUCAAUGUGCACAGAGUCAGAAUUG*
anti-Nupr1	*AACCUCUAAACCUAGAGGAUGAAGA*	*UCUUCAUCCUCUAGGUUUAGAGGUUGC*
anti-Etv1	*AAGAUUGAGCUCUUGGUAAAAUAGA*	*UCUAUUUUACCAAGAGCUCAAUCUUGG*
anti-Atf5	*GGCUUCUCUGAUUGGAUGACUGAGC*	*GCUCAGUCAUCCAAUCAGAGAAGCCGU*
anti-Bnc1	*GAAUCUGUGAUUGAGUCACAUGGAG*	*CUCCAUGUGACUCAAUCACAGAUUCAA*
anti-Arid5a	*GAAUCUGUUGCCAAGUCACAGUGAT*	*AUCACUGUGACUUGGCAACAGAUUCAC*
anti-Cebpg	*GAGAAUACCUUGGAUUAAGAAAAGC*	*GCUUUUCUUAAUCCAAGGUAUUCUCUC*
anti-Hes1#1	*CUAAGCCAACUGAAAACACUGAUTT*	*AAAUCAGUGUUUUCAGUUGGCUUAGAC*
anti-Hes1 #2	*CUCUUCUGACGGACACUAAAAACGA*	*UCGUUUUUAGUGUCCGUCAGAAGAGAG*
anti-Nrf1	*GUCACUGUUGCCCAAGUGAAUUACT*	*AGUAAUUCACUUGGGCAACAGUGACUG*
anti-Prdm16	*GGCAUUGGACAACUUAUUCUGAAGA*	*UCUUCAGAAUAAGUUGUCCAAUGCCAA*
anti-Nr2f2	*CCAAGCAAGCUAAUCACAGAACUGT*	*ACAGUUCUGUGAUUAGCUUGCUUGGAC*

8. Protein isolation, BCA assay and immunoblotting

Total protein was isolated using RIPA buffer (50 mM Tris-Cl, 1 % (v/v) NP-40, 0.25 % (w/v) sodium deoxycholate, 150 mM NaCl, 1 mM EDTA, 1:1000 protease inhibitor (P8340, Sigma)) as the lysis reagent. Cells were lysed with 150-400 µl of RIPA buffer for 12-well and 6-well plates, respectively. Cells were scraped off the plate with rubber cell scrapers and transferred to pre-chilled reaction tubes. Samples were incubated on ice for 30 min and vortexed every 10 min. Samples were then centrifuged for 15 min with 22,000 x g at 4 °C, and supernatant was collected for downstream applications. Total protein concentrations were determined using the Pierce™ BCA Assay Kit (Thermo Fisher Scientific), which is based on the reduction of Cu^{2+} to Cu^{1+} in alkaline medium coupled to the colorimetric detection of Cu^{1+} with bicinchoninic acid (BCA).

Western blot samples were prepared in Laemmli buffer (33 mM Tris-HCl, pH 6.8, 5 % sodium dodecyl sulfate (SDS), 25 % (w/v) glycerol, 0.01 % bromophenol blue) with 5 % (v/v) beta-mercaptoethanol and were denatured for 5 min at 95 °C. Equal amounts of protein were loaded onto 4–20 % Mini-PROTEAN® TGX Stain-Free™ precast gels (Biorad). A Mini-PROTEAN® Tetra cell system (Biorad) was used with a Tris-glycine running buffer (25 mM Tris, 250 mM glycine, 0.1 % SDS, pH 8.3) to separate the proteins. Electrophoresis was run at 80 V for the first 20 min and was then switched to 100 V for the remaining time. Proteins were blotted onto a nitrocellulose membrane (P/N 926-31092, LI-COR) using the Trans-Blot semi-dry transfer cell (Biorad) in combination with the Bjerrum Schafer-Nielsen transfer buffer (48 mM Tris, 39 mM glycine, 1.3 mM SDS, pH 9.2) with 20 % (v/v) methanol. Blotting was run at 1 mA per cm^2 of gel area for 60 min. Membranes were blocked in 3% (w/v) BSA in Tris-buffered saline (TBS). Blocked membranes were incubated with primary antibody solution overnight at 4 °C. The following primary antibodies were used in a 1:1000 dilution in TBS with 3 % (w/v) BSA: rabbit anti-UCP1 (ab23841, Abcam), rabbit anti-FGFR1 (#9740, Cell Signaling Technology) and mouse anti-β-Actin, clone C4 (MAB1501, Merck Millipore). After an overnight incubation with primary antibodies, membranes were washed with TBS-0.1 % Tween-20 for 10 min for a total of three times. Membranes were then incubated with secondary antibody goat anti-rabbit IRDye® 800CW and donkey anti-mouse IRDye® 680CW for 1 h at room temperature. Membranes were washed again with TBS-0.1 % Tween-20 for 10 min for a total of three times. Before imaging, membranes were washed one last time with TBS and dried for 5 min to enhance signal acquisition. Membranes were scanned on an

Odyssey Infrared Imaging System (LI-COR) and acquired images were analyzed using the Image Studio™ Lite Software (LI-COR) v.5.2.

9. Proliferation assays

The proliferative effect of fibroblast growth factors and other growth factors were evaluated in white epididymal and brown preadipocytes based on a cellular redox assay and automated cell counting.

Epididymal preadipocytes were incubated with the redox dye resazurin (20 µl per 100 µl cell media) for 4 h at 37 °C (CellTiter-Blue® Cell Viability Assay, Promega). As a result of cellular redox metabolism resazurin is converted to its reduced form resorufin in proportion to cell number. Resorufin containing cell media was collected and transferred into a black 96-well plate for fluorescence measurement on a spectrophotometer at 560/590 nm (Ex/Em).

Culture media of brown preadipocytes was aspirated and cells were washed with PBS. Cells were detached from the plate by sufficient incubation with a trypsin/EDTA solution (250 µl per well in a 12-well format) at 37 °C in the cell incubator. Detached cells were thoroughly resuspended in 250 µl of standard culture media. 10 µl of cell suspension per sample were transferred onto a cell counting slide (#1450011, Biorad) and cells were counted automatically on a TC20™ Cell Counter (Biorad).

10. Lactate measurement

Lactate in cell culture supernatant of brown preadipocytes was measured to evaluate the effect of FGF8b on glucose catabolism. The principle of the lactate assay is based on the quantitative and enzymatic conversion of lactate and NAD^+ (Carl Roth) to pyruvate and NADH by lactate dehydrogenase (LDH, 10127230001, Roche) in the presence of hydrazine at alkaline pH. The amount of lactate in cell culture supernatant is proportional to the amount of NADH formed. Standards (in the range between 0-10 mM lactate) and samples were diluted five-fold in PBS. Next, 5 µl of standards and samples were mixed with 95 µl PBS and the resulting 100 µl were pipetted onto a clear bottom black 96-well plate. Standards and samples were mixed with 100 µl cold hydrazine buffer (2 g/l EDTA, 13 g/l hydrazine sulfate, 25 g/l hydrazine hydrate, pH 9) containing 0.2 mg NAD^+ and 1 µl of undiluted LDH per reaction. The plate was incubated for 30 min at room temperature before measurement at 340 nm on a spectrophotometer.

11. Glucose measurement

Glucose concentrations in cell culture supernatant of brown preadipocyes were evaluated to study the effect of FGF8b on glucose uptake and metabolism. Glucose concentration in cell culture supernatant was measured with a glucometer (FreeStyle Lite, Abbott). The principle of glucose determination in test strips of a glucometer is based on the conversion of glucose to gluconolactone by glucose oxidase/flavin adenine dinucleotide (FAD). This biochemical reaction is, in turn, linked to the redox reaction of the mediator n-methyl pyridine. The mediator n-methyl pyridine shuttles electrons between glucose oxidase-FAD and the working electrode. The total charge is proportional to the glucose concentration in cell culture supernatant. Cell culture supernatant was measured mixed with 100 % glycerol in a ratio of 6:4 (sample:glycerol). Glucose consumption over time was calculated as the difference between glucose levels in fresh media and used media.

12. Glucose uptake assay

A non-radioactive glucose uptake assay was used based on the luciferase-coupled detection of 2-deoxyglucose-6-phosphate (Glucose Uptake-Glo™ Assay, Promega). Glucose uptake capacity was measured in brown preadipocytes (129S) treated with different doses of FGF8b for 48 h. On the day of the assay, cells were incubated in glucose free medium for 2 h before stimulation with 2.5 mM 2-deoxy-D-glucose (2-DG) for 20 min at 3°C. The uptake of 2-DG was stopped by the addition of lysis buffer. The luciferase signal was acquired on a luminometer (Berthold Detection Systems). Background signal was determined in the absence of 2-DG. Glucose transporter 1 (SLC2A1) independent glucose uptake was evaluated in the presence of 10 µM BAY876, a glucose transporter 1 inhibitor, during the 2-DG incubation step.

13. Glycerol measurement

Free glycerol in cell culture supernatant was measured as a surrogate measure for the effect of FGF8b on lipid accumulation and lipolytic capacity (ab65337, Free Glycerol Assay Kit, Abcam). The principle of free glycerol determination in cell culture supernatant is based on the enzymatic oxidation of glycerol. The oxidized glycerol reacts with a probe to generate color. The shift in color can be measured spectrophotometrically at 570 nm. Free glycerol was measured in white differentiated adipocytes upon treatment with 125 ng/ml FGF8b for 48 h. Glycerol release was also examined upon activation of lipolysis by 200 nM isoproterenol for 1 h.

14. Next Generation Sequencing

Gene expression profiling was performed to study global changes in transcript abundances upon treatment with fibroblast growth factors. The sequencing was run by Dr. Christine Wurmser at the Chair of Animal Breeding (Liesel-Beckmann-Str. 1, TUM School of Life Sciences, Technical University of Munich, 85354-Freising, Germany).

The first of two RNA sequencing experiments involved immortalized brown and white preadipocytes derived from the *Ucp1*-reporter mouse model (C57BL/6N). Preadipocytes were treated with 125 ng/ml FGF8b + 1 µg/ml heparin (control groups were stimulated with 1 µg/ml heparin only) for 48 h. Thus, the experimental design divided all samples into four groups (brown x control, white x control, brown x FGF8b, white x FGF8b) with four replicates in each. The passage number of the used preadipocyte cell lines was # 5.

The second of two RNA sequencing experiments involved immortalized brown preadipocytes derived from the 129S6Sv/EvTac mouse. Preadipocytes were treated with either no FGF, 5.55 nM FGF1, 5.55 nM FGF9, 5.55 nM (= 125 ng/ml) FGF8b and 5.55 nM FGF8b + 2 µM of BAY-876, a glucose transporter 1 inhibitor. All groups were co-simulated with 1 µg/ml heparin. Thus, the experimental design divided all samples into 5 groups (control, FGF1, FGF9, FGF8b, FGFb + BAY876) with three replicates in each. The passage number of the used preadipocyte cell line used # 10.

Prior to cDNA library preparation, purity of total RNA was evaluated on a spectrophotometer (Nanodrop-1000) and integrity was evaluated on a 2100 Bioanalyzer system (Agilent) based on the RNA Integrity Number (RIN). RNA integrity of cell culture samples are usually very good (RIN ≥ 9). For cDNA library preparation 500 ng of total RNA was used per sample. Briefly, mRNA was purified and fragmented, followed by cDNA synthesis, adapter ligation and amplification (TruSeq® Stranded mRNA Library Prep, 20020594, Illumina GmbH). For indexing and pooling TruSeq RNA Single Indexes Set A (20020492, Illumina GmbH) was used. The sequencing reaction was run on an Illumina HiSeq2500 instrument using HiSeq Rapid SR Cluster Kit v2 (GD-402-4002, Illumina GmbH) for cluster generation and HiSeq Rapid SBS Kit v2 (FC-402-4022, Illumina GmbH) as the component for the synthesis by sequencing part. The sequencing run parameters were multiplexed single indexed single-end reads, run for 50 cycles, with an average read depth of approximately 22 M reads per sample. The sequencing workflow required the use of several software tools, i.e. for sequencing (HiSeq control software 2.2.70), image analysis and base calling (Real-

Time Analysis 1.18.66.4) and fastq file generation (bcl2fastq conversion software v2.20). Read mapping was performed with the Genomatix Mapping tool, an implemented tool in the Genomatix Software Suite, which allowed mapping against the proprietary ElDorado genome annotation database (2013 version). Based on the mapped reads, the Genomatix Genome Analyzer computed the count matrix. Differential gene expression analysis was performed with the DESeq2 package in R version 3.6.3 using only RefSeq annotated transcripts.

The correlation analysis for the transcription factor screening was performed in R. Briefly, log 2 transformed, normalized counts of all transcripts across all samples were correlated with *Ucp1* expression. All correlations higher than r = 0.900 were extracted (408 transcripts). All proteins with transcription factor activity were extracted resulting in 18 transcripts. Ten transcripts including *Arid5a*, *Atf5*, *Bnc1*, *Cebg*, *Etv1*, *Hes1*, *Nrf1*, *Nr2f2*, *Nupr1* and *Prdm16* were selected, which fulfilled the following requirements: r > 0.925 and mean sum of normalized counts per sample > 50.

15. Bioluminescent quantitation

The *Ucp1*-reporter mouse model offered a reliable system to assess luciferase activity as a surrogate readout for *Ucp1* expression (*Ucp1*-LUC), as published previously (Wang *et al*, 2019). After aspiration of cell culture medium, cells were washed with PBS once and frozen at -80 °C for at least 15 min. Reporter lysis buffer (E397A, Promega) was added to cells (150 µl per well for a 12-well plate), and the plate was incubated on a horizontal shaker at 100 rpm for 15 minutes. In the meantime, 50 µl luciferase substrate (E1501, Promega) were added to 5 ml polystyrene tubes. After complete cell lysis, 10 µl of cell lysate was added to the luciferase substrate, samples were briefly vortexed and measured on a single tube luminometer within 60 s (Berthold Detection Systems). Luminescence signals were acquired (delay time of 10 s, integration time of 10 s) and normalized to protein concentration.

16. Pharmacological inhibition

The role of various signaling molecules and metabolic proteins in FGF8b induced *Ucp1* expression was investigated using small molecule inhibitors (**Table 3.**). Lyophilized inhibitors were reconstituted in dimethyl sulfoxide (DMSO). Sodium oxamate was dissolved in water.

Table 3. Small molecule inhibitors used in cell culture studies.

Molecule Name	Target	Inhibited Pathway	conc.	Catalog no.
LY2874455	Phospho-FGFR	FGF signaling	250 nM	HY-13304-5mg*
SH-4-54	STAT 3, 5	STAT signaling	250 nM	B1637-5*
TAK632	Pan-RAF	MAPK pathway	250 nM	HY-15767-5mg*
Trametinib	MEK1/2	MAPK pathway	250 nM	HY-10999-50mg*
SCH772984	ERK1/2	MAPK pathway	250 nM	B1682-5*
SB202190	P38MAPK	MAPK pathway	250 nM	AOB2557-10*
Wortmannin	PI3K	PI3K-Akt pathway	250 nM	W499400-5mg*
Bisindolylmaleimide I	Pan-PKC	PLCγ-PKC pathway	250 nM	Cay13298-5
Diclofenac	PTGS1, PTGS2	Prostaglandin metabolism	20 µM	Cay70680-5000
Celecoxib	PTGS2	Prostaglandin metabolism	20 µM	Cay10008672-50
BAY-876	SLC2A1	Glucose metabolism	2 µM	Cay19961-1
Sodium Oxamate	LDHA	Glucose metabolism	20 mM	Cay19057-5
GW6471	PPARα	PPAR signaling	20 µM	Cay11697-1
GSK3787	PPARβ/δ	PPAR signaling	20 µM	Cay15219-5
GW9662	PPARγ	PPAR signaling	20 µM	Cay70785-5
CAY10678	PTGES1	Prostaglandin metabolism	25 µM	Cay15129-1
CAY10526	PTGES1	Prostaglandin metabolism	25 µM	Cay10010088-1
U-51605	PTGIS	Prostaglandin metabolism	25 µM	Cay16465-1

Abbreviations:* purchased from Biotrend, otherwise from Biomol working concentration (conc.).

17. LC-MS/MS oxylipin analysis

Oxylipins were measured to identify potential mediators of FGF8b induced *Ucp1* expression within the prostaglandin metabolic pathway. LC-MS/MS based measurements were performed by M. sc. Fiona Henkel at the Research Unit Molecular Endocrinology and Metabolism (Ingolstädter Landstrasse 1, Helmholtz Center Munich, German Research Center for Environmental Health, 85764-Neuherberg, Germany).

Cell culture media of treated brown preadipocytes was collected and centrifuged for 2 min at 5,000 x g at 4 °C to remove cell debris. Supernatant was mixed with ice cold LC-MS grade methanol in a 1:1 ratio, inverted a few times and then frozen at -80°C until measurement. On day of measurement, samples were thawed and diluted with LC-MS grade water to a methanol content of 15 % and internal standard stock solutions were added. Samples underwent automated solid phase extraction with a Microlab STAR robot (Hamilton) und were extracted on Strata-X 96-well plates (30 mg, Phenomenex). After extraction, samples were eluted with methanol, evaporated to dryness under a constant stream of nitrogen, and then redissolved in 100 µl of 50 % methanol in water. Oxylipins were separated by chromatography using a 1260 Series HPLC (Agilent) with a Kinetex C18 reversed phase column (2.6 µm, 100 x 2.1 mm, Phenomenex) and a SecurityGuard Ultra Cartridge C18 (Phenomenex) precolumn. Samples were injected via an autosampler at 7.5 °C (HTC PAL, CTC Analytics) coupled to a QTRAP 5500 mass spectrometer (Sciex) with a Turbo-VTM ion source. The mass spectrometer operated in negative ionization mode. Retention time and scheduled multiple reaction monitoring were used to identify specific oxylipin species. Analyst Software 1.6.3 (Sciex) was used for acquisition of LC-MS/MS data. Data were quantified with the MultiQuant Software 3.0.2 (Sciex). The entire oxylipin panel including limit of detection for every metabolite is listed in the Appendix.

18. Respirometry and glycolysis assay

Oxygen consumption and extracellular acidification was measured on an Extracellular Flux analyzer (Seahorse XF96, Agilent Technologies). Proton production rates, derived exclusively from the glycolytic pathway, were obtained according to a published protocol (Mookerjee *et al*, 2016; Mookerjee & Brand, 2015). Cells were cultured in glucose free medium (DMEM Base D5030, 5 mM Hepes, 31 mM NaCl, 2 mM GlutaMAX™ (Gibco), 0.1 % (w/v) free fatty acid free BSA, 15 mg/l phenol red, pH 7.4) on a collagen-coated (10 µg/well) 96-well plate for 1 h before measurement.

Leak respiration was measured upon addition of 5 µM oligomycin, followed by the addition of 1 µM isoproterenol for UCP1-dependent respiration, and 7.5 µM Carbonyl cyanide 4-(trifluoromethoxy) phenylhydrazone (FCCP) for maximal respiration. Non-mitochondrial oxygen consumption was assessed after the addition of 5 µM antimycin A. The glycolysis assay measured basal glycolytic rates upon addition of 10 mM glucose. Glycolytic flux was increased with the addition of 1 µM rotenone and 1 µM myxothiazol or 5 µM antimycin A, which inhibited ATP production by oxidative phosphorylation. Maximal glycolytic capacity was assessed after the addition of 400 µM monensin and 2 µM FCCP, drastically increasing the cellular ATP demand.

19. Statistics

GraphPad Prism version 6.07 (GraphPad Software, San Diego, California, USA) was used to perform all statistical analyses. Parametric tests with Bonferroni correction were used, when data followed an approximate normal distribution and when variances across groups were similar (Student's t-test, one-way ANOVA, two-way ANOVA). Approximate normal distribution and variance homogeneity were visually assessed by plotting the residuals. Non-parametric tests with Dunn's correction were used when data failed to show normal distribution and variance homogeneity (Mann-Whitney test, Kruskal-Wallis). RNA sequencing data were bioinformatically analyzed in R-Studio (R version 3.6.3) using the R package *DESeq2*, as published (Love *et al*, 2014). For data visualization *ReactomePA*, *pheatmap*, *vidger*, *EnhancedVolcano*, *venndiagramm* packages were used. Data were presented as means ± SD, except noted otherwise in figure captions. Statistically significant results were indicated with asterisks: * = $p < 0.05$. ** = $p < 0.01$, *** = $p < 0.001$, **** = $p < 0.0001$.

20. Prepublication statement

Data presented in the following figures: Fig. 2A-C, Fig. 3A-C, Fig. 4A-D, Fig. 5A-D, Fig. 6B-C, were solely generated and contributed by Thomas Gantert and have been published previously in:

Westphal S, Gantert T, Kless C, Hüttinger K, Klingenspor M & Fromme T (2019) Fibroblast growth factor 8b induces uncoupling protein 1 expression in epididymal white preadipocytes. Sci Rep 9: 1–11

RESULTS

1. The effect of FGF8b on differentiated adipocytes.

Paracrine fibroblast growth factors (FGFs) constitute the largest class within the FGF protein family and encode for 15 secreted polypeptides (Ornitz & Itoh, 2015). The human *Fgf8* gene, unlike most other FGFs, gives rise to four protein isoforms (a, b, e, f) due to alternatively spliced transcripts. The FGF8b isoform was previously identified as the strongest of all paracrine FGFs to induce *Ucp1* transcription in white adipocytes (Westphal *et al*, 2019). Based on these initial findings FGF8b was comprehensively evaluated as a promising browning agent in cultured white adipocytes derived from the stromal-vascular fraction (SVF).

1.1 FGF8b induces *Ucp1* expression in white adipocytes.

FGF8b treatment during the entire differentiation dose-dependently increased *Ucp1* expression in white adipocytes from the epididymal and inguinal adipose tissue (**Fig. 1A**). White epididymal adipocytes demonstrated a significantly higher capacity to induce *Ucp1* expression than inguinal adipocytes (**Fig. 1A**), possibly due to a higher degree of differentiation (**Fig. 1B**). The recruitment of brite adipocytes is routinely

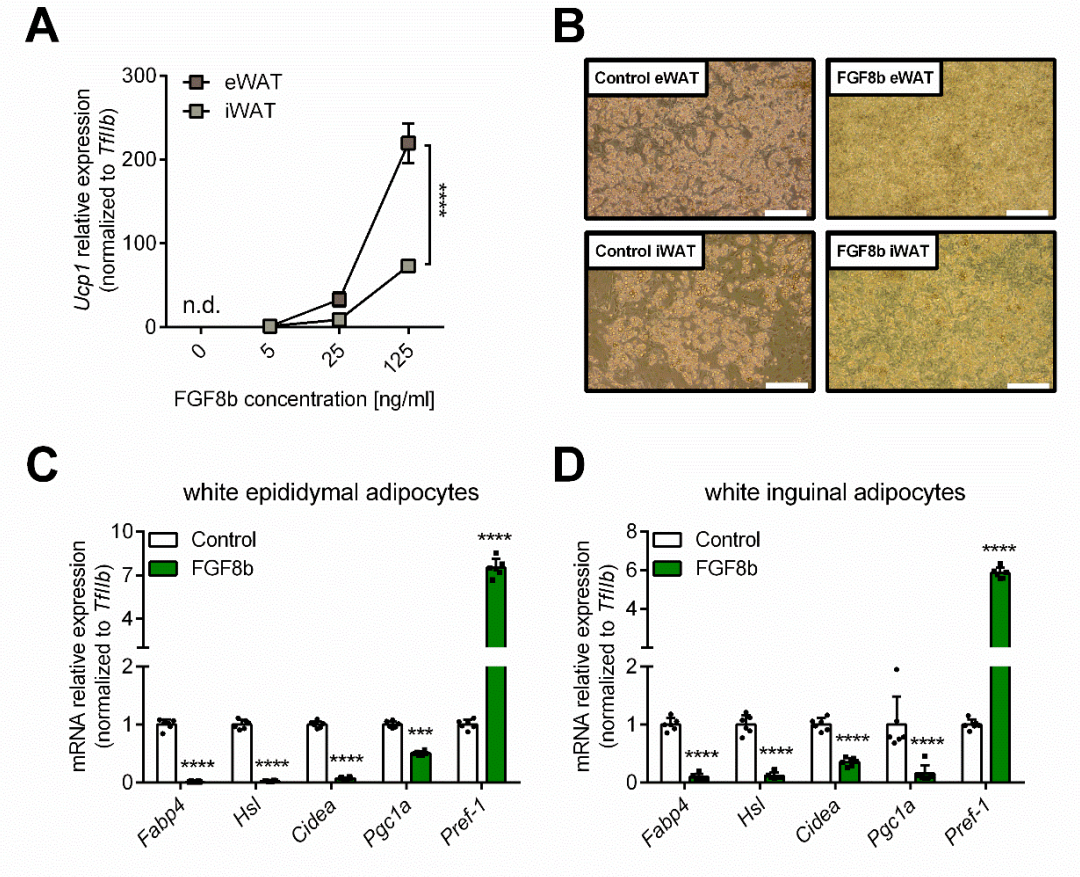

Figure 1. FGF8b induces *Ucp1* expression in white adipocytes. (**A**) Relative *Ucp1* expression in differentiated white epididymal and inguinal adipocytes treated with 5, 25 and 125 ng/ml FGF8b during differentiation (N=3 for each group). (**B**) Representative brightfield images of fully differentiated untreated and FGF8b-treated adipocytes of epididymal white adipose tissue (eWAT) and inguinal adipose tissue (iWAT). Scale bar 200 µm. (**C-D**) Relative mRNA expression of adipogenic and thermogenic markers in untreated and FGF8b-treated white epididymal and inguinal adipocytes (N=6 for each group). Adipocytes in all panels were differentiated according to differentiation protocol A. Two-way ANOVA in A, C and D. Statistically significant results were indicated with asterisks: * = $p < 0.05$. ** = $p < 0.01$, *** = $p < 0.001$, **** = $p < 0.0001$.

screened on the basis of increased *Ucp1* gene expression, but other thermogenic, adipogenic and mitochondrial markers are helpful in evaluating the effect of browning agents. White epididymal and inguinal adipocytes treated with 125 ng/ml FGF8b during differentiation were characterized by lower adipogenic (*Fabp4*, *Hsl*), thermogenic (*Cidea*) and mitochondrial marker (*Pgc1a*) gene expression (**Fig. 1C-D**). In contrast, *Pref-1*, a preadipocyte marker gene was consistently upregulated in white adipocytes (**Fig. 1C-D**). Taken together, FGF8b induced *Ucp1* gene expression in white adipocytes, but failed to activate a broader thermogenic transcriptional program. Moreover, treatment of adipocytes with FGF8b during differentiation markedly suppressed adipogenesis, as highlighted by a decrease in adipogenic and an increase in preadipocyte markers. Further experiments were conducted with the aim to validate these unexpected findings and white epididymal adipocytes were chosen as the preferred cell model due to their higher capacity for *Ucp1* induction.

1.2 *Ucp1* expression by FGF8b is independent of thermogenic differentiation.

Putative brite adipocyte markers have been identified in the past, including *Tmem26*, *Tbx1*, *Cd137*, *Hocx9*, *Shox2*, *Slc27a1* (Wu *et al*, 2012b; Waldén *et al*, 2012), and can be used complementarily to the browning markers *Ucp1*, *Cidea* and *Prdm16* to validate browning treatments. Rosiglitazone, a PPARγ agonist commonly used as a browning agent, was used as a positive control to confirm thermogenic differentiation of the cell line used. While rosiglitazone treatment strongly induced both *Ucp1* and *Cidea* expression in white epididymal adipocytes, treatment with FGF8b merely induced *Ucp1* expression (**Fig. 2A**), whereas *Cidea* expression remained unchanged (**Fig. 2A-B**). Expression levels of *Prdm16* tended to be higher in rosiglitazone treated adipocytes and lower in adipocytes treated with FGF8 than in control cells (**Fig. 2A**). The induction of *Ucp1* transcript abundance by FGF8b was confirmed on the protein level (**Fig. 2B**) Rosiglitazone treatment of epididymal adipocytes resulted in the upregulation of 1 of 6 (*Tbx1*) putative brite markers, while FGF8b induced 3 of the 6 (*Tmem26*, *Tbx1*, *Cd137*) marker genes. (**Fig. 2C**). Thus, these data demonstrated that FGF8b robustly increased *Ucp1* gene expression in white adipocytes, in the absence of a coordinated

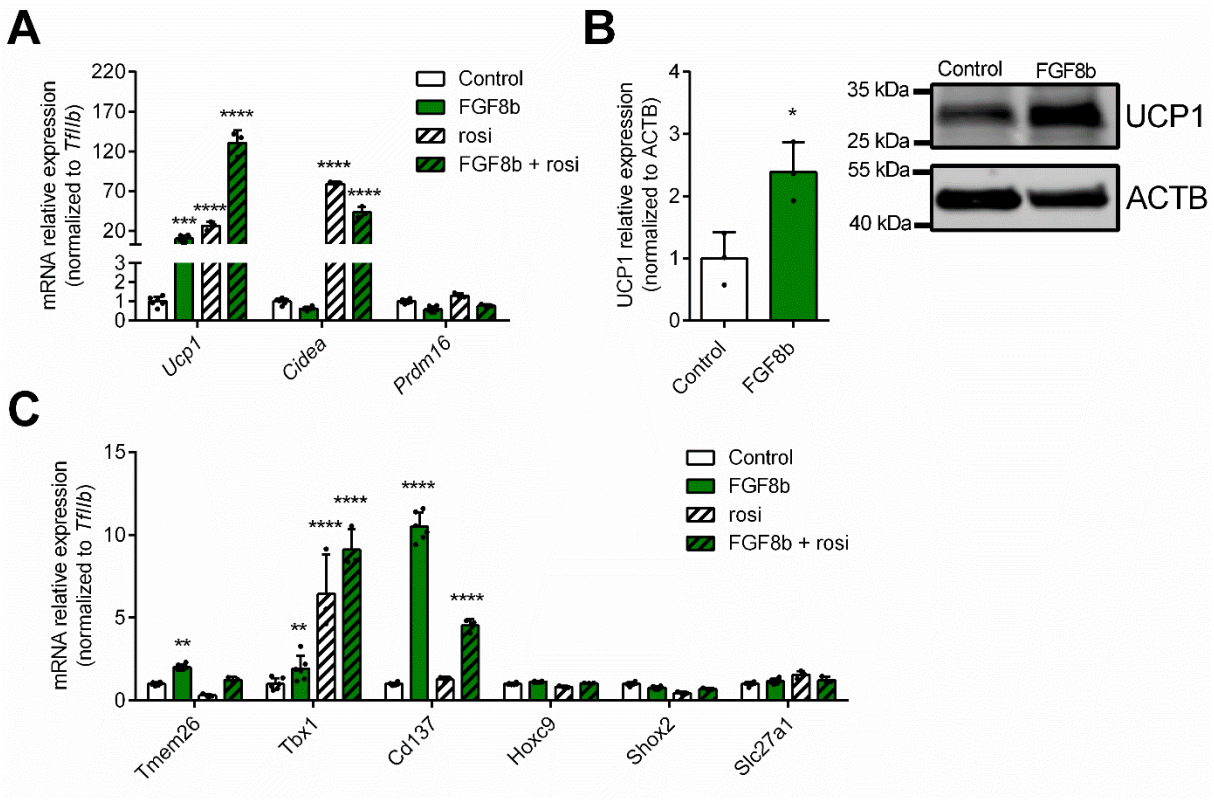

Figure 2. The effect of FGF8b on brite adipocyte marker gene expression. (**A**) Relative mRNA expression of thermogenic genes in epididymal adipocytes treated with a combination of 1 µM rosiglitazone (rosi) and 125 ng/ml FGF8b (N=3-6 for each group). (**B**) UCP1 protein expression in epididymal adipocytes treated with FGF8b, normalized to reference protein ACTB expression (N=3 for each group). (**C**) Relative mRNA expression of brite adipocyte marker genes in epididymal adipocytes treated with a combination of 1 µM rosiglitazone (rosi) and 125 ng/ml FGF8b (N=3-6 for each group). Adipocytes in all panels were differentiated according to differentiation protocol A. Two-way ANOVA in A and C and Student's t-test in B. Statistically significant results were indicated with asterisks: * = $p < 0.05$. ** = $p < 0.01$, *** = $p < 0.001$, **** = $p < 0.0001$. Data in panel A-C previously published in Westphal et al, 2019.

induction of other thermogenic genes such as *Cidea* and P*rdm16*. Notably, the observation that rosiglitazone treatment was not very effective in elevating most brite markers questioned the validity of these markers in the employed cell line. Hence, it remained unclear to what extent FGF8b constituted a *bona fide* browning agent. Thermogenic competency is acquired via the combined activation of the adipogenic and thermogenic transcriptional program. Hence, the effect of FGF8b on adipogenesis in white epididymal adipocytes was examined more closely.

1.3 FGF8b suppresses adipogenesis and lipid accumulation.

Expression levels of genes involved in lipid metabolism and adipogenesis such as *Fabp4*, *Hsl* and *Pparg* were robustly increased by rosiglitazone treatment (**Fig. 3A**). However, FGF8b treatment tended to decrease the expression levels of these adipogenic genes, including *Fasn*, well below control levels, while concomitantly inducing the preadipocyte marker *Pref-1* (**Fig. 3A**). Software-assisted lipid droplet analysis showed that less lipid droplets accumulated in FGF8b treated adipocyte

cultures (**Fig. 3B**) and that these changes occurred uniformly across the entire range of lipid droplet sizes (**Fig. 3C**). Thus, FGF8b treatment effectively suppressed lipid accumulation in epididymal adipocytes during differentiation.

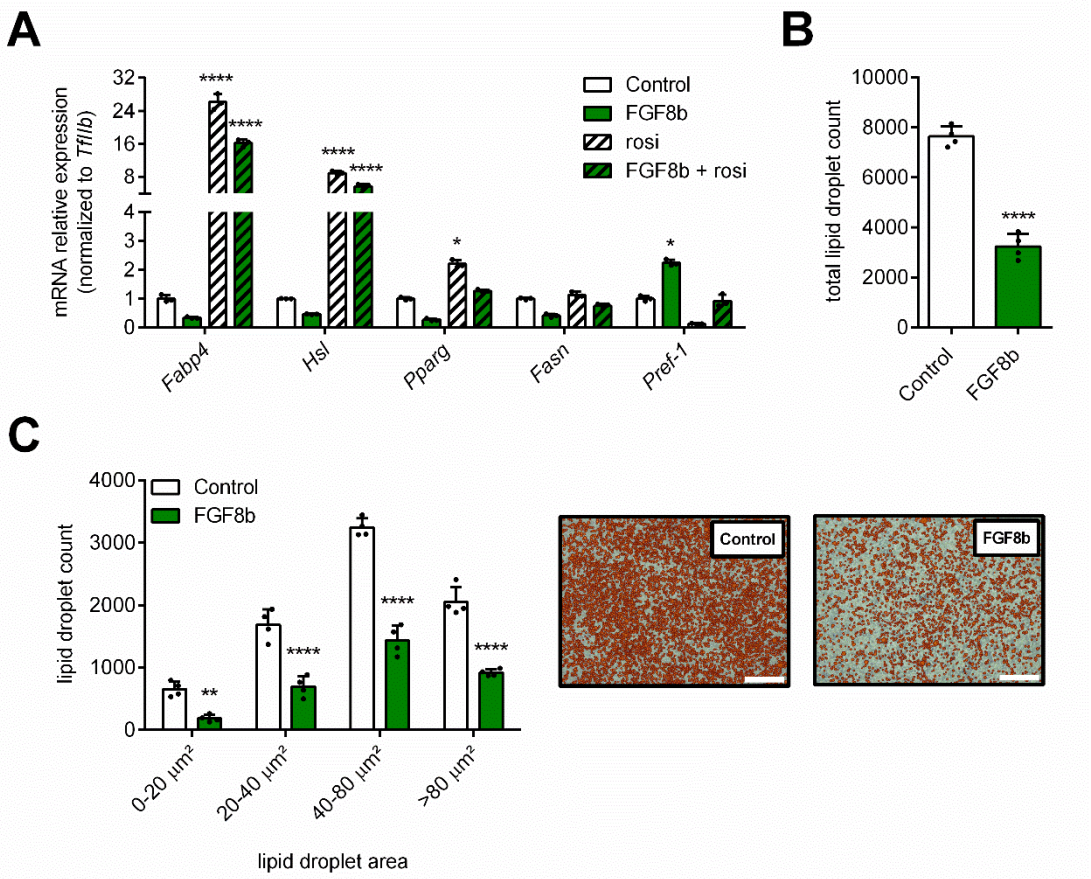

Figure 3. FGF8b suppresses adipogenesis and lipid accumulation. (**A**) Relative mRNA expression of adipogenic genes in epididymal adipocytes treated with a combination of 1 µM rosiglitazone (rosi) and 125 ng/ml FGF8b (N=3-6 for each group). (**B-C**) Lipid droplet analysis including total count and size distribution in epididymal adipocytes treated with 125 ng/ml FGF8b (N=4 for each group). Representative WimLipid post-run images of marked lipid droplets based on brightfield images of adipocyte cultures. Scale bars 200 µm. Adipocytes in all panels were differentiated according to differentiation protocol A. Two-way ANOVA in A, C and Student's t-test in B. Statistically significant results were indicated with asterisks: * = $p < 0.05$. ** = $p < 0.01$, *** = $p < 0.001$, **** = $p < 0.0001$. Data in panel A-C previously published in Westphal et al, 2019.

1.4 UCP1-dependent respiration is not changed upon FGF8b treatment.

Lipolytic stimulation of adipocytes results in the release of free fatty acids (FFAs) from triglycerides, which interact directly with UCP1 to activate its thermogenic function. Lipolytic capacity and UCP-dependent respiration were assessed in white adipocytes to functionally evaluate the effects of FGF8b on thermogenesis. Glycerol constitutes the backbone of triglycerides and is released upon lipolytic breakdown of triglycerides. Glycerol concentrations in cell culture supernatant of FGF8b treated adipocytes were consistently lower than in media of control cells, and independent of the fact whether a lipolytic stimuli was applied or not (**Fig. 4A**). These observations correlated well with overall lipid content in adipocyte cultures as assessed by oil red o staining (**Fig. 4B**). The baseline oxygen consumption rate was higher in FGF8b treated cells, but UCP1-

dependent respiration, in the presence of oligomycin and isoproterenol, remained unchanged (**Fig. 4C**), which was indicative of no meaningful thermogenic activity in both the control and FGF8b groups. Interestingly, FGF8b treated adipocytes showed higher extracellular acidification upon inhibition of ATP synthase, possibly indicating higher glycolytic capacity in these cells (**Fig. 4D**).

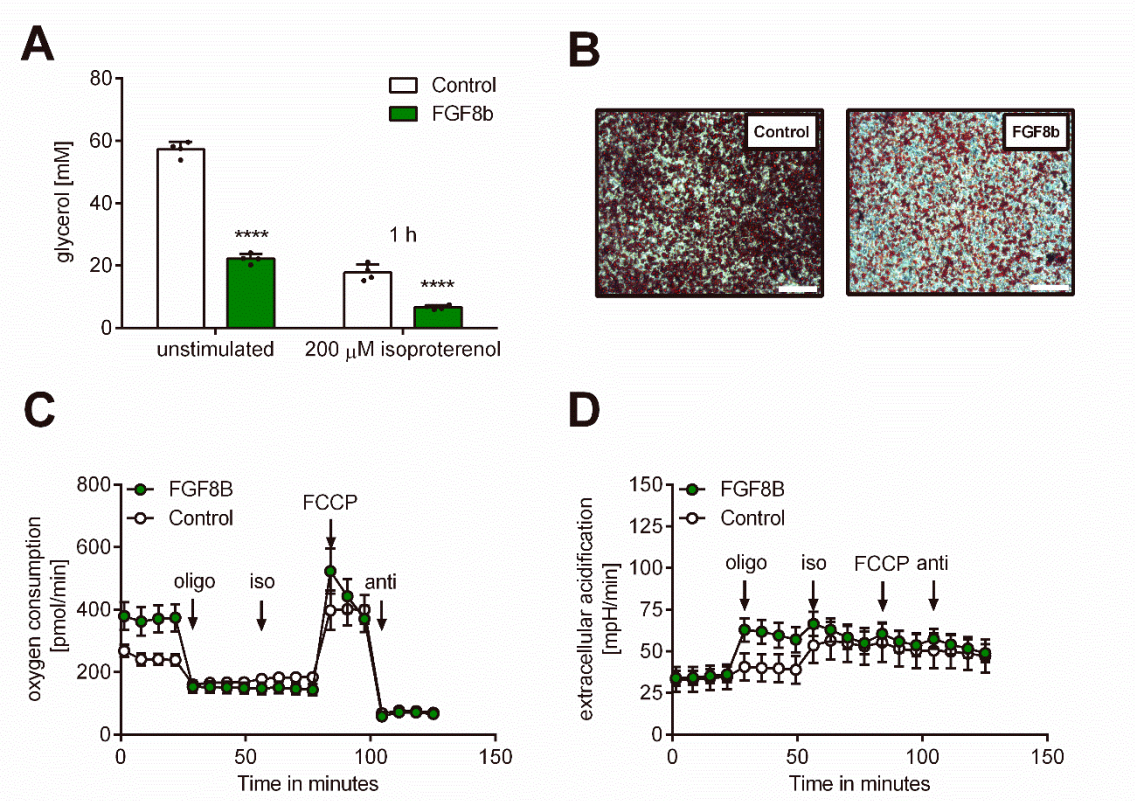

Figure 4. UCP1-dependent respiration is not changed upon FGF8b treatment. (**A**) Glycerol release from epididymal adipocytes treated with 125 ng/ml FGF8b during differentiation under unstimulated conditions for 48 h and stimulated with 200 µM isoproterenol for 1 h (N=4 for each group). (**B**) Representative brightfield images of epididymal adipocytes treated with FGF8b and stained with oil red o (lipid staining). Scale bars 200 µm. (**C-D**) Oxygen consumption and extracellular acidification of epididymal adipocytes treated with FGF8b during differentiation. Injection A: 5 µM oligomycin, B: 1 µM isoproterenol, C: 7.5 µM FCCP, D: 5 µM antimycin A. Adipocytes in all panels were differentiated according to differentiation protocol A. Two-way ANOVA in A. Statistically significant results were indicated with asterisks: * = $p < 0.05$. ** = $p < 0.01$, *** = $p < 0.001$, **** = $p < 0.0001$. Data in panel A-D previously published in Westphal et al, 2019.

1.5 FGF8b increases glycolytic capacity in cultured adipocytes.

Expression analysis of genes involved in lactate and glucose metabolism revealed increased expression of genes regulating lactate efflux (*Mct4*), glucose uptake (*Glut1*) and glycolysis (*Pdk1*) (**Fig. 5A**). In fact, lactate levels in cell culture supernatant of FGF8b treated adipocytes were significantly higher than in the control group, which coincided with a visible acidification of cell culture media (**Fig. 5B**). Next, glycolytic capacity of FGF8b treated adipocytes was functionally evaluated using a validated and published glycolysis assay (Mookerjee & Brand, 2015). Adipocytes were briefly incubated in glucose free medium, followed by glucose stimulation in the presence of respiratory inhibitors rotenone and antimycin A. As a consequence, oxygen

consumption was halted, while extracellular acidification increased (**Fig. 5C-D**). Subsequently, cellular ATP demand was artificially increased by the addition of FCCP and monensin to stimulate maximal glycolytic capacity as evidenced by an additional rise in media acidification (**Fig. 5D**). Higher increments in extracellular acidification were observed in FGF8b treated adipocytes, which indicated higher glycolytic capacity in these cells. Taken together, functional assessment of the effects of FGF8b treatment on white epididymal adipocytes revealed no meaningful thermogenic activity as evidenced by respiratory measurements, but a pronounced reprogramming of cellular metabolism towards glycolysis.

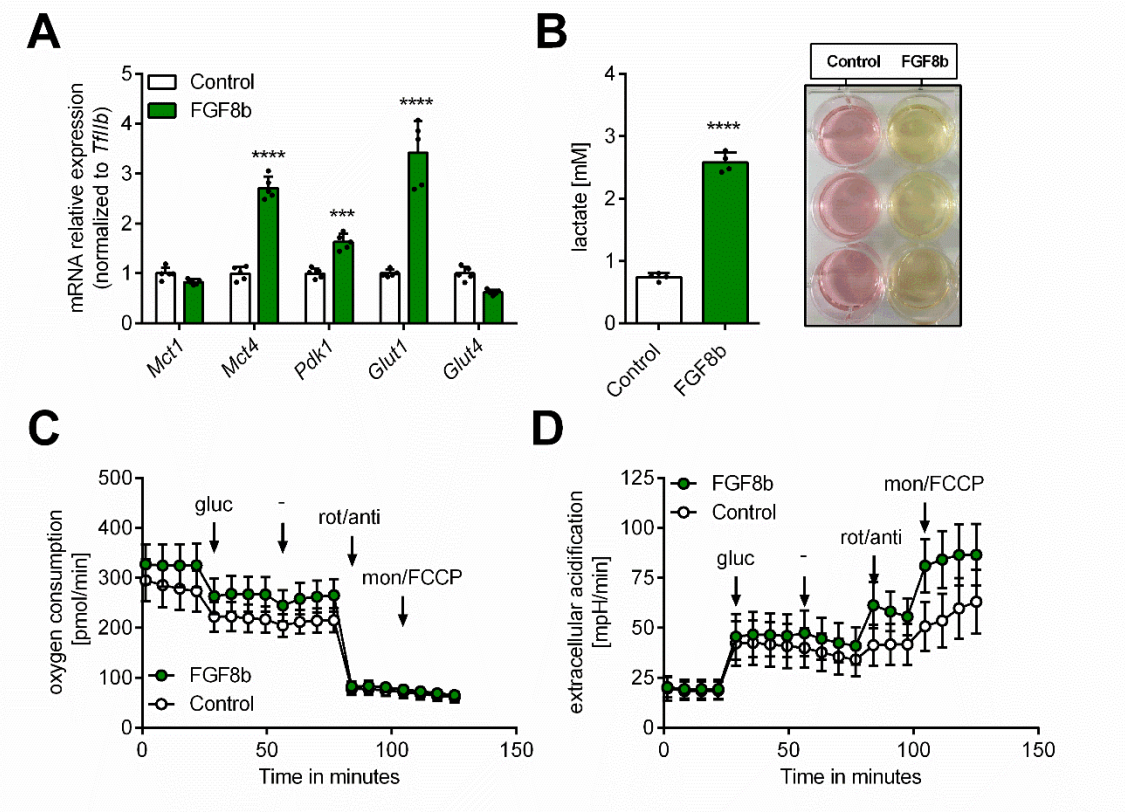

Figure 5. FGF8b treated adipocytes show enhanced glycolytic capacity. (**A**) Relative mRNA expression of genes involved in lactate and glucose metabolism in epididymal adipocytes treated with 125 ng/ml FGF8b (N=5 for each group). (**B**) Lactate levels in cell culture supernatant of epididymal adipocytes treated with 25 ng/ml FGF8b (N=4 for each group). (**C-D**) Oxygen consumption and extracellular acidification of epididymal adipocytes treated with FGF8b during differentiation. Injection A: 10 mM glucose, B: assay medium, C: 1 µM rotentone and 5 µM antimycin A, D: 400 µM monensin and 2 µM FCCP. Adipocytes in all panels were differentiated according to differentiation protocol A. Two-way ANOVA in A and Student's t-test in B. Statistically significant results were indicated with asterisks: * = $p < 0.05$. ** = $p < 0.01$, *** = $p < 0.001$, **** = $p < 0.0001$. Data in panel A-D previously published in Westphal et al, 2019.

1.6 Treatment with FGF8b stimulates cell proliferation in cultured adipocytes.

Glycolysis is a hallmark of rapidly proliferating cells and serves the purpose of maximizing biomass assimilation rather than ATP production through the provision of glycolytic intermediates for biosynthetic pathways (DeBerardinis *et al*, 2008). Since high glycolytic rates were observed in epididymal adipocytes upon FGF8b treatment, the effect of FGF8b on cell proliferation and biomass assimilation was investigated.

Incubation of NIH/3T3 mouse fibroblasts with increasing concentrations of FGF8b induced cell proliferation with an EC_{50} = 5.1 ng/ml (**Fig. 6A**). Likewise, treatment of epididymal preadipocytes with FGF8b for 48 h resulted in a significant increase in cell proliferation (**Fig. 6B**), and RNA/protein yields were consistently higher in FGF8b treated adipocytes than in the control group (**Fig. 6C**). Thus, FGF8b elicited a strong mitogenic effect in both epididymal preadipocytes and adipocytes, providing a rationale for the observed metabolic switch towards glycolysis in cultured cells.

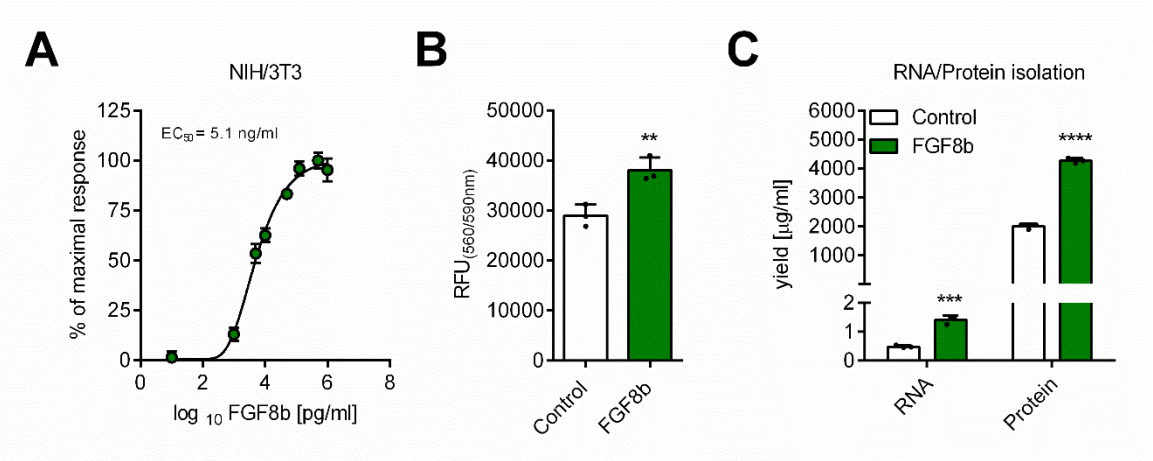

Figure 6. FGF8b treatment stimulates cell proliferation in (pre)adipocytes. (**A**) Mitogenic assay based on resazurin oxidation in NIH/3T3 fibroblasts stimulated with increasing concentrations of FGF8b for 48 h (n=6 for each group). (**B**) Mitogenic assay based on resazurin oxidation in epididymal preadipocytes stimulated with 125 ng/ml FGF8b for 48 h (N=3 for each group). (**C**) Typical RNA/protein yield from cultured epididymal adipocytes treated with FGF8b during differentiation (N=3 for each group). Adipocytes in panel C were differentiated according to differentiation protocol A. Student's t-test in B and two-way ANOVA in C. Statistically significant results were indicated with asterisks: * = $p < 0.05$. ** = $p < 0.01$, *** = $p < 0.001$, **** = $p < 0.0001$. Data in panel B-C previously published in Westphal et al, 2019.

1.7 FGF8b strongly upregulates *Ucp1* expression in white preadipocytes.

Treatment with FGF8b stimulated cell proliferation during the differentiation procedure, which was metabolically supported by an activation of the glycolytic pathway. Moreover, lipid metabolism and adipogenesis were suppressed, while the preadipocyte marker *Pref-1* was increased. Combined, these data supported the view that FGF8b acted as a mitogenic cue for some preadipocytes*, while other preadipocytes differentiated to mature adipocytes within the same cell culture. This

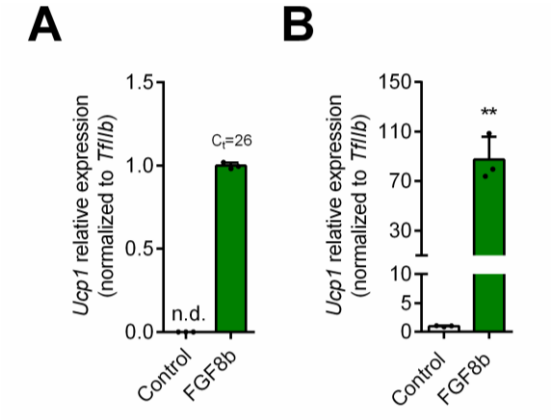

**for ease of use, the term 'preadipocyte' will be used interchangeably with the more accurate terminology 'primary or immortalized cell from the stromal-vascular fraction'. The stromal-vascular fraction is a complex mixture of progenitor/stem cells (preadipocytes), fibroblast, vascular and immune cells, but its dominant cell type is the preadipocyte. In addition, the tautological term undifferentiated preadipocyte will be used to emphasize the fact that these cells were not differentiated, in the same way some researchers refer to the differentiated adipocytes.*

Figure 7. FGF8b strongly upregulates *Ucp1* expression in preadipocytes. (**A**) *Ucp1* mRNA expression in epididymal preadipocytes (FVB/N) treated with 125 ng/ml FGF8b for six days (N=3 for each group). (**B**) *Ucp1* mRNA expression in inguinal preadipocytes (129S) treated with 125 ng/ml FGF8b for six days (N=3 for each group). Student's t-test in A and B. Statistically significant results were indicated with asterisks: * = $p < 0.05$. ** = $p < 0.01$, *** = $p < 0.001$, **** = $p < 0.0001$.

opened the possibility that FGF8b would, in fact, target *Ucp1* expression in preadipocytes rather than adipocytes, explaining the lack of overall thermogenic differentiation. Treatment of epididymal preadipocytes with FGF8b for the duration of six days (equal to the duration of the differentiation period), indeed, strongly upregulated *Ucp1* expression (**Fig. 7A**), which was corroborated in a white preadipocyte cell line derived from the 129S mouse strain (**Fig. 7B**). Thus, FGF8b induced *Ucp1* expression in the proliferating and pro-glycolytic preadipocyte, while negatively affecting the outcome of adipogenic and thermogenic differentiation.

In summary, FGF8b induced *Ucp1* expression in immortalized white epididymal and inguinal adipocytes. Surprisingly, the effect on *Ucp1* expression was neither embedded in a coordinated upregulation of the adipogenic, nor thermogenic programm. As a result, adipocytes treated with FGF8b were characterized by impaired lipid accumulation and a lack of thermogenic activity. Instead, adipocyte cell cultures treated with FGF8b showed signs of increased cell proliferation and a pro-glycolytic metabolism to support it. Finally, FGF8b was demonstrated to regulate *Ucp1* gene expression in the undifferentiated preadipocyte, highlighting a formerly unrecognized site for *Ucp1* expression in cell cultures derived from white adipose tissue.

1.8 FGF8b lowers *Ucp1* expression in differentiated brown adipocytes.

FGF8b increased *Ucp1* expression in immortalized white epididymal and inguinal adipocytes, but its effect on brown adipocytes, the main site of *Ucp1* expression *in vivo*, was not known. Immortalized brown preadipocytes derived from two different mouse strains, the 129S mouse and the *Ucp1*-reporter mouse (C57BL/6N), a transgenic mouse model, which accurately reports endogenous *Ucp1* expression via a luciferase reporter (Wang *et al*, 2019), were used. Consistent with previous findings, FGF8b treatment in brown adipocytes led to lower gene expression of adipogenic and thermogenic genes (**Fig. 8A**), and resulted in less overall lipid accumulation (**Fig. 8B**). However, brown adipocytes treated with FGF8b had lower *Ucp1* expression than control cells (**Fig. 8A**). These data were reproduced in brown *Ucp1*-reporter adipocytes showing less *Ucp1* expression in brown adipocytes upon treatment with FGF8b during the entire differentiation (**Fig. 8C**) or when added to fully differentiated adipocytes for another 48 h (**Fig. 8D**).

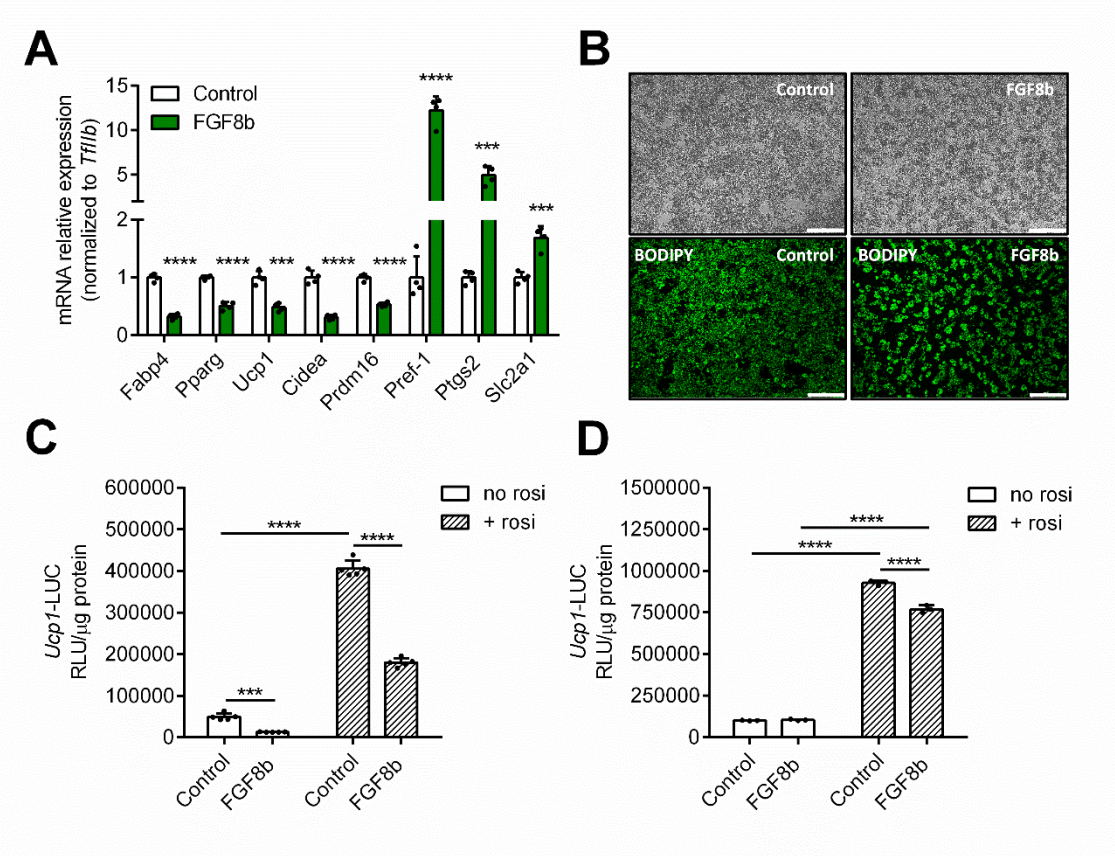

Figure 8. FGF8b lowers *Ucp1* expression brown adipocytes. (**A**) Relative mRNA expression of adipogenic and thermogenic genes in brown adipocytes (129S) treated with FGF8b (N=4 for each group). (**B**) lipid staining with the fluorescent dye BODIPY in brown adipocytes treated with or without FGF8b. Ex/Em: 488–503/515–545. Scale bar 200 µm. (**C**) luciferase linked *Ucp1* expression (*Ucp1*-LUC) in rosiglitazone (1 µM) treated brown adipocytes stimulated with FGF8b over the entire differentiation period (N=5 for each group). (**D**) luciferase linked *Ucp1* expression (*Ucp1*-LUC) in rosiglitazone (1 µM) treated brown adipocytes stimulated with FGF8b for 48 at the end of differentiation (N=3 for each group). Adipocytes in all panels were differentiated according to differentiation protocol B. Multiple Student's t-test with Bonferroni correction in A, two-way ANOVA in C and D. Statistically significant results were indicated with asterisks: * = $p < 0.05$. ** = $p < 0.01$, *** = $p < 0.001$, **** = $p < 0.0001$.

Taken together, these data demonstrated a clear discrepancy with respect to the effect of FGF8b on *Ucp1* expression between adipocytes derived from white fat depots and interscapular brown fat. Whether this discrepancy would be a disposition of the preadipocyte or a consequence of differentiation remained to be tested.

2. The effect of FGF8b on undifferentiated preadipocytes.

2.1 FGF8b strongly upregulates *Ucp1* expression in brown preadipocytes.

Preadipocyte-specific *Ucp1* expression was comprehensively characterized using both immortalized and primary brown and white preadipocytes. *Ucp1* gene expression significantly increased in immortalized brown preadipocytes derived from 129S mice upon treatment with FGF8b for 72 h (**Fig. 9A**). These changes in transcript abundance translated to a 20-fold increase in UCP1 protein expression in the same cell model (**Fig. 9B**). Lentivirus mediated overexpression of FGF8b in immortalized brown preadipocytes replicated these findings (**Fig. 9C**). For an extensive characterization of FGF8b induced *Ucp1* expression, we employed our established *Ucp1*-luciferase-reporter model (Bl/6N background), which provides a reliable and efficient luminescence based readout for *Ucp1* expression (Wang *et al*, 2019). Treatment of immortalized brown and white preadipocytes of the *Ucp1*-reporter model with FGF8b

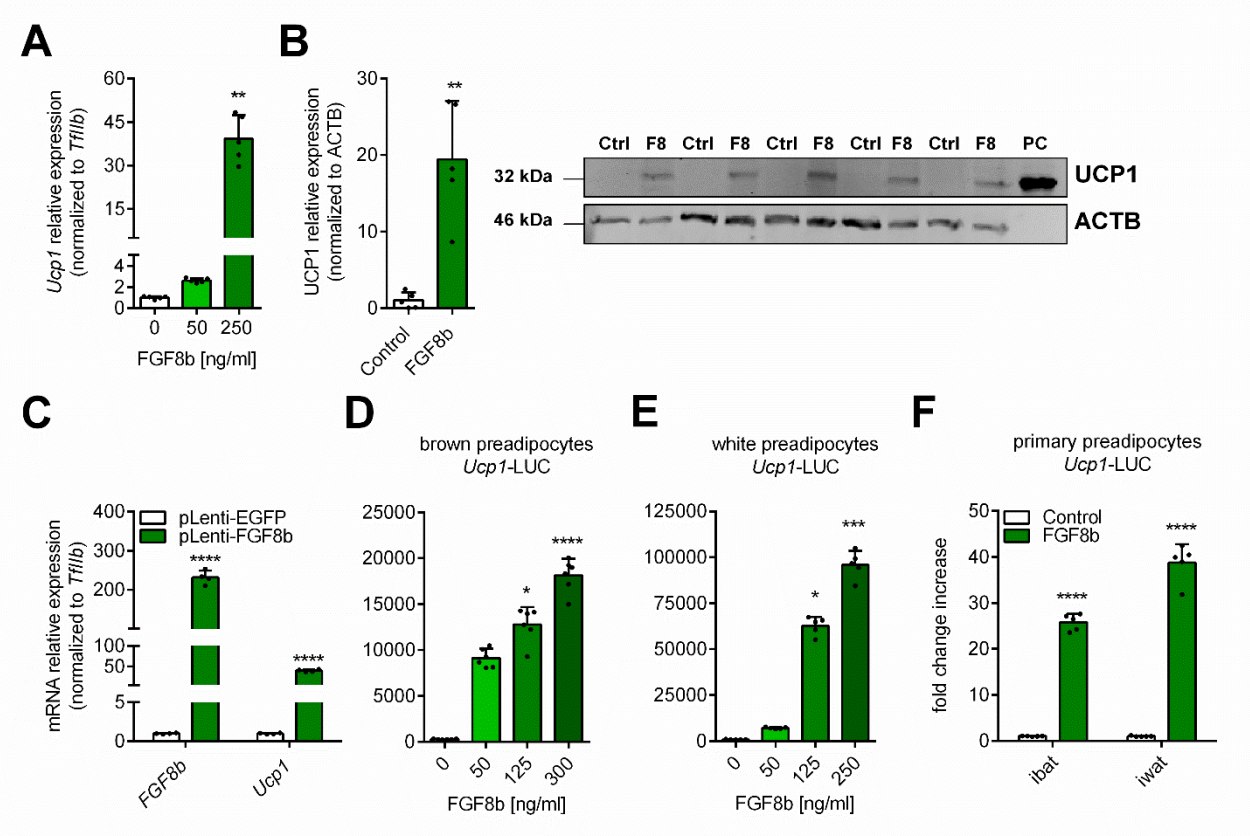

Figure 9. FGF8b induces *Ucp1* expression in brown and white preadipocytes. (**A**) *Ucp1* mRNA expression in brown preadipocytes (129S) treated with 50 and 250 ng/ml FGF8b (N=5 for each group). (**B**) UCP1 protein expression in brown preadipocytes (129S) treated with 125 ng/ml FGF8b (N=4 for each group). (**C**) *Fgf8b* and *Ucp1* mRNA expression in brown preadipocytes (129S) as a result of lentiviral overexpression of enhanced green fluorescent protein (EGFP) and FGF8b (N=4 for each group). (**D-E**) luciferase activity linked *Ucp1* expression (*Ucp1*-LUC) in immortalized *Ucp1*-reporter derived brown and white preadipocytes (N=5-6 for each group). (**F**) luciferase activity linked *Ucp1* expression (*Ucp1*-LUC) in primary brown and white preadipocytes (N=5 for each group). All experiments were carried out in the presence of 1µg/ml heparin. Kruskal-Wallis test in A, D, E, Mann-Whitney in B, two-way ANOVA in C, F. Statistically significant results were indicated with asterisks: * = $p < 0.05$. ** = $p < 0.01$, *** = $p < 0.001$, **** = $p < 0.0001$.

for 48 h increased *Ucp1* expression dose-dependently (**Fig. 9D-E**). Similarly, treatment of primary preadipocytes isolated from the interscapular brown and white inguinal adipose tissue with FGF8b induced *Ucp1* expression 25-40 fold, respectively. Thus, FGF8b treatment upregulated *Ucp1* expression in immortalized and primary brown and white preadipocytes, independent of mouse strain (129S vs. Bl/6N) and mode of delivery (pharmacological vs. lentivirus).

2.2 The biological activity of FGF8b is modulated by its cofactor heparin.

The effect of FGF8 on *Ucp1* expression followed a dose-response relationship, with an experimentally determined EC_{50} value of 55 ng/ml in brown preadipocytes (**Fig. 10A**). A single dose of 125 and 250 ng/ml FGF8b induced *Ucp1* expression significantly above control levels after 48 h, peaking at 72 h, before declining again towards the end of the experiment (**Fig. 10B**), possibly due to diminished FGF signaling. Next, the ability of the cofactor heparin to modulate FGF signaling was evaluated in a dose-response experiment with varying concentrations of both FGF8b

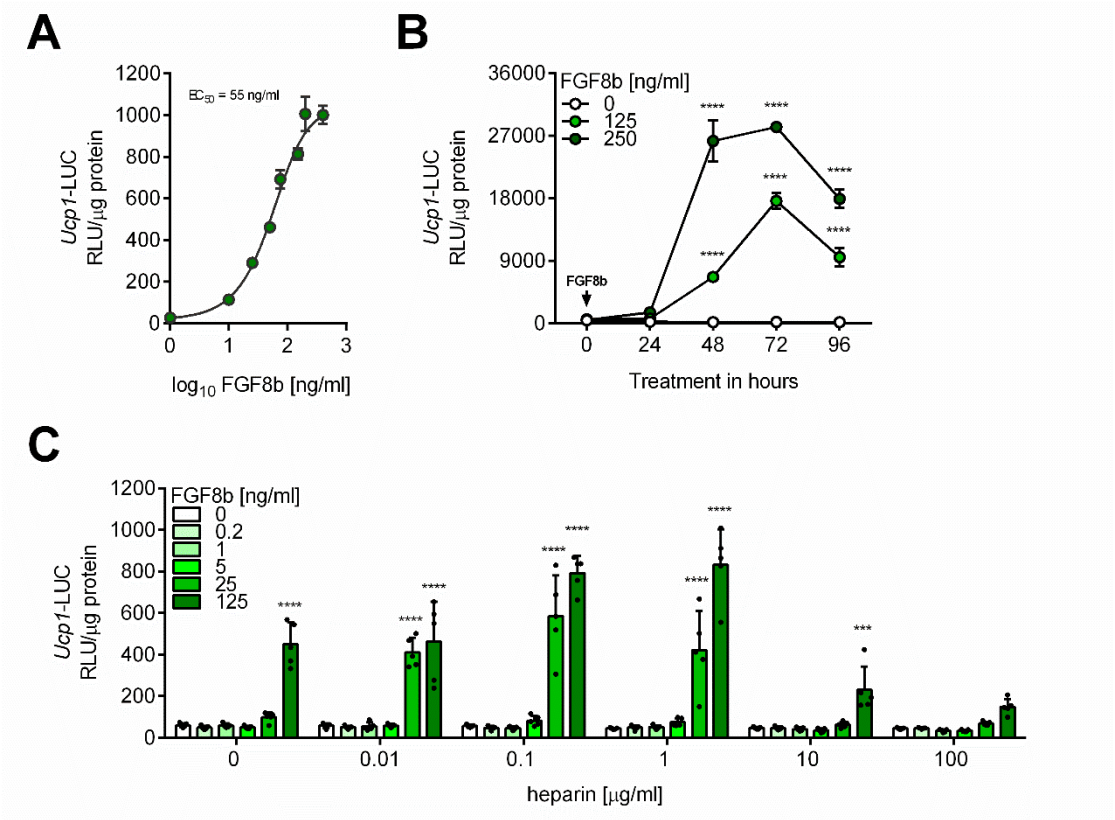

Figure 10. The biological activity of FGF8b is modulated by heparin. (**A**) Dose-response relationship between FGF8b concentration and luciferase linked *Ucp1* expression (*Ucp1*-LUC) in brown preadipocytes (N=5 for each group). (**B**) luciferase activity linked *Ucp1* expression (*Ucp1*-LUC) in brown preadipocytes following a single application of 125 and 250 ng/ml FGF8b without media exchange (N=3-5 for each group). (**C**) luciferase activity linked *Ucp1* expression (*Ucp1*-LUC) in brown preadipocytes treated with increasing concentrations of FGF8b (0.2, 1, 5, 25, 125 ng/ml) and heparin (0.01, 0.1, 1,10, 100 µg/ml) (N=5 for each group). Experiments in panel A and B were carried out in the presence of 1 µg/ml heparin. Two-way ANOVA in B and C. Statistically significant results were indicated with asterisks: * = $p < 0.05$. ** = $p < 0.01$, *** = $p < 0.001$, **** = $p < 0.0001$.

(0, 0.2, 1, 5, 25, 125 ng/ml) and heparin (0.01, 0.1, 1, 10, 100 µg/ml). Interestingly, heparin amplified FGF8b induced *Ucp1* expression 2-6 fold in the range between 0.01 to 1 µg/ml of added heparin, but blunted or even abrogated the effect of FGF8b on *Ucp1* expression at 10 µg/ml and 100 µg/ml, respectively (**Fig. 10C**). Taken together, these data demonstrated a clear dose-response relationship between FGF8b concentration and the magnitude of *Ucp1* expression in brown preadipocytes and highlighted the cofactor heparin as a strong modulator of FGF8b signaling. In all of the following experiments a heparin concentrations of 1 µg/ml was used to amplify FGF8b signaling activity.

2.3 Paracrine FGFs with high mitogenicity induce *Ucp1* expression.

The effect of FGF8b on *Ucp1* expression in preadipocytes was compared to other paracrine and endocrine members of the FGF protein family. FGF6 and FGF9 were selected due to a recent publication, demonstrating FGF6/FGF9 induced *Ucp1* expression in preadipocytes (Shamsi *et al*, 2020). FGF21 was included based on its demonstrated browning effect on cultured white adipocytes and WAT *in vivo* (Emanuelli *et al*, 2014; Fisher *et al*, 2012). All paracrine FGFs (FGF6, FGF8b, FGF9), except FGF1 induced *Ucp1* expression in brown preadipocytes, when equimolar concentrations were used (**Fig. 11A**). Increasing the concentration of FGF1 resulted in a significant upregulation of *Ucp1* expression, but it remained less potent than

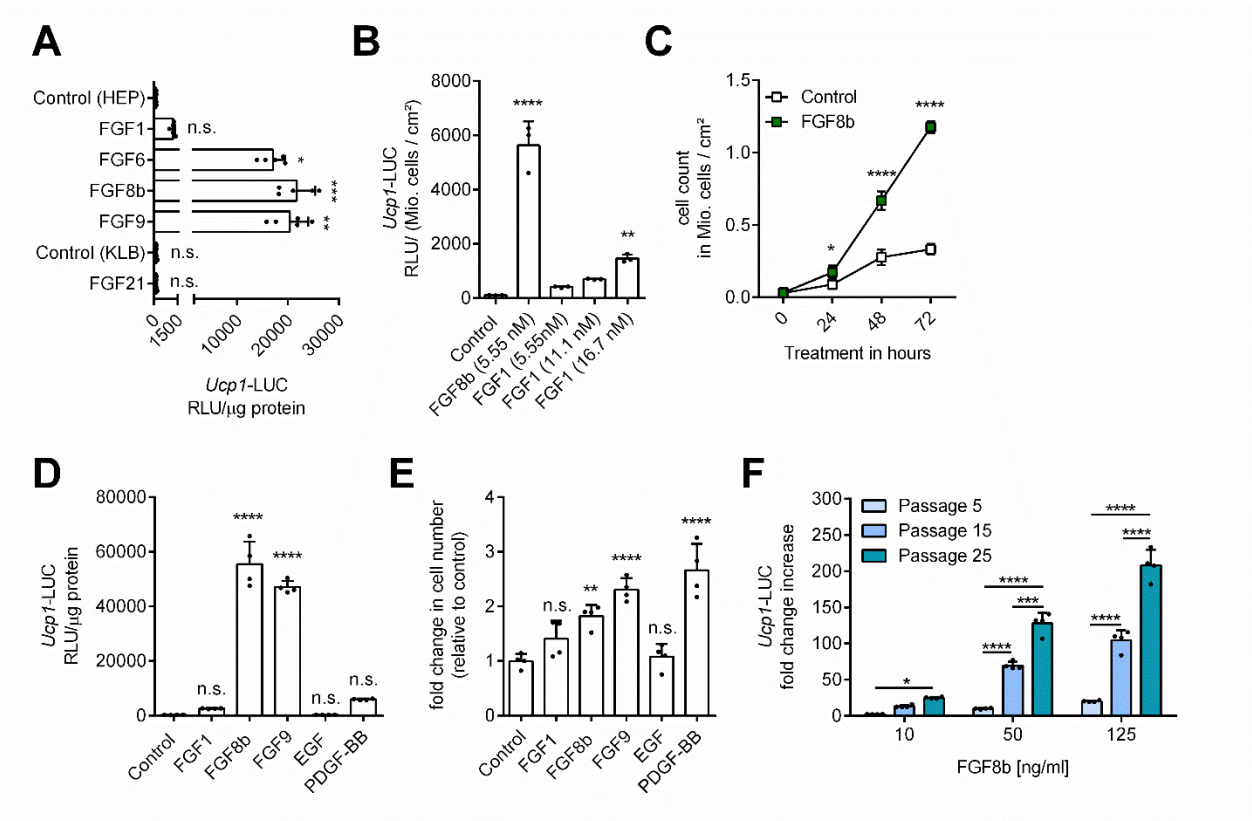

Figure 11. Mitogenic FGFs induce *Ucp1* expression. (**A**) luciferase activity linked *Ucp1* expression (*Ucp1*-LUC) in brown preadipocytes treated with equimolar concentrations (5.55 nM) of FGF1, FGF6, FGF8b, FGF9 and FGF21 compared to heparin control (HEP, 1 µg/ml) and beta-klotho control (KLB, 1 µg/ml) (N=5 for each group). (**B**) luciferase activity linked *Ucp1* expression (*Ucp1*-LUC) in brown preadipocytes treated with increasing concentrations of FGF1 (5.55, 11.1, 16.7 nM) (N=3 for each group). (**C**) Cell count over a period of 72 h in brown preadipocytes treated with FGF8b (N=4 for each group). (**D**) luciferase activity linked *Ucp1* expression (*Ucp1*-LUC) and (**E**) fold change in cell number in brown preadipocytes treated with equimolar concentrations of FGF1, FGF8b, FGF9, 5 µg/ml epidermal growth factor (EGF) and 200 ng/ml platelet-derived growth factor (PDGF-BB) (N=4 for each group). (**F**) fold induction of luciferase activity linked *Ucp1* expression (*Ucp1*-LUC) by FGF8b depending on passage number of preadipocytes used (passaged 5, 15 and 25 times) (N=4 for each group). All experiments were carried out in the presence of 1 µg/ml heparin. Kruskal-Wallis test in A and B, one-way ANOVA in D, E, two-ay ANOVA in C and F. Statistically significant results were indicated with asterisks: * = $p < 0.05$. ** = $p < 0.01$, *** = $p < 0.001$, **** = $p < 0.0001$.

FGF8b (**Fig. 11B**). FGF21 failed to increase *Ucp1* expression in the presence of its cofactor beta-Klotho (**Fig. 11A**). A possible relationship between the mitogenic effect of paracrine FGFs and other mitogens such as epidermal growth factor (EGF) and platelet-derived growth factor (PDGF), and their ability to induce *Ucp1* expression was investigated. Brown preadipocytes treated with FGF8b showed higher cell proliferation with cell numbers diverging between untreated and treated cells as soon as after 24 h of incubation, culminating in a 3-fold difference in cell numbers after 72 h (**Fig. 11C**). FGF9 and PDGF exhibited strong mitogenic potency in brown preadipocytes, while FGF1 and EGF remained ineffective in stimulating cell proliferation above control levels (**Fig. 10E**). Interestingly, paracrine FGFs induced *Ucp1* expression only if they also possessed high mitogenic potency, but mitogenic potency alone as in the case of PDGF did not affect *Ucp1* expression (**Fig. 11D-E**). Notably, brown preadipocyes with higher passage numbers demonstrated higher fold inductions of *Ucp1* upon FGF8b treatment (**Fig. 11F**), possibly indicating that a highly proliferative subpopulation exists in the stromal-vascular fraction of brown adipose tissue, which was disproportionately responsive to FGF8b treatment. Taken together, FGF6, FGF8b and FGF9 induced *Ucp1* expression in preadipocytes to similar degrees, whereas FGF1 was less effective than the other paracrine FGFs. Interestingly, the ability to strongly induce *Ucp1* expression correlated with the mitogenicity of studied FGFs, highlighting an unexpected interplay between cell proliferation and *Ucp1* gene expression. Conversely, preadipocytes of higher passages, which likely contained cells with a higher proliferative capacity due to continuous positive selection, were demonstrated to induce *Ucp1* more effectively. Thus, highly passaged cell lines might be more responsive to FGF8b treatment.

2.4 The FGF8b induced transcriptome is not fat-depot dependent.

Global gene expression signatures in white and brown preadipocytes upon FGF8b treatment were assessed by transcriptomic analyses. Immortalized preadipocytes derived from both fat depots were treated with 125 ng/ml FGF8b and 1 µg/ml heparin for 48 h. Control cells were treated with 1 µg/ml heparin over the same period. Differential gene expression analysis revealed a large overlap of significantly down- and upregulated transcripts between the fat depots, indicating that treatment effects overrode potential depot effects (**Fig. 12A-B**). The most downregulated genes included *Ptn*, *Igfbp3*, *Igfbp4*, *Nov*, *Wisp2* and *Aspn*, and the most upregulated genes were *Spp1*, *Angptl4, Slc14a1, Hmga2* and *Ptgs2*. Notably, prostaglandin endoperoxidase synthase 2 (*Ptgs2*), also known as cyclooxygenase 2, is an enzyme located in the prostaglandin biosynthetic pathway, a pathway associated with browning of white adipose tissue (Vegiopoulos *et al*, 2010; Madsen *et al*, 2010). Pathways enriched within the subset of highly downregulated genes included *Extracellular matrix organization*, *Degradation of the extracellular matrix*, *Collagen formation* and *Collagen biosynthesis and modifying enzymes*, demonstrating remodeling of the extracellular matrix by FGF8b treatment. Analysis of highly upregulated genes revealed enriched pathways such as *Extracellular matrix organization*, *MAPK family signaling cascade*, *Metabolism of carbohydrates*, *Glucose metabolism* and *Glycolysis*, indicating that FGF8b controlled glucose utilization via the MAPK signaling pathway (**Fig. 12D**).

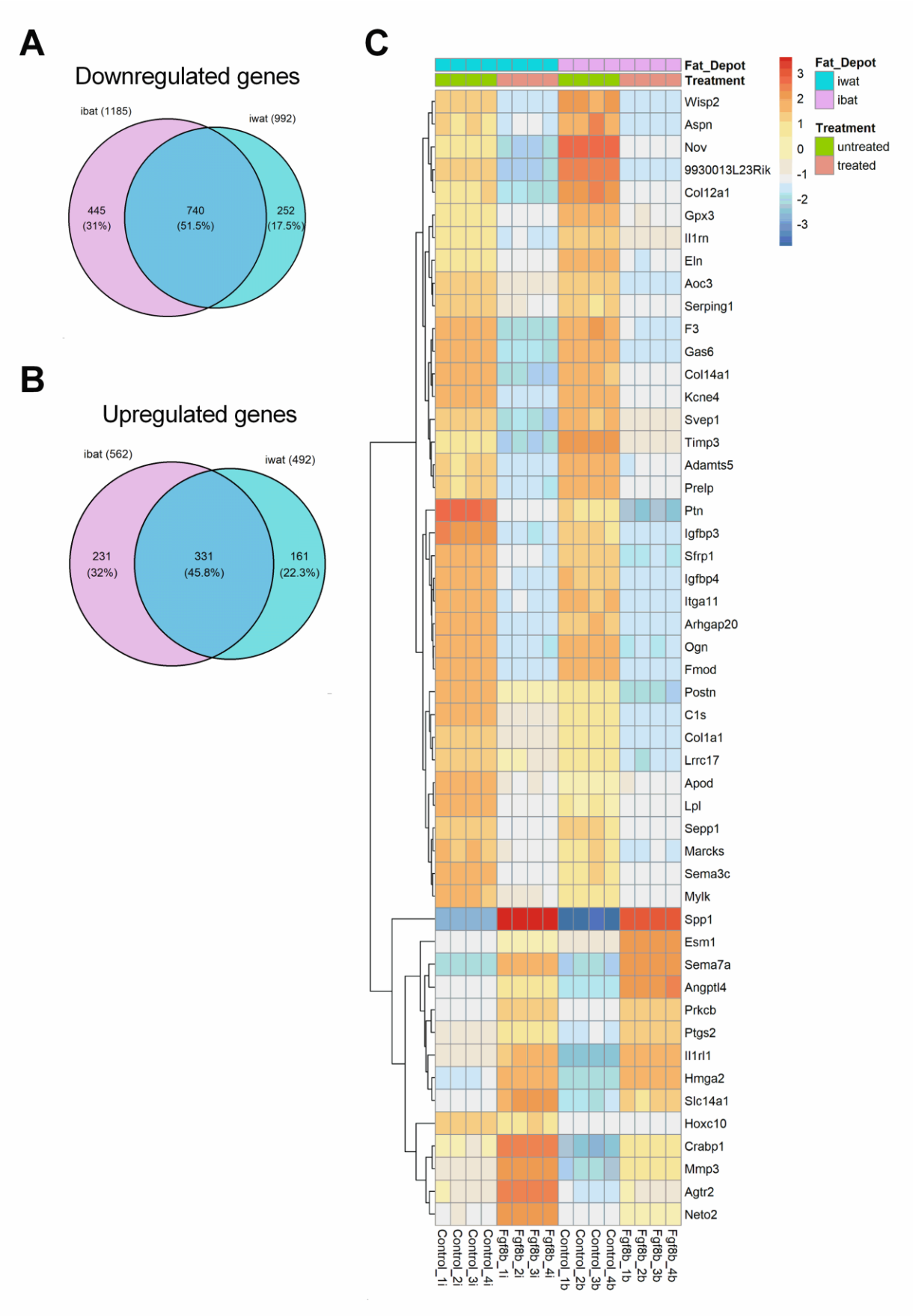
A
Downregulated genes
ibat (1185)
iwat (992)
445
(31%)
740
(51.5%)
252
(17.5%)
B
Upregulated genes
ibat (562)
iwat (492)
231
(32%)
331
(45.8%)
161
(22.3%)
C
Fat_Depot
Treatment
Fat_Depot
iwat
ibat
Treatment
untreated
treated
3
2
1
0
-1
-2
-3
Wisp2
Aspn
Nov
9930013L23Rik
Col12a1
Gpx3
Il1rn
Eln
Aoc3
Serping1
F3
Gas6
Col14a1
Kcne4
Svep1
Timp3
Adamts5
Prelp
Ptn
Igfbp3
Sfrp1
Igfbp4
Itga11
Arhgap20
Ogn
Fmod
Postn
C1s
Col1a1
Lrrc17
Apod
Lpl
Sepp1
Marcks
Sema3c
Mylk
Spp1
Esm1
Sema7a
Angptl4
Prkcb
Ptgs2
Il1rl1
Hmga2
Slc14a1
Hoxc10
Crabp1
Mmp3
Agtr2
Neto2
Control_1i
Control_2i
Control_3i
Control_4i
Fgf8b_1i
Fgf8b_2i
Fgf8b_3i
Fgf8b_4i
Control_1b
Control_2b
Control_3b
Control_4b
Fgf8b_1b
Fgf8b_2b
Fgf8b_3b
Fgf8b_4b

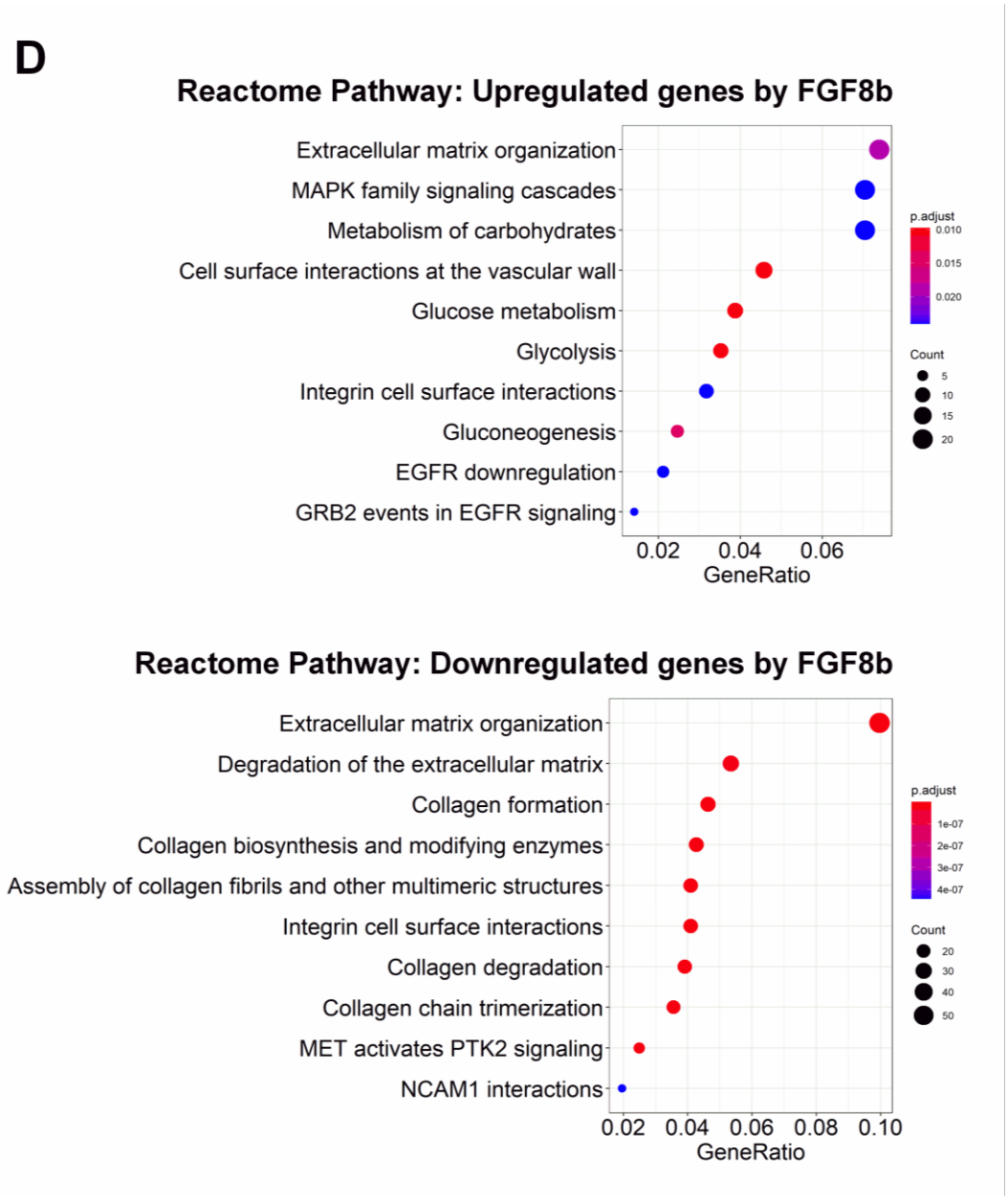

Figure 12. Transcriptomic analysis of FGF8b treatment in preadipocytes. (**A**) Venn diagrams showing the overlap between subsets of down- and upregulated transcripts (adjusted p-value < 0.01 and $\log_2$ fold change > 1 or < -1) beween fat depots (ibat vs. iwat). (**B**) Subset of genes with highest variance across all groups based on normalized count matrix. Scale bar reflects fold changes after variance stabilizing transformation and are centered around the mean (≙ $\log_2$ fold change). Analyzed with the *DESeq2* R package. (**C**) Pathway analysis of down-and upregulated genes (adjusted p-value < 0.01 and $\log_2$ fold change > 1 or < -1) in brown preadipocytes. Analyzed with the *ReactomePA* R package.

Taken together, transcriptomic analyses of cultured preadipocytes treated with FGF8b revealed three key findings, which warranted further investigation. Firstly, which fibroblast growth factor receptor gene is activated and are there signaling pathways besides the MAPK pathway contributing to FGF8b signaling? Secondly, is the induction of *Ptgs2* causally linked to FGF8b induced *Ucp1* expression? And thirdly, does FGF8b control glucose metabolism with a potential link to *Ucp1* expression?

2.5 FGF8b induced *Ucp1* expression is mediated by FGFR1.

Fibroblast growth factors signal via four fibroblast growth factor receptor (*Fgfr*) genes, designated *Fgfr1-4*. The most abundant *Fgfrs* in preadipocytes were, according to the transcriptomic data, *Fgfr1* and *Fgfr2*, whereas *Fgfr3* showed very weak and *Fgfr4* no meaningful expression at all (**Fig. 13A**). Gene silencing of *Fgfr1* and *Fgfr2* was performed using DsiRNAs and efficiency of knockdown was validated by RT-qPCR. Knockdown of *Fgfr1* increased *Fgfr2* expression, while *Fgfr2* knockdown did not change *Fgfr1* transcript levels (**Fig. 13B-C**). The effect of FGF8b on *Ucp1* expression was completely abrogated in cells lacking *Fgfr1*, but remained unchanged, when *Fgfr2*

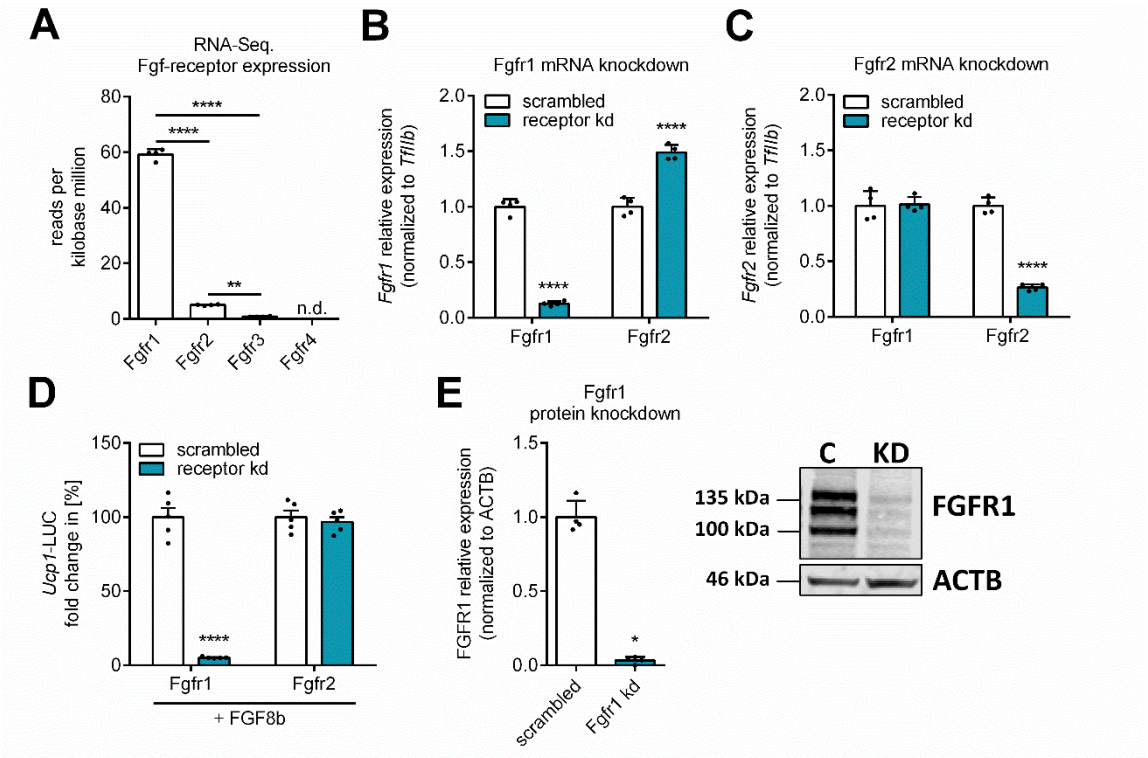

Figure 13. FGF8b induced *Ucp1* expression is mediated by FGFR1. (**A**) mRNA expression of fibroblast growth factor genes in reads per million mapped reads (RPKM) in brown preadipocytes from the first RNA sequencing experiment (N=4 for each group). *Fgfr4* was non-detectable (n.d.). (**B-C**) *Fgfr1/Fgfr2* mRNA expression in *Fgfr1/Fgfr2* knockdown (kd) experiments with 20 nM DsiRNA in brown preadipocytes (N=4 for each group). (**D**) luciferase activity linked *Ucp1* expression (*Ucp1*-LUC) in brown preadipocytes treated with FGF8b during *Fgfr1/Fgfr2* knockdown (N=5 for each group). (**E**) FGFR1 protein expression in brown preadipocytes upon *Fgfr1* knockdown 72 h post-transfection (N=4 for each group). FGFR1 protein expression was normalized to ACTB protein expression. Control (C) and Knockdown (KD) N=4 for each group). All experiments were carried out in the presence of 1 µg/ml heparin. One-way ANOVA in A, two-way ANOVA in B-D, Mann-Whitney test in E. Statistically significant results were indicated with asterisks: * = $p < 0.05$. ** = $p < 0.01$, *** = $p < 0.001$, **** = $p < 0.0001$.

was silenced (**Fig. 13D**). Efficiency of gene silencing of FGFR1 was confirmed on the protein level (**Fig. 13E**). Thus, initiation of FGF8b signaling occurred via binding of FGF8b to FGFR1, followed by downstream pathway activation.

2.6 FGF8b signals via a FGFR1-MEK1/2-ERK1/2 axis to upregulate *Ucp1*.

Several intracellular signaling pathways have been shown to underly the biological activity of FGFs. These include the RAS-MAPK, PI3K-Akt, STAT and PLCγ-PKC pathways (Ornitz & Itoh, 2015). A panel of small molecule inhibitors was used to target these pathways in brown preadipocytes to validate the contribution of each signaling branch in FGF8b mediated *Ucp1* induction (**Table 4.**).

Table 4. Small molecule inhibitors targeting the FGF signaling pathway.

No.	Inhibitor Name	Abbreviation	Target	Pathway
1	LY2874455	LY	pan-FGFR	-
2	SH-4-54	SH	Stat3,5	STAT
3	TAK632	TAK	pan-RAF	RAS-MAPK
4	Trametinib	TRA	MEK1/2	RAS-MAPK
5	SCH772984	SCH	ERK1/2	RAS-MAPK
6	SB202190	SB	p38MAPK	RAS-MAPK
7	Wortmannin	WOR	PI3K	PI3K-AKT
8	Bisindolylmaleimide I	BIS	PKC	PLCγ-PKC

The ability to inhibit FGF8b induced *Ucp1* expression was evaluated in comparison to a vehicle/DMSO (negative) control and the pan-FGFR inhibitor LY2874455, which served as a (positive) inhibition control. FGF8b induced *Ucp1* expression 75-fold in the vehicle control group and was completely abolished in the presence of the pan-FGFR inhibitor LY2874455 (**Fig. 14A**). FGF signaling remained unchanged in the presence of four out of seven inhibitors (TAK632, SB2020190, Wortmannin, Bisindoylmaleimide I) (**Fig. 14A**). One inhibitor (SH-4-54) moderately amplified the effect of FGF8b on *Ucp1* expression above control values and two inhibitors (Trametinib, SCH772984) abrogated FGF8b induced *Ucp1* expression entirely (**Fig. 14A**). These data demonstrated that FGF8b signaled via a MAPK pathway-dependent MEK1/2-ERK1/2 axis to control *Ucp1* expression. Nuclear receptors are direct transcriptional regulators downstream of signaling pathways and control gene expression. Peroxisome proliferator-activated receptors (PPARs) regulate brown adipocyte differentiation. The role of PPARs as nuclear effectors downstream of the MAPK pathway was investigated. Brown preadipocytes were treated with FGF8b and antagonists for

PPARα, PPARβ/δ and PPARγ. Surprisingly, FGF8b induced *Ucp1* expression remained unaffected in each case (**Fig. 14B**).

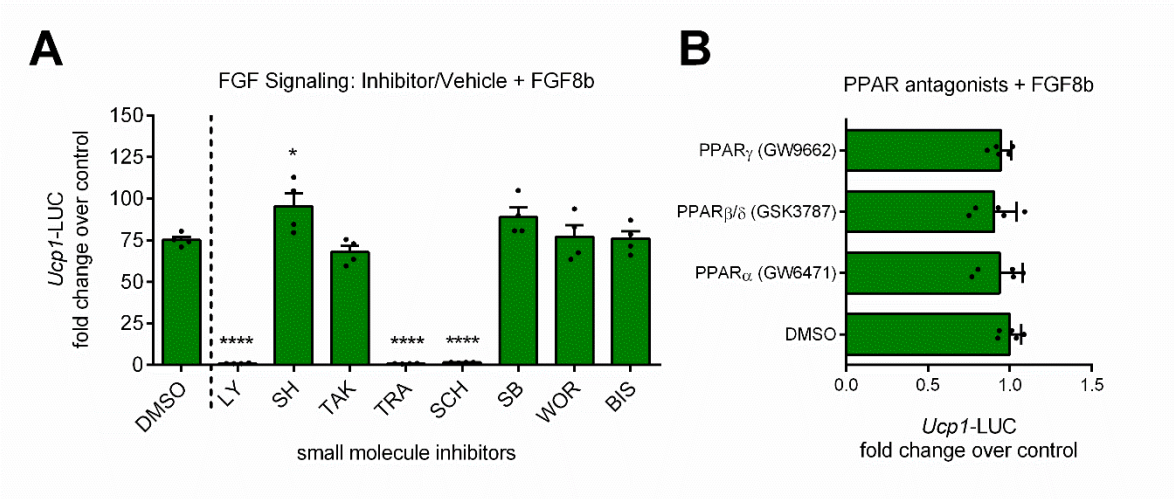

Figure 14. FGF8b signals via a MEK1/2-ERK1/2 axis, independent of PPARs. (**A**) luciferase activity linked *Ucp1* expression (*Ucp1*-LUC) in brown preadipocytes treated with 125 ng/ml FGF8b and 250 nM of the following inhibitors (abbreviation, target) for 48 h: LY2874455 (LY, pan-FGFR), SH-4-54 (SH, Stat3,5), TAK632 (TAK, pan-RAF), Trametinib (TRA, MEK1/2), SCH772984 (SCH, ERK1/2),SB2020190 (SB, p38MAPK), Wortmannin (WOR, PI3K), Bisindoylmaleimide I (BIS, PKC), N=4 for each group. (**B**) luciferase activity linked *Ucp1* expression (*Ucp1*-LUC) in brown preadipocytes treated with 125 ng/ml FGF8b and one of the following inhibitors (target) for 48 h: GW6471 (PPARα), GSK3787 (PPARβ/δ), GW9662 (PPARγ), N=5 for each group. Data were normalized to inhibitor treatment control in panel A and B. All experiments were carried out in the presence of 1 µg/ml heparin. One-way ANOVA in A and B. Statistically significant results were indicated with asterisks: * = $p < 0.05$. ** = $p < 0.01$, *** = $p < 0.001$, **** = $p < 0.0001$.

Taken together, these data delineated a clear route of the FGF signal transduction from the receptor level to the downstream effectors involving a FGFR1-MEK1/2-ERK1/2 axis, which indicated activation of the RAS-MAPK pathway (**Fig. 15**). Furthermore, control over *Ucp1* expression in brown preadipocytes occurred independent of canonical PPAR signaling, which suggested that non-canonical transcriptional regulators were involved instead.

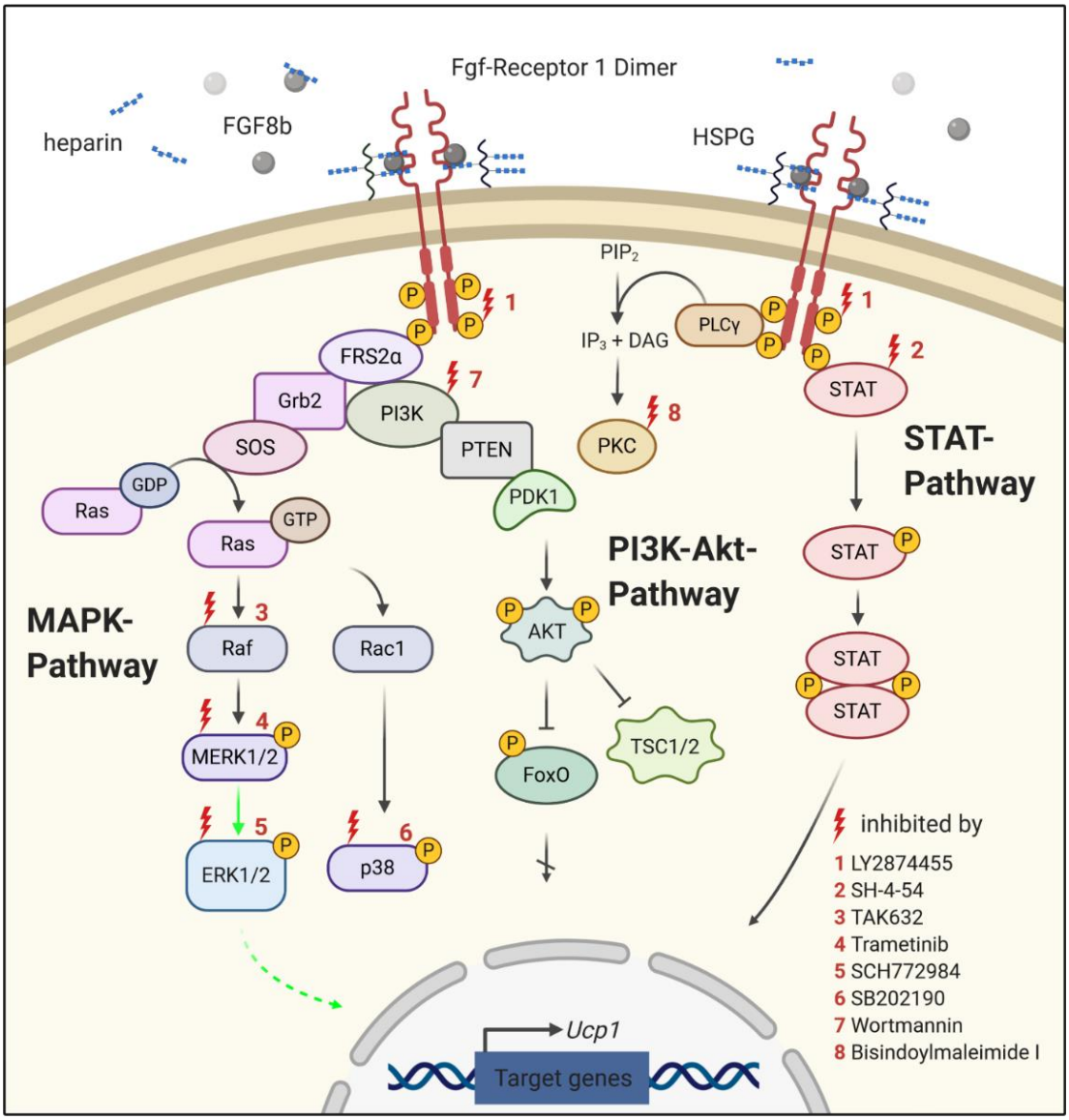

Figure 15. The FGF signaling pathway in control of *Ucp1*. The FGF signaling pathway is activated by formation of the ternary FGF8b/FGFR1-cofactor complex. Heparin or heparan sulfate proteoglycans (HSPG) serve as cofactors in FGF signaling. FGF signaling is initiated by receptor dimerization and autophosphorylation of the intracellular receptor tyrosine kinase domains, which results in activation of several signaling branches such as RAS-MAPK, PI3K-AKT, STAT and PLCγ-PKC. Individual branches of FGF signaling were targeted with small molecule inhibitors. These inhibitors were (abbreviation + target) used: (1) LY2874455 (LY, pan-FGFR), (2) SH-4-54 (SH, Stat3,5), (3) TAK632(TAK, pan-RAF), (4) Trametinib (TRA, MEK1/2), (5) SCH772984(SCH, ERK1/2), (6) SB2020190 (SB, p38MAPK), (7) Wortmannin (WOR, PI3K), (8) Bisindoylmaleimide I (BIS, PKC). Target proteins are indicated with a red bolt. Green arrows indicate the experimentally established molecular axis, which mediated FGF8b induced *Ucp1* expression. Figure was created with biorender.com.

2.7 Prostaglandin metabolism is coordinately upregulated by FGF8b.

The impact of FGF8b on prostaglandin metabolism was investigated based on the observed upregulation of *Ptgs2* in the transcriptomic data. Expression levels of several other genes involved in prostaglandin metabolism including *Pla2g4a*, *Ptgs1*, *Ptges1* and *Slco2a1* were significantly upregulated upon FGF8b treatment (**Fig. 16A**). Inhibition of PTGS1 and PTGS2 by non-selective PTGS inhibitors diclofenac and indomethacin partially blunted, while selective PTGS2 inhibitor celecoxib completely abolished FGF8b induced *Ucp1* expression (**Fig. 16B**), demonstrating that the molecular mechanism underlying FGF8b induced *Ucp1* expression was PTGS2-dependent. The prostaglandin biosynthetic pathway gives rise to a multitude of arachidonic acid derived lipid mediators. LC-MS/MS based measurements were

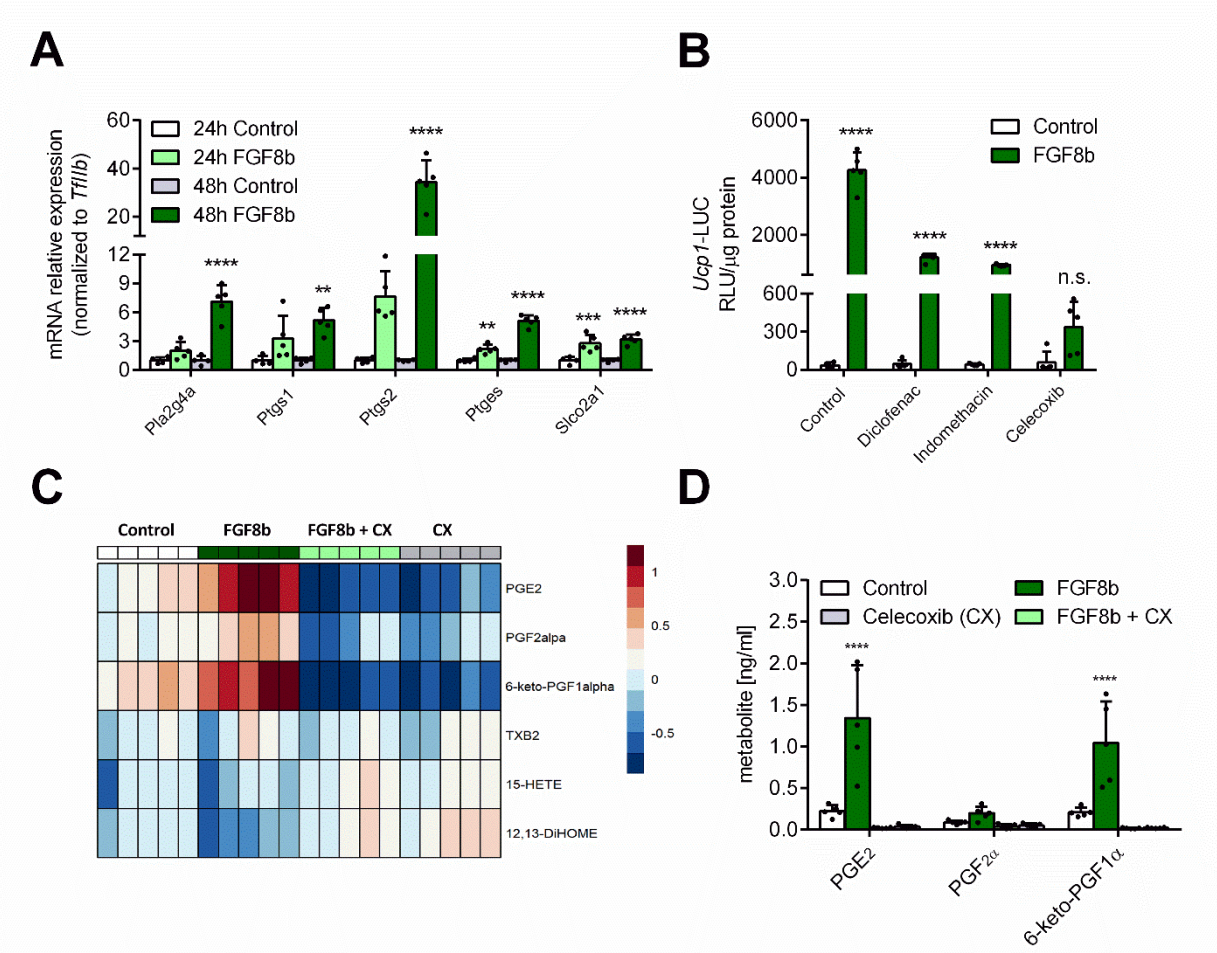

Figure 16. FGF8b coordinately upregulates prostaglandin metabolism. (**A**) mRNA expression of genes involved in prostaglandin metabolism in brown preadipocytes treated with 125 ng/ml FGF8b for 24 and 48 h (N=5 for each group). (**B**) luciferase activity linked *Ucp1* expression (*Ucp1*-LUC) in FGF8b treated brown preadipocytes upon inhibition of prostaglandin endoperoxidase synthase (PTGS) 1 and 2 by unselective inhibitor diclofenac (20 µM), indomethacin (125 µM), and selective PTGS2 inhibitor celecoxib (20 µM) for 48 h (N=5 for each group). (**C-D**) LC-MS/MS measurements of oxylipin species in FGF8b conditioned media of brown preadipocytes treated with or without celecoxib (20 µM) for 48 h (N=5 for each group). Scale in C represents $\log_{10}$ transformed metabolite concentrations in pg/ml and are centered around the mean. All experiments were carried out in the presence of 1 µg/ml heparin. Two-way ANOVA in A, B and D. Statistically significant results were indicated with asterisks: * = $p < 0.05$. ** = $p < 0.01$, *** = $p < 0.001$, **** = $p < 0.0001$.

performed with the aim to identify potential candidate compounds that were causally involved in controlling *Ucp1* expression by FGF8b. Brown preadipocytes were treated with either FGF8b, celecoxib or a combination of both substances for 48 h. Conditioned media was collected and assayed for 52 lipid mediators. Six oxylipin species were robustly detectable and passed internal quality control (**Fig. 16C**). The candidates with the most promising profiles were prostaglandin E_2 (PGE_2) and 6-keto-$PGF_{1\alpha}$, a degradation product of prostaglandin I_2 (PGI_2). Both metabolites were selected for further investigations due to their high abundance in cell culture supernatant, strong responsiveness to both FGF8b and celecoxib treatment, and overall correlation to *Ucp1* expression.

2.8 The PGE_2 biosynthetic pathway controls *Ucp1* expression.

The role of the prostaglandin biosynthetic pathway was validated by inhibition of the PGE_2 synthesizing enzyme PTGES1 with two different inhibitors CAY10678 and CAY10526. PTGES1 inhibition strongly blunted FGF8b induced *Ucp1* expression in brown preadipocytes by single inhibitor treatment and more effectively when both inhibitors were combined (**Fig. 17A**). These data were confirmed using a gene silencing approach of *Ptges1*, which significantly reduced both the induction of *Ucp1* in preadipocytes by FGF8b and PGE_2 levels in cell media (**Fig. 17C-D**). Inhibition of the PGI_2 producing enzyme PTGIS, on the other hand, did not impair FGF8b induced *Ucp1* expression, despite robustly reducing 6-keto-$PGF_{1\alpha}$ concentrations (**Fig. E-F**). The temporal sequence between rising PGE_2 levels in relation to the induction of *Ucp1* was resolved to establish causality. Upon treatment with FGF8b, PGE_2 levels increased rapidly within hours (**Fig. 17G**), peaking at around 24 h, while *Ucp1* followed with a delay of approximately 24 h (**Fig. 17H**). Thus, PGE_2 production preceded *Ucp1* induction, lending further support for a causal role of PGE_2. Whether PGE_2 alone would be sufficient to upregulate *Ucp1* in preadipocytes was subsequently examined. Incubation of brown preadipocytes with high micromolar concentrations of PGE_2 for 8 and 48 h revealed a significant 8-fold increase after 8 h, but not 48 h (**Fig. 17I**), indicating that PGE_2 was able to elicit a moderate, albeit transient effect on *Ucp1* expression. Taken together, FGF8b treatment induced a broad upregulation of genes involved in prostaglandin metabolism, and FGF8b induced *Ucp1* expression was shown to be controlled in a PTGS2 and PTGES1-dependent manner. The product of the sequential action of PTGS2-PTGES1 catalyzed reactions, PGE_2, was identified as an abundant FGF8b-responsive lipid mediator, which was able to rapidly induce *Ucp1*

expression in preadipocytes in a transient manner. Thus, the transcriptional regulation of *Ucp1* by FGF8b required a mechanism involving the PGE_2 biosynthetic pathway.

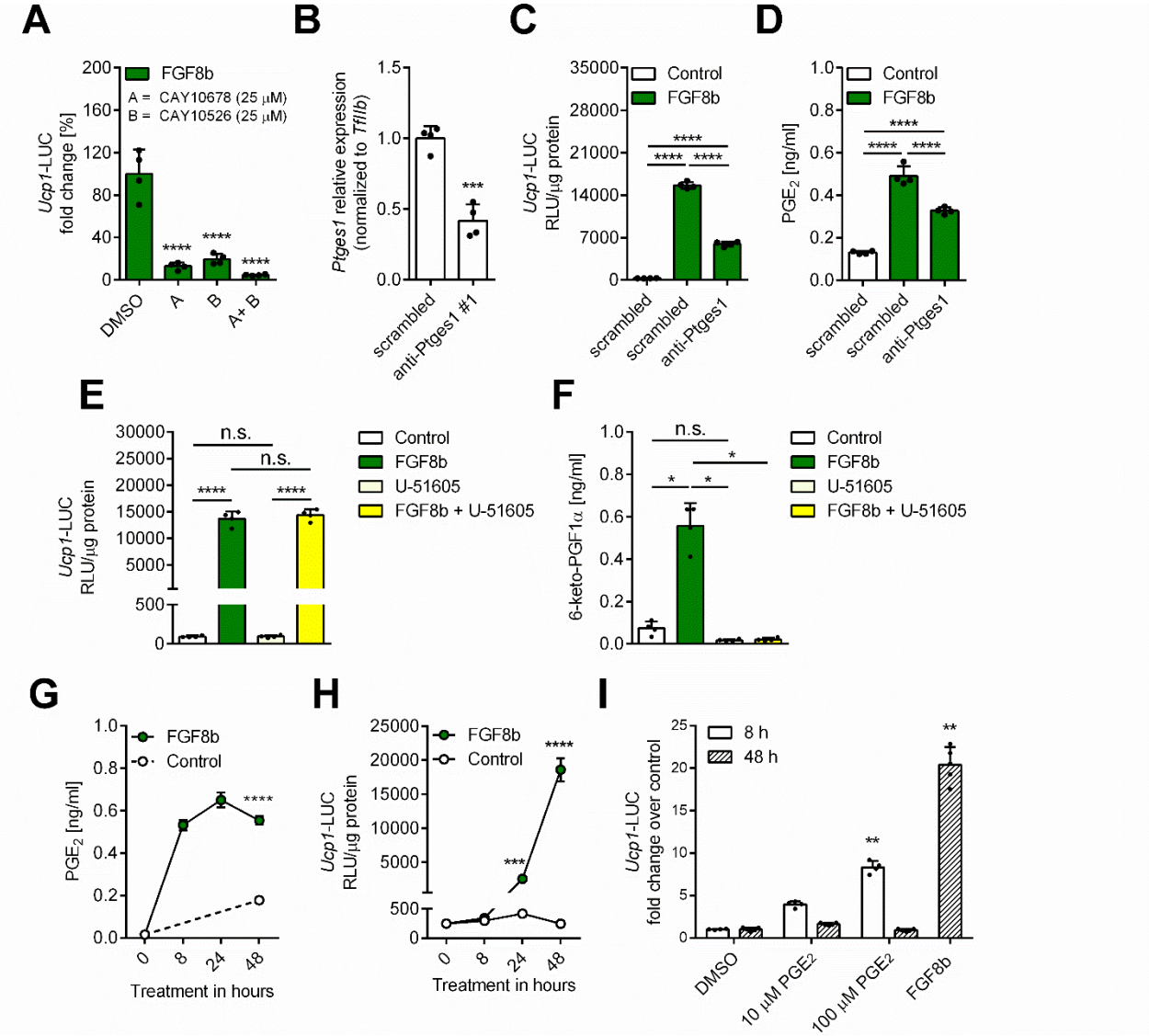

Figure 17. FG8b induces PGE_2 biosynthesis to control *Ucp1* expression. (**A**) luciferase activity linked *Ucp1* expression (*Ucp1*-LUC) upon PTGES1 inhibition by CAY10678 and/or CAY10526 (25 μM each) in brown preadipocytes treated with FGF8b for 48 h (N=4 for each group). (**B**) *Ptges1* mRNA expression upon *Ptges1* knockdown in brown preadipocytes, 48 h post-transfection (N=4 for each group). (**C**) luciferase activity linked *Ucp1* expression (*Ucp1*-LUC) in FGF8b treated brown preadipocytes upon *Ptges1* knockdown (N=4 for each group). (**D**) PGE_2 levels in media of FGF8b treated brown preadipocytes (N=4 for each group). (**E**) luciferase activity linked *Ucp1* expression (*Ucp1*-LUC) upon PTGIS inhibition by U-51605 (25 μM) in brown preadipocytes treated with FGF8b for 48 h (N=4 for each group). (**F**) 6-keto-$PGF_{1\alpha}$ levels in media of FGF8b/U-51605 treated brown preadipocytes (N=4 for each group). (**G**) PGE_2 levels in media and (**H**) luciferase activity linked *Ucp1* expression (*Ucp1*-LUC) in FGF8b treated brown preadipocytes over 48 h (N=4 for each group). (**I**) Stimulation of brown preadipocytes with 10 and 100 μM PGE_2 for 8 and 48 h (N=4-5 for each group). All experiments were carried out in the presence of 1 μg/ml heparin. One-way ANOVA in A, C, D, two-way ANOVA in F and H, Student's t test in B and G (for timepoint 48 h only) and Kruskal-Wallis test in I for each treatment duration. Statistically significant results were indicated with asterisks: * = $p < 0.05$. ** = $p < 0.01$, *** = $p < 0.001$, **** = $p < 0.0001$.

2.9 The glycolytic pathway is upregulated by FGF8b.

The impact of FGF8b on glucose metabolism was investigated based on the observed enrichment of the glycolytic pathway in the transcriptomic data. On the level of individual genes an induction upon FGF8b treatment was observed for *Slc2a1*, *Hk2*, *Gpi1*, *Pfkl*, *Aldoa*, *Tpi1*, *Eno1*, *Pkm* and *Ldha* (**Fig. 18A**), highlighting the coordinated activation of the glycolytic pathway. Preadipocytes treated with increasing concentrations of FGF8b were functionally evaluated in terms of metabolic activity and proton production capacity. Preadipocytes treated with FGF8b demonstrated a dose-dependent increase in oxygen consumption and extracellular acidification (**Fig. 18B-C**), possibly to some extent driven by the mitogenic effect of FGF8b. Maximal glycolytic capacity as assessed by proton production rates after the addition of FCCP and monensin were dose-dependently increased by FGF8b (**Fig. 18D**). Notably, the calculated proton production rate already accounted for the generation of protons by respiration and was normalized to the protein content of the well to control for

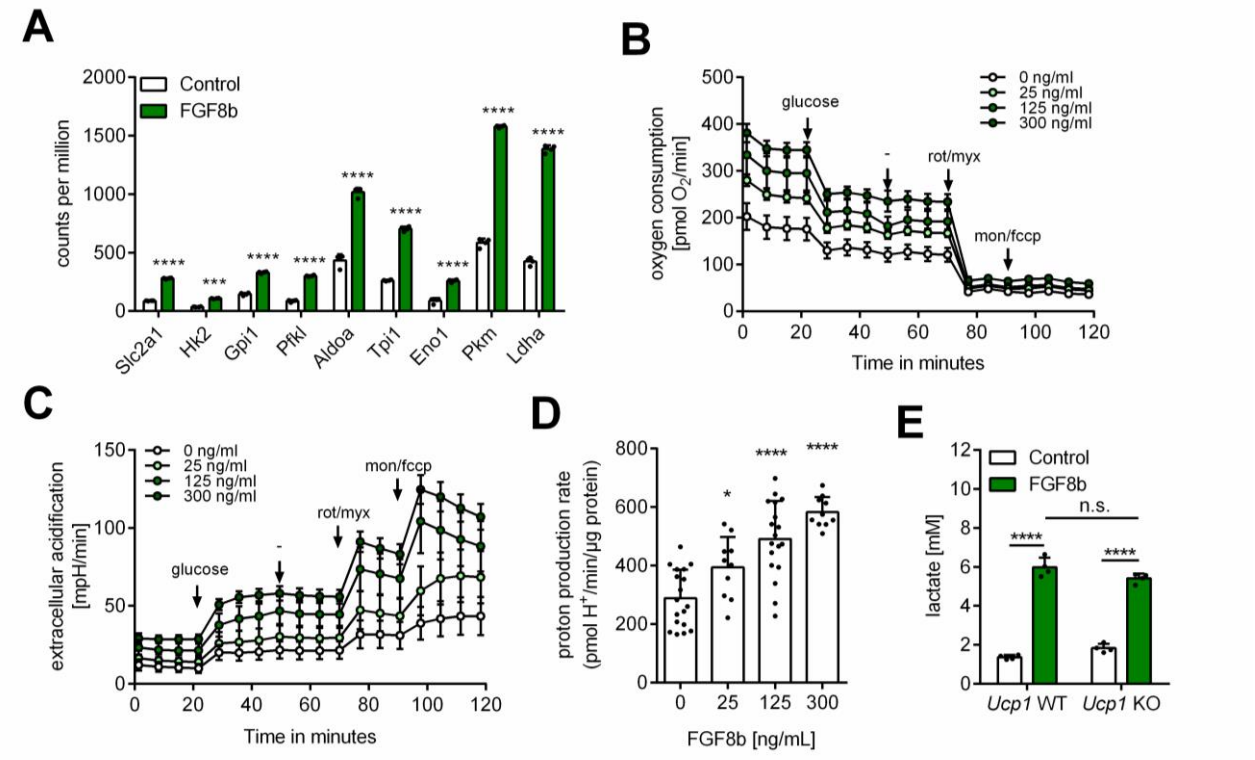

Figure 18. Glycolysis is activated in preadipocytes treated with FGF8b. (**A**) Expression data of glycolyic genes from the first RNA sequencing experiment in counts per million in brown preadipocytes treated with FGF8b (N=4 for eah group). (**B**) oxygen consumption rate in pmol O_2/min and (**C**) extracellular acidification rate in mpH/min in brown preadipocytes treated with 25, 125 and 300 ng/l FGF8b for 48 h on collagen coated 96-well plate on a XF96 flux analyzer (N=10-18 for each group). (**D**) glycolytic proton production rate in pmol H^+/min/µg protein in brown preadipocytes treated with 25, 125 and 300 ng/l FGF8b for 48 h, normalized to protein concentration (N=10-18 for each group). Injections A: 25 mM glucose, B: media, C: 1 µM rotenone, 1 µM myxothiazol, D: 400 µM monensin, 2 µM FCCP. (**E**) lactate levels in FGF8b treated preadipocytes from wild-type and *Ucp1*-knock-out mice (N=4 for each group). All experiments were carried out in the presence of 1 µg/ml heparin. Multiple Student's t test with Bonferroni correction in A, one-way ANOVA in D and two-way ANOVA in E. Statistically significant results were indicated with asterisks: * = $p < 0.05$. ** = $p < 0.01$, *** = $p < 0.001$, **** = $p < 0.0001$.

differences in cell number. The glycolytic phenotype, as assessed by lactate release into media, did not require the presence of *Ucp1* in brown preadipocytes as genotype comparisons showed (**Fig. 18E**). Thus, FGF8b induced a coordinated upregulation of glycolysis and rendered preadipocytes pro-glycolytic on a functional level, but *Ucp1* itself was not required to function as a glucose sink.

2.10 FGF8b stimulates glucose uptake and lactate release in preadipocytes.

Enhanced glucose catabolism requires higher rates of glucose uptake. Glucose uptake capacity was assayed in brown preadipocytes treated with increasing concentrations of FGF8b. The proportion of uptake mediated by the most abundant glucose transporter in preadipocytes, glucose transporter 1 (SLC2A1), was assessed by employing the SLC2A1 inhibitor BAY-876. Glucose uptake was dose-dependently increased up to 6-fold with FGF8b treatment and was completely blunted by BAY-876 (**Fig. 19A**), suggesting that SLC2A1 was the dominant glucose transporter in brown preadipocytes. The IC_{50} value of BAY-876 was subsequently determined to be in the low micromolar range (**Fig. 19B**). Another key feature of highly glycolytic cells is lactate production. Lactate accumulation over time was therefore evaluated following a single dose of FGF8b in brown preadipocytes. Lactate levels in cell culture supernatant continuously increased over a time span of 96 h in both control and treatment groups (**Fig. 19C**). Culture media of cells stimulated with FGF8b accumulated 5 mM of lactate, while the control group only accumulated 2 mM in the same time period (**Fig. 19C**). These data showed that FGF8b increased glucose uptake and lactate release.

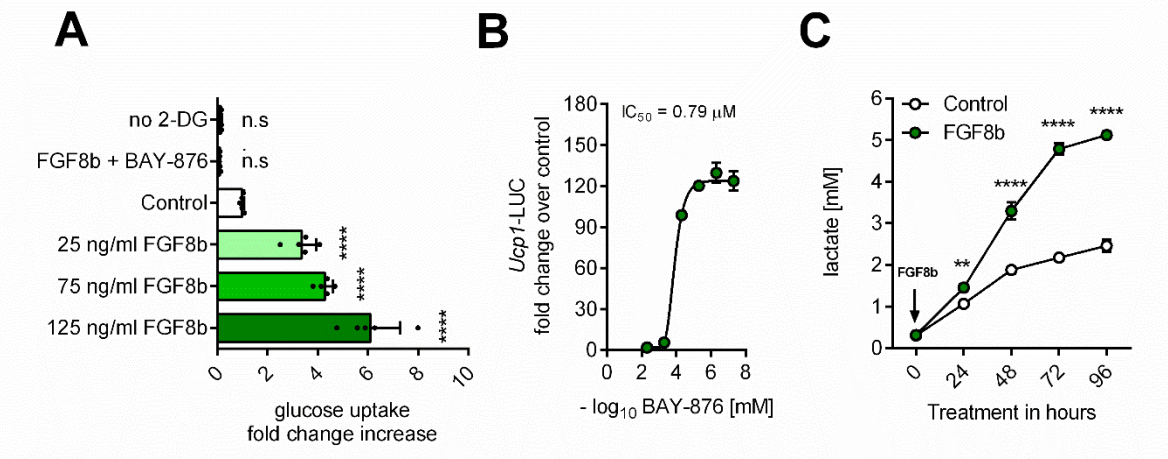

Figure 19. FGF8b stimulates glucose uptake and lactate release. (**A**) glucose uptake assay with 2.5 mM 2-deoxy-D-glucose (2-DG) in brown preadipocytes treated with 25, 75 and 125 ng/ml FGF8b. Negative controls included stimulation with 10 µM BAY-876 during uptake and a no 2-deoxy-D-glucose (2-DG) condition (N=4 for each group). (**B**) Dose-response curve between SLC2A1 inhibitor BAY-876 and FGF8b induced *Ucp1* expression in brown preadipocytes (N=3 for each group (**C**) lactate in cell culture media upon a single dose of 125 ng/ml FGF8b over a time course of 96 h without media exchange (N=3 for each group). All experiments were carried out in the presence of 1 µg/ml heparin. One-way ANOVA in B and two-way ANOVA in C. Statistically significant results were indicated with asterisks: * = $p < 0.05$. ** = $p < 0.01$, *** = $p < 0.001$, **** = $p < 0.0001$.

Additionally, experiments employing the specific glucose transporter 1 inhibitor BAY-876 demonstrated that FGF8b induced *Ucp1* expression required SLC2A1 mediated glucose uptake.

2.11 FGF8b induced *Ucp1* expression requires glycolytic flux.

FGF8b induced glycolysis in brown preadipocytes, but whether glycolytic flux *per se* was a requirement for the induction of *Ucp1* remained unclear. Glycolytic flux was manipulated based on two different strategies. Firstly, glucose levels in cell culture media were controlled to represent groups with low, intermediate and high levels of glucose. Secondly, glycolytic flux was slowed down by 2-deoxy-D-glucose (2-DG) treatment of preadipocytes. In addition, inhibition of glucose uptake by BAY-876 was used as a positive intervention control. Inhibition of glycolytic flux resulted in significant reductions in FGF8b induced *Ucp1* expression (**Fig. 20A**). Lactate levels were drastically reduced in each of these experiments validating the successful inhibition of glycolytic flux (**Fig. 20B**). Taken together, these data demonstrated that the activation of glycolysis in preadipocytes was required for the induction of *Ucp1* gene expression.

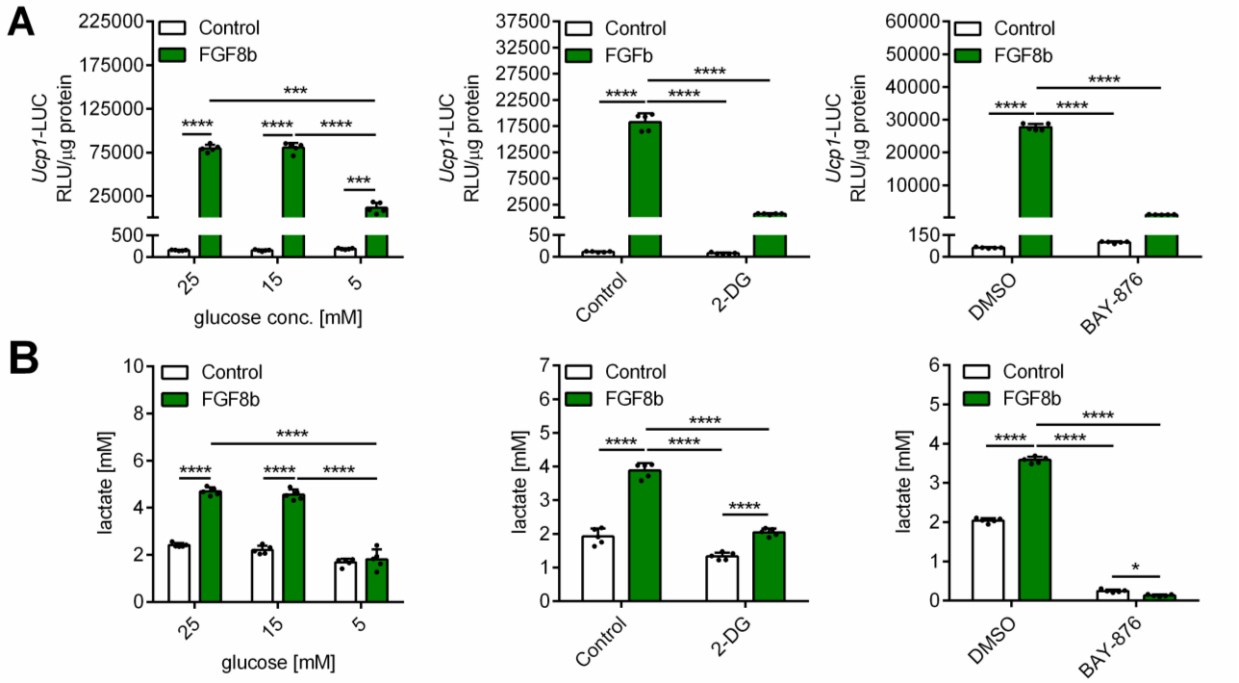

Figure 20. FGF8b induced *Ucp1* expression requires glycolytic flux. (**A**) luciferase activity linked *Ucp1* expression (*Ucp1*-LUC) and (**B**) in FGF8b treated brown preadipocytes depending on (from left to right) glucose levels in cell media, glucose uptake inhibition by 2 µM BAY-876, inhibition of the glycolytic pathway by 2.5 mM 2-deoxy-D-glucose (2-DG), N=5 for each group. All experiments were carried out in the presence of 1 µg/ml heparin. Two-way ANOVA in A and B. Statistically significant results were indicated with asterisks: * = $p < 0.05$. ** = $p < 0.01$, *** = $p < 0.001$, **** = $p < 0.0001$.

2.12 Endogenous lactate is not required for FGF8b induced *Ucp1* expression.

The catabolic product of the glycolytic pathway lactate regulates *Ucp1* expression in white adipocytes (Carrière *et al*, 2014). Interestingly, lactate levels in brown preadipocytes treated with the signaling inhibitors (**Table. 1**), used previously, correlated with the induction of *Ucp1* by FGF8b (**Fig. 21A**). The ability of exogenously and endogenously produced lactate to control or modulate FGF8b induced *Ucp1* expression in preadipocytes was studied. In fact, *Ucp1* expression increased dose-dependently when exogenous lactate was added to FGF8b treated preadipocytes (**Fig. 21B**), but not when lactate was added to untreated preadipocytes (**Fig. 21C**). However, inhibition of endogenous lactate production by the lactate dehydrogenase inhibitor sodium oxamate in FGF8b treated preadipocytes resulted in no changes in *Ucp1*

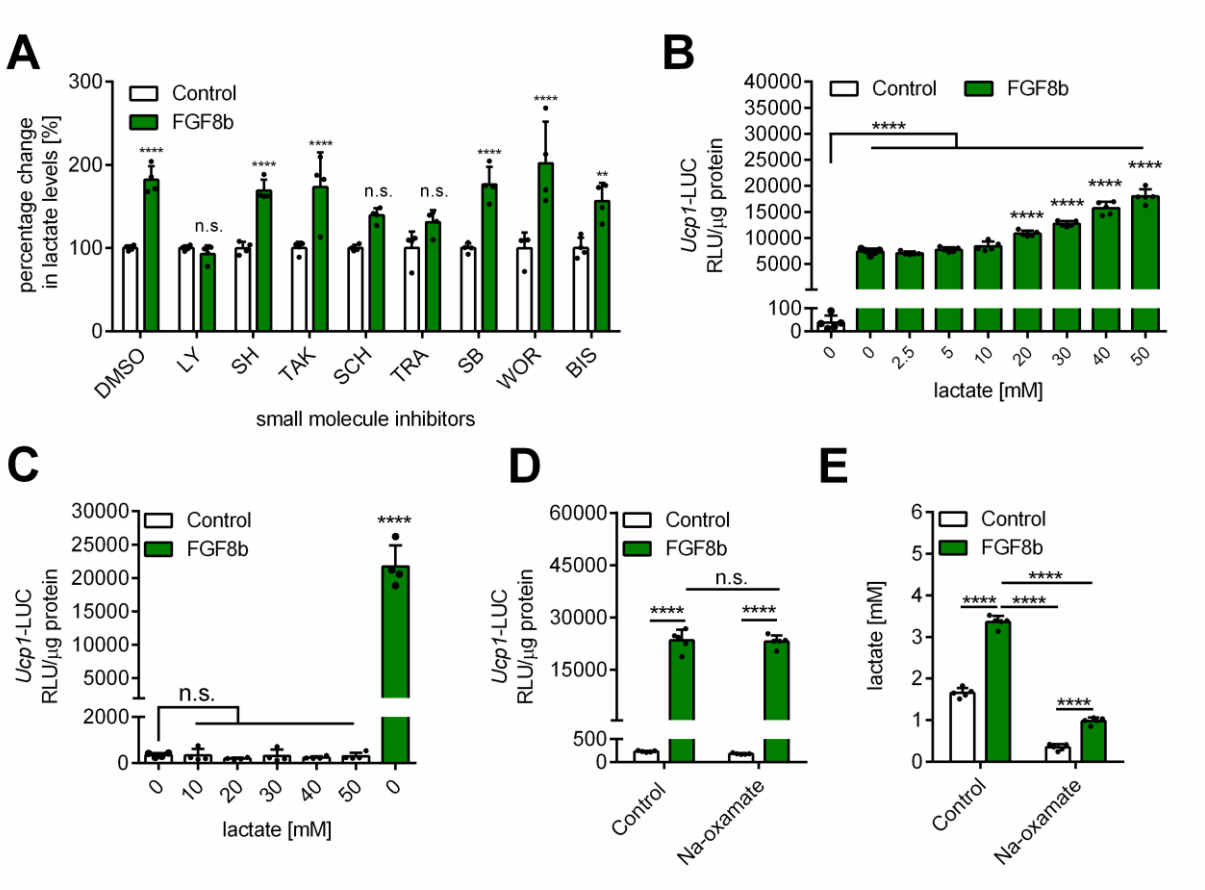

Figure 21. Lactate is not required for FGF8b induced *Ucp1* induction. (**A**) effect of small molecule inhibitors on lactate levels in brown preadipocytes treated with FGF8b (N=4 for each group). Inhibitor (abbreviation, target): LY2874455 (LY, pan-FGFR), SH-4-54 (SH, Stat3, 5), TAK632 (TAK, pan-RAF), Trametinib (TRA, MEK1/2), SCH772984 (SCH, ERK1/2), SB2020190 (SB, p38MAPK), Wortmannin (WOR, PI3K), Bisindoylmaleimide I (BIS, PKC). (**B-C**) luciferase activity linked *Ucp1* expression (*Ucp1*-LUC) in brown preadipocytes with or without FGF8b treatment, incubated with increasing concentrations of lactate (2.5-50 mM) for 48 h (N=4 for each group). (**C**) lactate levels and (**E**) luciferase activity linked *Ucp1* expression (*Ucp1*-LUC) in FGF8b treated brown preadipocytes incubated with lactate dehydrogenase inhibitor sodium oxamate (20 mM) for 48 h (N=5 for each group). One-way ANOVA in A, B and two-way ANOVA in A, D and E. All experiments were carried out in the presence of 1 µg/ml heparin. Two-way ANOVA in A and B. Statistically significant results were indicated with asterisks: * = $p < 0.05$. ** = $p < 0.01$, *** = $p < 0.001$, **** = $p < 0.0001$.

induction (**Fig. 21D**), despite effectively preventing a rise in lactate levels in cell media upon FGF8b treatment (**Fig. 21E**). Thus, lactate metabolism was not required for the upregulation of *Ucp1* by FGF8b and did not mediate the effects of glycolytic flux on *Ucp1* expression.

2.13 Glycolytic flux does not control PGE_2 biosynthesis.

Glycolytic flux and PGE_2 biosynthesis were independently demonstrated to regulate FGF8b induced *Ucp1* expression in preadipocytes. A potential link between these two metabolic pathways was studied. PGE_2 measurements were performed in cell culture supernatant of brown preadipocytes treated with FGF8b and BAY-876. Interestingly, impeding glycolytic flux did not reduce PGE_2 concentrations in FGF8b conditioned media (**Fig. 22A**). On the contrary, inhibition of glucose uptake appeared to stimulate the prostaglandin biosynthetic pathway in preadipocytes (**Fig. 22A**), which was corroborated by increased transcript levels of *Pla2g4a*, *Ptgs1* and *Ptgs2* (**Fig. 22B**). These data demonstrated an interaction between glucose and prostaglandin metabolism, providing evidence that PGE_2 alone was not sufficient to fully induce *Ucp1* expression without high glycolytic flux.

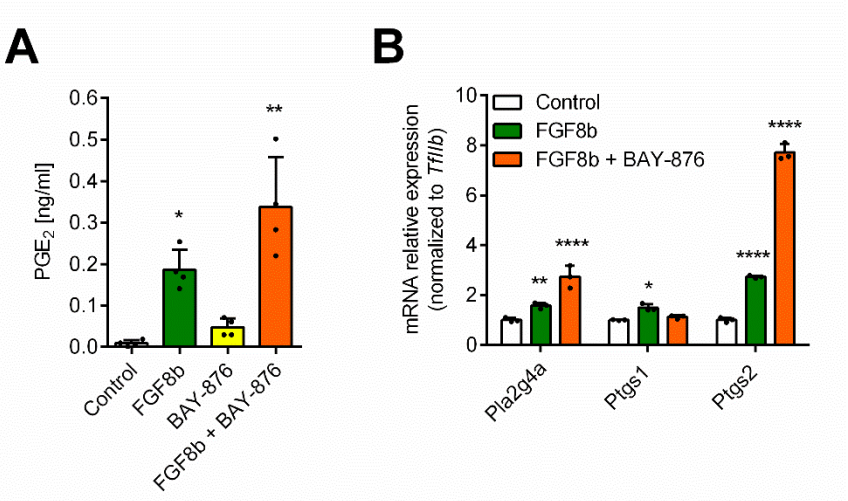

Figure 22. Inhibiting glycolytic flux does not abolish PGE_2 biosynthesis. (**A**) PGE_2 levels in media of brown preadipocytes treated with 125 ng/ FGF8b, 2 µM BAY-876, or a combination of both (N=4 for each group). (**B**) Relative mRNA expression of prostaglandin metabolism related genes in brown preadipocytes treated with FGF8b with and without 2 µM BAY-876 (N=3 for each group). All experiments were carried out in the presence of 1 µg/ml heparin. Kruskal-Wallis test in A, two-way ANOVA in B. Statistically significant results were indicated with asterisks: * = $p < 0.05$. ** = $p < 0.01$, *** = $p < 0.001$, **** = $p < 0.0001$.

2.14 FGF1 fails to induce glycolytic flux and *Ucp1* expression.

Given the important interplay between glucose and prostaglandin metabolism in controlling *Ucp1* gene expression, the hypothesis was tested that the lack of effectiveness of FGF1 to upregulate *Ucp1*, as presented earlier (**Fig. 11**), was linked to either a failed induction of glycolysis or PGE_2 biosynthesis. Treatment of brown preadipocytes with both FGF8b and FGF1 increased PGE_2 levels in cell culture media to similar degrees (**Fig. 23A**) and the upregulation of the key enzyme *Ptgs2* was fully intact in FGF1 treated preadipocytes (**Fig. 23B**). Thus, FGF1 and FGF8b evoked the same activation of the prostaglandin biosynthetic pathway. Glucose uptake capacity, on the other hand, was much lower in FGF1 than in FGF8b treated preadipocytes (**Fig.**

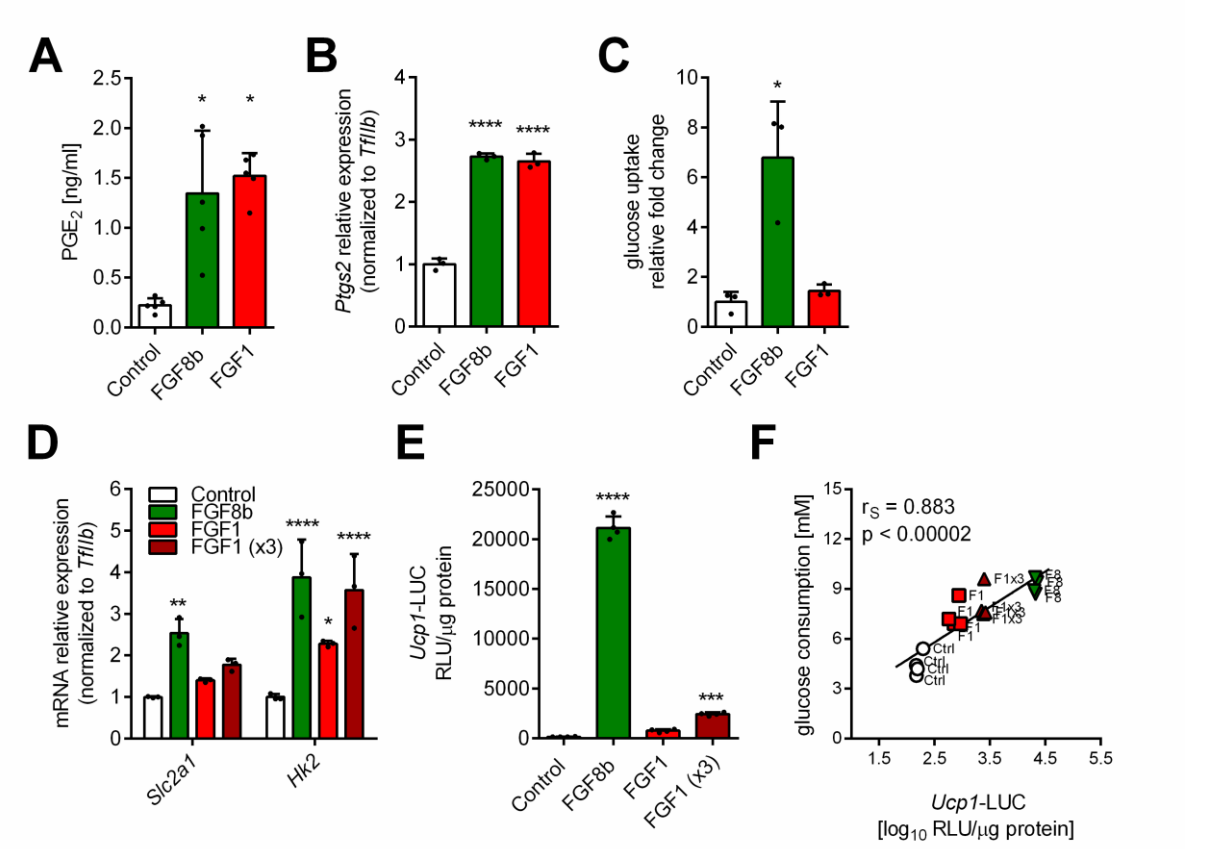

Figure 23. The glycolytic effect of FGFs correlate with *Ucp1* induction. (**A**) PGE_2 levels in media and (**B**) *Ptgs2* mRNA expression in brown preadipocytes treated with 5.55 nM FGF8b and 5.55 nM FGF1 (N=5 for each group in PGE_2 data, N=3 for each group in *Ptgs2* data). (**C**) relative fold change in glucose uptake of brown preadipocytes (129S) treated with 5.55 nM FGF8b and 5.55 nM FGF1 (N=3 for each group). (**D**) Relative mRNA expression of *Slc2a1* and *Hk2* and (**E**) luciferase linked *Ucp1* expression (*Ucp1*-LUC) in brown preadipocytes treated with 5.55 nM FGF8b, 5.55 nM FGF1 and 16.5 nM FGF1 (FGF1x3) for 48 h (N=3 for each group in *Slc2a1*/*Hk2* data, N=4 for each group in *Ucp1*-LUC data). (**F**) Spearman correlation between glucose consumption and luciferase linked *Ucp1* expression (*Ucp1*-LUC) in brown preadipocytes treated with 5.55 nM FGF8b, 5.55 nM FGF1 and 16.5 nM FGF1 (FGF1x3) for 48 h (N=4 for each group). Kruskal-Wallis test in A and C, one-way ANOVA in B and E, two-way ANOVA in D. All experiments were carried out in the presence of 1 µg/ml heparin. Kruskal-Wallis test in A, two-way ANOVA in B. Statistically significant results were indicated with asterisks: * = $p < 0.05$. ** = $p < 0.01$, *** = $p < 0.001$, **** = $p < 0.0001$.

23C). In fact, FGF1 did not enhance glucose uptake above control levels (**Fig. 23C**). In addition, transcript levels of genes essential for high glycolytic flux such as *Slc2a1* and *Hk2* were much lower expressed in FGF1 than in FGF8b treated preadipocytes, but higher concentrations of FGF1 (16.5 nM) reduced the difference to the FGF8b group (**Fig. 23D**). These data clearly illustrated a dose-dependent effect of FGF1 on glycolytic genes, which was reminiscent of the dose-dependency observed for FGF1 induced *Ucp1* expression (**Fig. 23E**). In fact, when glucose consumption was plotted against *Ucp1* expression from preadipocytes treated with either FGF8b or FGF1, a high correlation (r = 0.883) was observed (**Fig. 23F**). Taken together, it was demonstrated that co-regulation of the prostaglandin biosynthetic pathway and glycolysis were required events and failure to activate one or the other prevented the maximal induction of *Ucp1* in preadipocytes.

2.15 FGF8b and FGF9 induce highly similar molecular signatures.

Two metabolic pathways, PGE_2 biosynthesis and glycolysis, were identified as metabolic regulators of FGF8b induced *Ucp1* expression in preadipocytes. The underlying transcriptional regulators, however, particularly those which were able to explain the discrepancy between the effects of FGF1 and FGF8b on *Ucp1* expression, remained unidentified. A second RNA sequencing experiment was performed comparing the effects of three different paracrine FGFs, FGF1, FGF8b and FGF9 on the transcriptome of brown preadipocytes. In addition, the effect of low glycolytic flux in FGF8b treated preadipocytes was studied by including a group co-treated with the glucose transporter inhibitor BAY-876.

The principal components of the transcriptomic data was analyzed and revealed extremely high similarities in gene expression signatures between FGF8b and FGF9 groups (**Fig. 24A**). Moreover, gene expression changes induced by FGF1 were found to be more similar to the control group than to any other group (**Fig. 24A**). On the level of *Ucp1* expression, treatments elicited the expected effects. While FGF8b and FGF9 strongly induced transcription of *Ucp1*, FGF8b + BAY-876 co-treatment led to a mild and FGF1 to no induction of *Ucp1* (**Fig. 24B**). Since FGF8b and FGF9 induced molecular signatures, which were virtually identical, and both upregulated *Ucp1*, the expression level of a ternary transcriptional complex, recently implicated in FGF9 induced *Ucp1* expression in preadipocytes (Shamsi *et al*, 2020), was evaluated. Three proteins are part of the transcriptional complex: estrogen-related receptor α (*Esrra*), flightless-1 (*Flii*) and leucine-rich-repeat-(in Flii)-interacting-protein-1 (*Lrrfip1*). While

Esrra and *Flii* expression levels in brown preadipocytes were not different between FGF1, FGF8b and FGF9 treatment groups, *Lrrfip1* expression correlated well with *Ucp1* expression between these three FGFs (**Fig. 24C**).

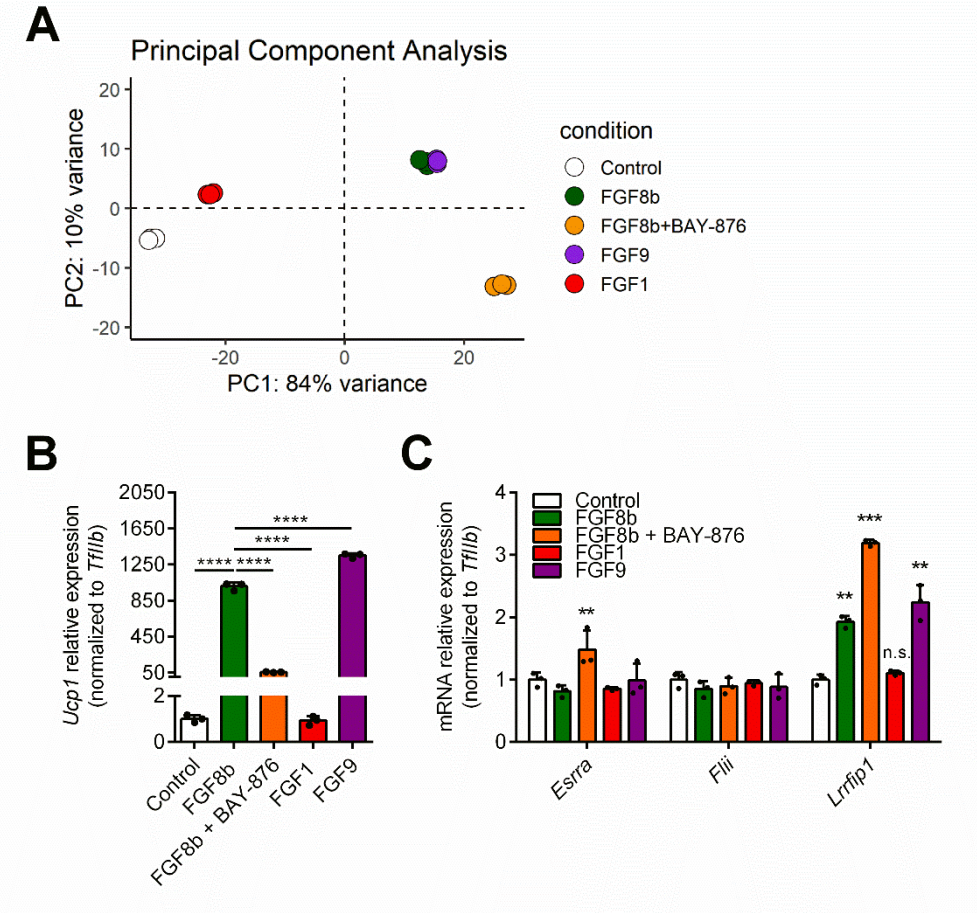

Figure 24. FGF8b and FGF9 induce highly similar expression changes. (**A**) principal component analysis of expression patterns and (**B-C**) mRNA expression of *Ucp1*, *Esrra*, *Flii* and *Lrrfip1* induced by treatment of brown preadipocytes (129S) with 5.55 nM FGF1, 5.55 nM FGF8b ± 2 µM BAY-876 and 5.55 nM FGF9 (N=3 for each group). All experiments were carried out in the presence of 1 µg/ml heparin. One-way ANOVA in B and two-way ANOVA in C. Statistically significant results were indicated with asterisks: * = $p < 0.05$. ** = $p < 0.01$, *** = $p < 0.001$, **** = $p < 0.0001$.

2.16 *Hes1* is required for the induction of *Ucp1* by FGF8b.

Both *Lrrfip1* and *Esrra* have been shown to be required for FGF9 induced *Ucp1* expression in preadipocytes (Shamsi *et al*, 2020). Gene silencing of *Lrrfip1* in FGF8b treated preadipocytes resulted in no significant changes in *Ucp1* expression (**Fig. 25A**), despite excellent knockdown efficiency (**Fig. 25B**). Similarly, loss-of-function of *Esrra* by DsiRNA mediated gene silencing did not impair FGF8b induced *Ucp1* expression, but rather increased it as observed with one of two DsiRNAs (**Fig. 25C**). Both DsiRNAs were validated and produced excellent knockdown efficiencies (**Fig. 25D**). Taken together, *Lrrfip1* and *Esrra* were not dispensable for FGF8b induced *Ucp1* expression. Using the transcriptomic data set, an unbiased screening of transcription factors, which highly correlated with *Ucp1* gene expression across treatment groups

was performed (**Table 5.**). The top 10 candidates (*Arid5a*, *Atf5*, *Bnc1*, *Cebg*, *Etv1*, *Hes1*, *Nrf1*, *Nr2f2*, *Nupr1* and *Prdm16*) were then individually silenced in brown preadipocytes upon treatment with FGF8b to evaluate their transcriptional involvement in controlling *Ucp1* expression.

Table 5. Transcription factor candidates for knockdown studies.

Rank	Gene symbol	Pearson r	mean counts per sample
1	*Nupr1*	0,987	2294
2	*Etv1*	0,986	376
3	*Atf5*	0,978	3910
4	*Bnc1*	0,963	452
5	*Arid5a*	0,958	446
6	*Cebpg*	0,953	2743
7	*Hes1*	0,945	214
8	*Nrf1*	0,944	1047
9	*Prdm16*	0,934	96
10	*Nr2f2*	0,926	886

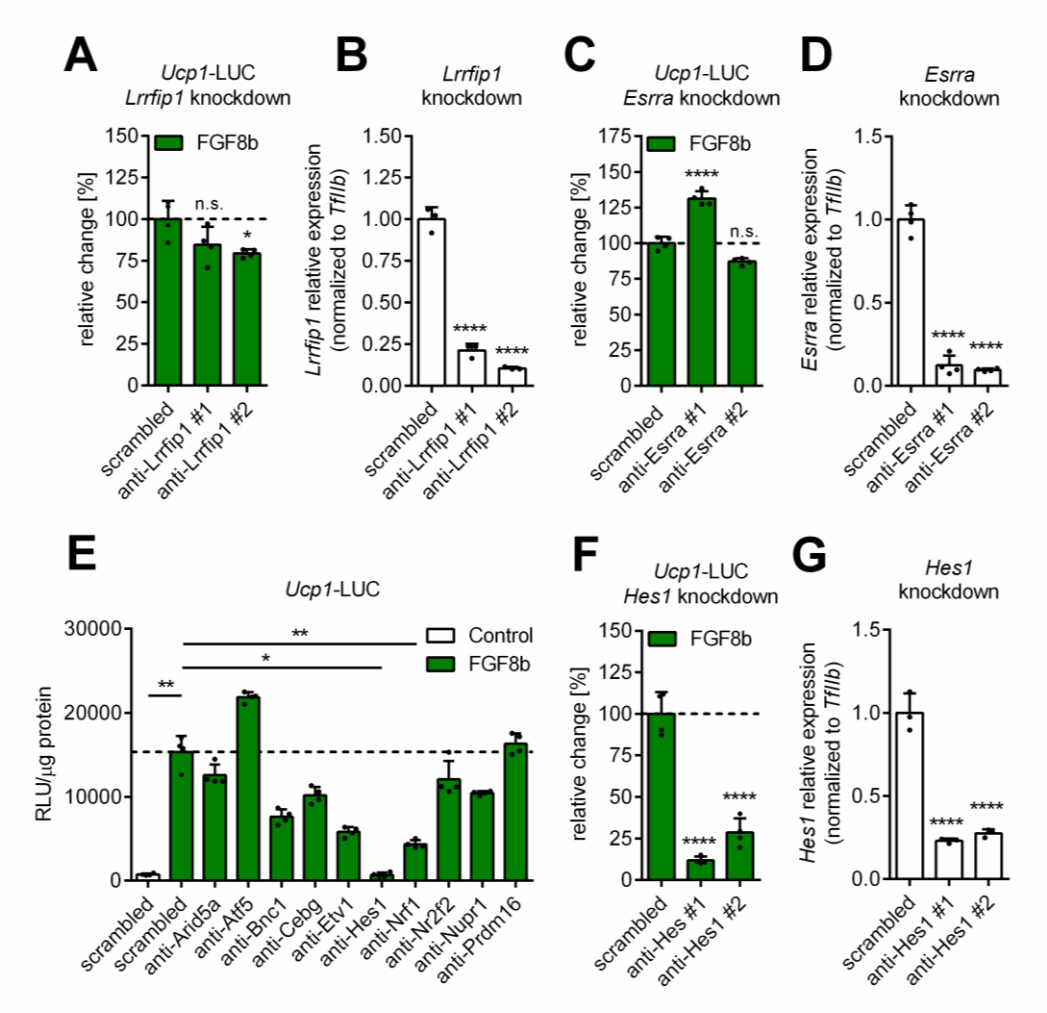

Figure 25. FGF8b induced *Ucp1* expression depends on *Hes1*. (**A**) luciferase activity linked *Ucp1* expression (*Ucp1*-LUC) upon *Lrrfip1* knockdown in brown FGF8b treated preadipocytes (N=4 for each group) and (**B**) *Lrrfip1* knockdown efficiency on transcript levels, 48 h post-transfection (N=3 for each group). (**C**) luciferase activity linked *Ucp1* expression (*Ucp1*-LUC) upon *Esrra* knockdown in brown FGF8b treated preadipocytes (N=4 for each group) and (**D**) *Essra* knockdown efficiency on transcript levels, 48 h post-transfection (N=4 for each group). (**E**) transcription factor screening based on DsiRNA mediated knockdown evaluated by luciferase activity linked *Ucp1* expression (*Ucp1*-LUC) in FGF8b treated preadipocytes (N=4 for each group). (**F**) luciferase activity linked *Ucp1* expression (*Ucp1*-LUC) upon *Hes1* knockdown in brown FGF8b treated preadipocytes (N=4 for each group) and (**G**) *Hes1* knockdown efficiency on transcript levels 48 h post-transfection (N=3 for each group). All experiments were carried out in the presence of 1 µg/ml heparin. One-way ANOVA in B and two-way ANOVA in C. Statistically significant results were indicated with asterisks: * = $p < 0.05$. ** = $p < 0.01$, *** = $p < 0.001$, **** = $p < 0.0001$.

Knockdown of two transcription factors (*Nrf1*, *Hes1*) impaired FGF8b induced *Ucp1* expression (**Fig. 25E**). *Nrf1* knockdown partially prevented the upregulation of *Ucp1*, while knockdown of *Hes1* completely abolished it (**Fig. 25E**). The most consequential transcription factor *Hes1* was validated with a second DsiRNA, confirming the initial results of the screening (**Fig. 25F-G**). These data revealed that the ternary complex implicated in FGF9 induced *Ucp1* expression was not required for the upregulation of *Ucp1* elicited by FGF8b. In contrast, it was demonstrated that FGF8b exerts its control over *Ucp1* expression via a formerly unknown, and non-canonical transcriptional regulator *Hes1*.

3. Summary

Recruitment of brite adipocytes within classical white adipose tissue has potential and wide-ranging metabolic benefits and therefore has garnered much attention in the scientific community in the past decade. Brite adipocytes, in contrast to white adipocytes, are characterized by much higher levels of the energy dissipating protein UCP1. The present study aimed to validate and comprehensively characterize the effect of the paracrine hormone FGF8b on *Ucp1* expression.

FGF8b was identified as the strongest putative browning agent among all members of the paracrine FGF protein family (Westphal *et al*, 2019) and immortalized white epididymal and inguinal SVF were used to study FGF8b in cell culture. While FGF8b treatment of white adipocytes induced *Ucp1* expression, it unexpectedly reduced transcript levels of other thermogenic and adipogenic genes. As a result, FGF8b treated adipocytes lacked thermogenic function and lipid stores characteristic of mature adipocytes. Contrarily, white adipocyte cultures treated with FGF8b showed signs of preadipocyte proliferation, instead of terminal differentiation and acquired a pro-glycolytic phenotype, possibly to metabolically support the high rate of proliferation. FGF8b treatment of undifferentiated preadipocytes recapitulated the strong induction

of *Ucp1* seen in adipocyte cultures. Thus, FGF8b acted on preadipocytes and controlled *Ucp1* expression in a formerly unrecognized cell type, the preadipocyte.

The effect of FGF8b on brown preadipocytes was subsequently characterized in depth with the aim to decipher the mechanism of FGF8b induced *Ucp1* expression. FGF8b dose-dependently increased *Ucp1* expression in brown and white preadipocytes. Other paracrine FGFs were also shown to effectively upregulate *Ucp1* expression such as FGF6 and FGF9, but FGF1 remained less effective. The underlying signaling pathway was demonstrated to rely on a FGFR1 MEK1/2-ERK1/2 axis, independent of PPARs, which pointed towards non-canonical regulators in control of *Ucp1* expression in preadipocytes. Analysis of gene expression changes upon FGF8b treatment in preadipocytes revealed the broad and coordinated upregulation of two metabolic pathways involving prostaglandins and glycolysis. Measurement of prostaglandin derived lipid mediators in FGF8b conditioned media identified PGE_2 as a potentially regulated mediator in FGF8b induced *Ucp1* expression. Loss-of-function by gene silencing and pharmacological inhibition of the PGE_2 producing enzyme PTGES1 clearly established that the induction of *Ucp1* by FGF8b was PGE_2 dependent and PGE_2 treatment of preadipocytes was sufficient to drive *Ucp1* expression in preadipocytes. However, high micromolar concentrations of PGE_2 were necessary to elicit these effects. The existence of an effect modulator of FGF8b induced *Ucp1* expression was therefore hypothesized, possibly linked to the mitogenic and pro-glycolytic effect of FGF8b.

FGF8 clearly promoted a pro-glycolytic phenotype in preadipocytes, thus a link between glucose metabolism and FGF8b induced *Ucp1* expression was investigated. Inhibition of glycolytic flux through various means significantly reduced FGF8b induced *Ucp1* expression. Notably, PGE_2 production was not impaired by suppression of glycolytic flux, highlighting that PGE_2 production alone was not able to fully upregulate *Ucp1* expression and that FGF8b induced *Ucp1* expression was dependent on high glycolytic flux. This was confirmed in FGF1 treated preadipocytes, which were characterized by intact PGE_2 biosynthesis, but insufficient glycolytic flux to upregulate *Ucp1* expression significantly. Thus, FGF8b induced *Ucp1* expression required the coordinated upregulation of both PGE_2 biosynthesis and glycolytic flux to maximize *Ucp1* expression.

A second transcriptomic data set was generated with the aim to identify potential transcriptional regulators of FGF8b induced *Ucp1* expression. The expression of the

transcriptional co-activator *Lrrfip1*, previously implicated in FGF9 induced *Ucp1* expression (Shamsi *et al*, 2020), correlated well with *Ucp1* expression in preadipocytes treated with either FGF1, FGF8b or FGF9. However, knockdown studies established that *Lrrfip1* was dispensable for FGF8b induced *Ucp1* expression. Subsequently, two transcription factors, *Nrf1* and *Hes1*, were demonstrated to highly correlate with *Ucp1* expression and were shown to be required for FGF8b induced *Ucp1* expression. In particular, knockdown of *Hes1* completely abolished the induction of *Ucp1* by FGF8.

Taken together, FGF8b was validated as a potent inducer of *Ucp1* expression in brown and white preadipocytes. Mechanistically, the FGF8b signal was transmitted via a FGFR1-MEK1/2-ERK1/2 axis, independent of PPARs and completely depended on the transcription factor *Hes1*. Two metabolic pathways, coordinately upregulated by FGF8b, acted in concert to maximize *Ucp1* expression and failure to induce either one of them would significantly hamper the magnitude of the induction. Thus, the present study revealed a novel and non-canonical mechanism for *Ucp1* expression in a formerly unrecognized cell type, the undifferentiated preadipocyte

DISCUSSION

Recruitment of thermogenic adipocytes is a desired clinical outcome inversely associated with body mass index (BMI), visceral fat and cardiometabolic health in human subjects (Keeley *et al*, 2019; Hondares *et al*, 2011; Becher *et al*, 2021). However, despite extensive ongoing efforts, there are still no effective therapeutics available for clinical use in humans, which utilize the remarkable plasticity of adipose tissue. In the mouse, brown adipose tissue has been shown to positively regulate glucose homeostasis, insulin sensitivity and triglyceride clearance (Stanford *et al*, 2013; Bartelt *et al*, 2011b), and the recruitment process of thermogenic adipocytes can be controlled by a multitude of transcription factors, secreted hormones and drugs (Lo & Sun, 2013; Kaisanlahti & Glumoff, 2019), including the well documented browning agent FGF21. While the endocrine hormone FGF21 has been shown to positively regulate metabolism via browning of WAT (Fisher *et al*, 2012; Kim *et al*, 2013), paracrine FGFs have been much less studied. The role of only a small number of paracrine FGFs in the recruitment and activation of thermogenic adipocytes has been investigated, for instance, FGF6 (Shamsi *et al*, 2020), FGF9 (Shamsi *et al*, 2020; Sun *et al*, 2019) and previous work of our own group on FGF8b (Westphal *et al*, 2019). In the latter study, a screening of all 15 paracrine FGFs was performed to identify those members of the paracrine FGF family with the highest capacity to induce *Ucp1* expression in differentiated white adipocytes (Westphal *et al*, 2019). The highest induction of *Ucp1* expression was subsequently demonstrated to be in response to FGF8b (Westphal *et al*, 2019).

1. FGF8b - a *bona fide* browning agent?

Browning of white adipocytes is transcriptionally regulated by canonical transcription factors such as *Pparγ*, *Prdm16* and *Pgc1a* (Maurer *et al*, 2020; Lo & Sun, 2013) and recruitment of brown adipocytes can be evaluated using these genes in combination with classical brown fat markers such as *Ucp1* and *Cidea*. In addition, putative brite marker genes can be used, which have been proposed to identify brite adipocytes. Surprisingly, FGF8b treated white adipocytes did not show a broad activation of the thermogenic program, as evidenced by lower expression levels of classical browning markers, despite high *Ucp1* induction. In an attempt to validate these unexpected findings, the brite marker genes *Tmem26*, *Tbx1*, *Cd137*, *Hocx9*, *Shox2*, *Slc27a1* were

evaluated (Wu *et al*, 2012b; Waldén *et al*, 2012). However, the analysis of brite marker gene expression levels generated inconclusive results as rosiglitazone treatment did not elevate most putative brite markers. Indeed, in a recent study none of the six aforementioned putative brite markers emerged as potential determinants of brown, brite and white adipocyte identity based on an in-depth characterization of mouse and human transcriptomes (Perdikari *et al*, 2018). Moreover, according to the study authors four of the six putative brite markers rather constituted general adipocyte markers or markers of specific fat depots, rendering these genes invalid for the evaluation of browning treatments. The use of these brite markers has therefore not been very illuminating, and classical brown markers remained the most important tool to differentiate between white and brite adipocytes. Thus, gene expression analysis of FGF8b treated adipocytes demonstrated that FGF8b cannot be classified as a *bona fide* browning agent, due to the absence of a coordinated induction of thermogenic gene expression. The effect of FGF8b on *Ucp1* expression can be interpreted as an unexpected, browning-independent event, and did therefore not result in increased thermogenic activity in white adipocytes. On the contrary, FGF8b appeared to act specifically on preadipocytes, a cell type usually not under consideration as a site for *Ucp1* expression.

2. FGF8b induced *Ucp1* expression is preadipocyte-specific.

FGF8b treatment clearly induced *Ucp1* expression in cultures of white preadipocytes and adipocytes. It is important to note that differentiated adipocyte cultures are a mixture of differentiated adipocytes and undifferentiated preadipocytes and the degree of differentiation often correlates with the overall *Ucp1* expression measured in the respective cell culture. This is mostly attributable to very low or even non-existing basal *Ucp1* expression in preadipocytes, whereas during differentiation *Ucp1* expression is strongly induced, particularly in the presence of PPARγ agonists. Increased *Ucp1* expression in adipocyte cultures can thus arise by several different routes. *Ucp1* expression can either be induced exclusively in the preadipocyte, in the adipocyte or in both cell types at the same time. The role of high *Ucp1* levels in preadipocytes remains largely speculative, while higher *Ucp1* expression in fully differentiated adipocytes should certainly lead to greater UCP1-dependent respiration. Moreover, an increase in *Ucp1* expression upon FGF8b treatment that is theorized to be disproportionately attributable to the mature adipocytes should lead to a smaller *Ucp1*

induction, when the same treatment is tested in cell cultures of undifferentiated preadipocytes. In fact, the opposite was experimentally established in both cases. FGF8b treated adipocytes did not show higher thermogenic function in a respiratory assay and pure preadipocyte cultures treated with FGF8b upregulated *Ucp1* more effectively than in adipocyte cultures (C_t = 26 in preadipocyte culture; C_t = 29 in adipocyte culture). The responsiveness to FGF8b treatment is also to some extent a function of receptor expression. In fact, *Fgfr1* expression is much higher in undifferentiated preadipocytes than in differentiated adipocytes, as available RNA-sequencing data suggest ((Li *et al*, 2019), E-MTAB-8344). These data supported a model in which FGF8b induced *Ucp1* expression is most likely a preadipocyte-specific and non-thermogenic event. As a consequence, FGF8b failed to increase thermogenic activity upon norepinephrine treatment in mice (Westphal *et al*, 2019). Whether these results reflect a preadipocyte rather than adipocyte-centered role for any possible experimental setting in living animals remains to be seen, but the literature on other paracrine FGFs points towards a much more nuanced picture. For instance, FGF9 loss-of function resulted in a significant reduction in maximal thermogenic capacity in response to cold exposure in mice, and chronic application of recombinant FGF9 improved cold tolerance in mice, highlighting the importance of FGF9 for BAT thermogenesis (Shamsi *et al*, 2020). However, no significant changes in brown and white fat *Ucp1* mRNA expression were reported in these experiments, possibly indicating that the metabolic improvements mediated by FGF9 on adaptive thermogenesis were a result of potential inter-organ crosstalk. Taken together, these data showed that paracrine FGFs most likely act on preadipocytes rather than adipocytes, and that different paracrine FGFs may also act differently on processes such as thermogenic differentiation in cultured cells and thermogenic activity in mice. As a consequence, conflicting results and interpretations arise easily, but can be diminished, for instance, by taking into account that preadipocyte are able to express *Ucp1*.

3. Resolving conflicting effects of paracrine FGFs in adipocytes.

FGF8b treatment of white adipocytes increased *Ucp1* expression, whereas FGF8b treatment of brown adipocytes decreased *Ucp1* expression relative to untreated adipocytes, despite suppression of adipogenesis in both cell lines. The absence of an induction of *Ucp1* in brown adipocytes was even more puzzling, as there was evidence

of an upregulation of prostaglandin metabolism and glucose uptake in these cells (**Fig. 8 A**), which was demonstrated to control *Ucp1* expression in brown preadipocytes. On the other hand, the anti-adipogenic effect of paracrine FGFs has been well documented in the case of FGF9 (Sun *et al*, 2019; Shamsi *et al*, 2020), even though conflicting results exist with respect to the effect of FGF9 on *Ucp1* expression in white inguinal adipocytes (Sun *et al*, 2019; Shamsi *et al*, 2020). These conflicting results can be at least partially resolved, when differences in the intrinsic *Ucp1* induction capacities between fat depots are considered. While brown adipocytes possess much higher transcript levels of *Ucp1* in absolute terms, white adipocytes show higher fold increases upon stimulation with browning agents, mostly due to much lower baseline *Ucp1* transcript levels within untreated adipocytes (Kalinovich *et al*, 2017). The most likely site of FGF8b induced *Ucp1* expression in brown and white adipocyte cultures was demonstrated to lie within the undifferentiated preadipocyte fraction, and when these two facts are taken into account discrepancies between brown and white adipocytes in response to FGF8b treatment can be resolved to some extent. While proliferation of preadipocytes with relatively high *Ucp1* expression can easily surpass *Ucp1* transcript levels of untreated differentiated white (epididymal) adipocytes, this is not the case in brown adipocyte cultures. Here, proliferation of the *Ucp1* positive preadipocyte fraction dilutes overall *Ucp1* transcript levels due to displacement of differentiated brown adipocytes containing very high amounts of *Ucp1*. Consequently, whether FGF treatment induces or reduces *Ucp1* expression in differentiated adipocytes significantly depends on absolute and relative *Ucp1* expression in adipocytes versus preadipocytes, which may also depend on mouse strains or whether cells were co-treated with a PPARγ agonist (Li *et al*, 2014; Xue *et al*, 2005). A finding that may be well suited to illustrate the relationship outlined above is that increased *Ptgs2* and *Ptges1* transcript levels and tissue PGE_2 concentrations correlated positively with *Ucp1* expression in eWAT, but not in iBAT in adipogenesis-deficient PPARγ-KO mice (García-Alonso *et al*, 2013).

Experiments with the same paracrine FGF occasionally yielded conflicting results in the literature in supposedly similar cell models. For example, *Ucp1* expression was reported to increase in white adipocytes upon treatment with FGF9 (Shamsi *et al*, 2020), while it was shown to be decreased by others (Sun *et al*, 2019). A thorough assessment of the methodological differences is helpful in clarifying whether these findings are contradictory. In the first study, FGF9 treatment was performed either as a 6 day pretreatment or as a 1-3 days lasting treatment on top of fully-differentiated

adipocytes, and led to higher *Ucp1* expression (Shamsi *et al*, 2020). In contrast, FGF9 treatment was applied during the entire differentiation procedure under co-stimulation with a PPARγ agonist in the second study, which resulted in lower *Ucp1* expression (Sun *et al*, 2019). It is conceivable that treatment of inguinal adipocytes with the browning agent troglitazone markedly elevated *Ucp1* transcript levels in the control group, while FGF9 treatment displaced adipocytes with abundant *Ucp1* expression via proliferation of the preadipocyte fraction. On the other hand, FGF9 pretreatment or treatment of fully-differentiated adipocyte cultures did not lead to a significant displacement of adipocytes by preadipocytes. Moreover, the cells were not treated with a PPARγ agonist, therefore absolute *Ucp1* expression levels were on a much lower level, which were more easily surpassed by preadipocyte-specific *Ucp1* expression. Taken together, these considerations showcase the importance of methodological differences between studies employing the same paracrine FGF, and careful interpretations are needed to resolve supposed discrepancies between studies.

Another variable potentially contributing to discrepancies between experiments pertained to the use of immortalized cell lines. Data from the present study, highlighted large differences in the magnitude of the induction of *Ucp1* expression upon FGF8b treatment as a function of passage number of the employed immortalized cell line. These results indicated that cell cultures undergoing positive selection for highly proliferative cells change their response to the same treatment regimen. It is important to note that the immortalization procedure itself represents such a selection process, since it includes an antibiotic selection step, which most likely enriches the immortalized cell line with more rapidly dividing cells. Hence, it is highly likely that immortalized cells *per se* showed higher sensitivity towards paracrine FGFs than primary SVF cells throughout the study. This was also evident in the study of Shamsi et al. (2020), where effect sizes derived from immortalized cells were one order of magnitude higher than in primary SVF cells. It is therefore imperative to validate any browning agent in primary cells before arriving to a final conclusion, as done in the present study. In addition, the use of immortalized versus primary cells needs to be considered in any comparison between publications such as the one outlined before in the case of FGF9 and can partially or even fully resolve an apparent lack of reproducibility.

4. FGF8b and FGF9 induce *Ucp1* in a PGE_2 dependent manner.

FGF8b and FGF9 induced highly similar gene expression signatures (r = 0.999) in brown preadipocytes. These similarities suggested a shared molecular mechanism in control of *Ucp1* expression between these two FGFs. Indeed, *Ucp1* expression in preadipocytes induced by FGF6 and FGF9 treatment was recently reported, and PGE_2 biosynthesis was demonstrated to play a key role (Shamsi *et al*, 2020). Similarly, the present study provided strong evidence of an activation of the prostaglandin metabolic pathway by FGF8b, which culminated into a coordinated upregulation of PGE_2 biosynthesis, and PGE_2 itself was shown to be sufficient to upregulate *Ucp1* expression in cultured preadipocytes. The ability of FGF8b to stimulate PGE_2 biosynthesis has been documented in cultured chondrocytes, corroborating a model, in which FGF8b controls prostaglandin metabolism (Uchii *et al*, 2008). Prostaglandins such as PGE_2 and carbaprostacyclin ($cPGI_2$), a stable analog of PGI_2, have been reported to regulate brite adipocyte recruitment in a PTGS-dependent manner before (García-Alonso *et al*, 2013; Madsen *et al*, 2010; Vegiopoulos *et al*, 2010). Importantly, acute treatment of progenitor cells, derived from the SVF of white adipose tissue, with PGE_2 resulted in an upregulation of *Ucp1* transcription (Vegiopoulos *et al*, 2010), mirroring the results obtained in this work. An important conceptual difference between these early studies and the present one is that activation of the prostaglandin pathway was initially seen as being a direct downstream effector of the cold-induced β-adrenergic signaling pathway in white adipocytes. Contrarily, the present work located the prostaglandin pathway directly downstream of the FGF signaling pathway within preadipocytes. Interestingly, paracrine FGF9 has been identified as a cold-induced secreted factor in brown preadipocytes (Shamsi *et al*, 2020). Conceivably, FGF mediated *Ucp1* expression in preadipocytes contributed to the observed prostaglandin-dependent regulation of *Ucp1* in murine white adipose. Contrarily, stimulation of cultured human white adipocytes, which were differentiated from omental preadipocytes, with low micromolar concentrations of PGE_2 did not induce *Ucp1* expression (García-Alonso *et al*, 2016), and treatment of human adipose derived stem cells with the precursor arachidonic acid inhibited brite adipocyte recruitment in a PGE_2-dependent manner (Pisani *et al*, 2014). Therefore, whether PGE_2 induced *Ucp1* expression can be translated to human adipocyte biology remains an open question.

5. High glycolytic flux is required for PGE_2 induced *Ucp1* expression.

High micromolar concentrations of PGE_2 were needed to evoke a significant upregulation of *Ucp1* in cultured preadipocytes. Whether this was due to weak stability under cell culture conditions or unspecific binding to media components such as BSA remained elusive. However, an unexpected interplay between high glycolytic flux and PGE_2 was observed. Firstly, impeding glycolytic flux in FGF8b treated preadipocytes by inhibiting glucose uptake, reduced the magnitude of the *Ucp1* induction despite elevated PGE_2 levels. Similarly, FGF1 failed to upregulate *Ucp1* expression due to a weak glycolytic response, despite increasing PGE_2 biosynthesis as effectively as FGF8b. These data illustrated a metabolic dependency of PGE_2 induced *Ucp1* expression on high glycolytic flux, essentially limiting the magnitude of PGE_2 induced *Ucp1* expression in non-glycolytic cells. Interestingly, a transmembrane gradient in lactate has been shown to regulate prostaglandin uptake into cells (Chan *et al*, 2002), and inhibition of glycolysis was reported to increase PGE_2 release (Herman *et al*, 1977), reminiscent of results presented earlier that showed an upregulation of prostaglandin metabolism when cellular glucose uptake was inhibited by BAY-876. These data strongly suggested a direct interaction between prostaglandin biosynthesis and glycolysis.

It is well known that PGE_2 promotes cell proliferation in normal and cancer cells by autocrine and paracrine mechanisms (Cao & Prescott, 2002). Three main signaling pathways have been shown to mediate PGE_2 induced cell proliferation and tumor growth. These pathways signal either via epidermal growth factor receptor (EGFR), PPARδ or the RAS-MAPK pathway (Wang & Dubois, 2006). The PGE_2-dependent increase in *Ucp1* expression in response to FGF8b, however, is unlikely to be the cause of EGFR or PPAR signaling as both EGF treatment and PPAR antagonists did not affect FGF8b induced *Ucp1* transcription. In contrast, inhibition of the RAS-MAPK pathway completely abolished the effect of FGF8b on *Ucp1* expression. Thus, PGE_2 most likely signals via the RAS-MAPK pathway to induce *Ucp1* expression. Notably, arachidonic acid, the precursor metabolite for PGE_2 biosynthesis, stimulates cell proliferation in brown preadipocytes via PKC and the MEK1/2-ERK1/2 pathway (Garcia *et al*, 2012), confirming the involvement of the MAPK pathway. Conversely, inhibition of the arachidonic acid pathway by PTGS2 inhibitors celecoxib or indomethacin suppresses cell proliferation and tumor progression (Leahy *et al*, 2002; Eli *et al*, 2001). Thus, the inhibitory effect of indomethacin on prostaglandin metabolism needs to be considered in any setting, where the effect of a treatment, e.g. paracrine FGFs, on

Ucp1 expression relies on the action of prostaglandins. This is particularly the case for *in vitro* differentiated adipocytes, which are routinely stimulated with high micromolar concentrations of indomethacin to induce differentiation.

Many proliferative cells, including cancer cells require high rates of glycolytic flux to meet their metabolic demand (Jeanson *et al*, 2015). The low effectiveness of FGF1 to induce *Ucp1* expression coincided with its weak mitogenic activity compared to other FGFs, such as FGF8b and FGF9. Moreover, higher glucose consumption was observed in FGF8b, than in FGF1 treated preadipocytes. Thus, the potential of paracrine FGFs to induce *Ucp1* expression in preadipocytes was linked to their mitogenic and pro-glycolytic activity. UCP1 expression has been documented by immunohistochemistry in some forms of human cancers such as non-small cell lung cancer (NSCLC) and colorectal cancer (Alnabulsi *et al*, 2019; Alexandra *et al*, 2017), and in a mouse xenograft model of breast cancer (Singh *et al*, 2016), but its relation to tumor cell proliferation remains poorly understood. Ectopic overexpression of UCP1 in human SGBS-adipocytes, derived from a patient with Simpson-Golabi-Behmel syndrome (Fischer-Posovszky *et al*, 2008), resulted in increased glucose transporter 1 mediated glucose uptake and lactate release, indicating enhanced glycolytic flux, and the existence of a feedback mechanism between UCP1 expression and glucose metabolism (Tews *et al*, 2019). Similarly, forced expression of UCP1 in the preadipocyte cell line 3T3-L1 increased glucose uptake and lactate release, and was demonstrated to increase glycolytic flux (Si *et al*, 2007, 2009). Conversely, knockdown of *Ucp1* in brown fat prevented the uptake of glucose into the tissue during optogenetic activation of thermogenesis in mice (Jeong *et al*, 2018). These data supported the view that *Ucp1* expression determines glucose uptake rates in adipocytes and that UCP1 is capable of acting as sink for glucose. However, results obtained from FGF8b treated brown preadipocytes revealed that the glycolytic phenotype was *Ucp1*-independent (**Fig. 18E**). Thus, the opposite directionality of control over *Ucp1* has been established in the case of the undifferentiated FGF8b treated preadipocyte, providing no evidence to suggest that increased *Ucp1* expression was the cause for higher glycolytic flux. Nevertheless, the interplay between glycolysis and *Ucp1* suggested a potential non-classical biological role for *Ucp1* in preadipocytes.

6. Exogenous lactate amplified FGF8b induced *Ucp1* expression.

Endogenous lactate production did not mediate the dependence of FGF8b induced *Ucp1* expression on high glycolytic flux, but addition of millimolar quantities of exogenous lactate amplified the induction of *Ucp1* in FGF8b treated preadipocytes. The ability of lactate to increase *Ucp1* gene expression in white adipocytes has been reported by several independent investigators (Carrière *et al*, 2014; Bai *et al*, 2016; Kim *et al*, 2017). Lactate induced browning has been proposed to act as an adaptive regulator during periods of high redox pressure (Jeanson *et al*, 2015). Large amounts of lactate are produced from hypoxic adipocytes and high redox pressure is a product of the oxidation of lactate to pyruvate and leads to a high $NADH/NAD^+$ ratio, which acts as a signal for the upregulation of *Ucp1* expression in cultured adipocytes. UCP1-dependent uncoupled respiration alleviates the elevated redox pressure by increasing the oxidation of NADH. Thus, browning is postulated by some researchers to be a by-product of a redox pressure alleviating mechanism. Cancer cell lines, which rely heavily on glycolysis are characterized by high $NADH/NAD^+$ ratios and inhibition of glycolytic flux decrease, whereas glucose supplementation increase the $NADH/NAD^+$ ratio (Zhao *et al*, 2015). With this in mind, FGF8b induced *Ucp1* expression can be interpreted as a redox regulatory mechanism with the aim to decrease high NADH concentrations. This is in line with multiple observations during FGF8b treatment in proliferating preadipocytes. Firstly, the addition of exogenous lactate likely increased the intracellular $NADH/NAD^+$ ratio by formation of pyruvate from lactate and reduction of NAD^+ to NADH. Consequently, as a redox regulatory response, *Ucp1* gene expression increased. Inhibition or slowing down of glycolytic flux in FGF8b treated preadipocytes decreased the induction of *Ucp1* because intracellular redox pressure was diminished. A recently published report demonstrated a strong correlation with *Ucp1* expression and a dependence of lactate fluxes in brite adipocytes on the monocarboxylate transporter 1 (MCT1) (Lagarde *et al*, 2021). Interestingly, treatment of brown preadipocytes with FGF8b and FGF9 markedly upregulated *Mct1* expression according to the transcriptomic data, whereas FGF1 did not have an effect, further supporting the model outlined above. Thus, *Ucp1* expression upon FGF8b treatment in proliferating preadipocytes may be a mechanism to alleviate high redox pressure produced by the glycolytic pathway. This model also explains the association of the mitogenic potential of individual paracrine FGFs and their capacity to induce *Ucp1* expression, as well as the dependence on glycolysis. However, the fact that inhibition of lactate dehydrogenase (LDH) did not have an impact on *Ucp1* expression is

unexpected, given that inhibition of LDH would likely result in a change of the NADH/NAD^+ ratio. Thus, even though many findings integrate well into the hypothesis that preadipocyte-specific *Ucp1* expression is part of a redox regulatory mechanism, more research is needed to experimentally validate it. Taken together, paracrine FGFs with high mitogenicity strongly induced *Ucp1* expression in a PGE_2 and glycolysis-dependent manner to potentially control cellular redox homeostasis.

7. Transcriptional regulators in control of FGF8b induced *Ucp1* expression.

The classical cold/norepinephrine induced signaling pathway regulates *Ucp1* transcription based on interactions between well-known transcription factors such as PRDM16 , PGC1A, PPARs and CREBs and regulatory regions within the *Ucp1* gene (Villarroya *et al*, 2017b). Whether these classical transcriptional regulators were involved in FGF8b induced *Ucp1* expression, which was experimentally demonstrated to rely on the MAPK signaling pathway, remained to be investigated. Experiments in white adipocytes revealed that treatment with FGF8b downregulated *Pparγ*, *Pgc1α* and *Prdm16* mRNA expression. This was consistent with reports demonstrating downregulation of the same genes in FGF6 and FGF9 treated brown preadipocytes (Shamsi *et al*, 2020). Moreover, pharmacological inhibition of PPAR signaling in brown preadipocytes did not affect FGF8b induced *Ucp1* expression. Similarly, FGF6/FGF9 induced *Ucp1* expression was preserved in PPAR-KO and PGC1A-KO cell models (Shamsi *et al*, 2020). Taken together, these results argued against a canonical transcriptional regulatory mechanism in control of preadipocyte-specific *Ucp1* expression. Indeed, Shamsi *et al.* (2020) elegantly identified ESRRA-FLII-LRRFIP1, a formerly unknown non-canonical ternary transcriptional complex in control of *Ucp1* expression in preadipocytes by using a combination of engineered DNA-binding molecule-mediated chromatin immunoprecipitation (enChIP) and quantitiative proteomics. The present work, however, provided strong evidence from loss-of-function studies that *Esrra* and *Lrrfip1* were dispensable for FGF8b induced *Ucp1* expression, in spite of virtually indistinguishable gene signatures between FGF8b and FGF9 treated brown preadipocytes. Two transcription factors, *Nrf1* and *Hes1* were identified as potential regulators of FGF8b induced *Ucp1* expression based on a combination of gene correlation analysis and knockdown studies. Even though using such an experimental strategy is not able to identify and prove direct interactions with

the *Ucp1* promoter, it did help to understand the regulatory network necessary to evoke preadipocyte-specific *Ucp1* expression.

Nuclear respiratory factor 1 (*Nrf1*) is known to orchestrate various biological responses to cellular stress including antioxidant defense, mitochondrial biogenesis and proteasomal function during ER stress (Kim *et al*, 2016; Weitzel *et al*, 2003). PGC1A induces *Nrf1* expression during mitochondrial biogenesis, which in turn affects *Tfam* expression (Wu *et al*, 1999). Thus, induction of *Nrf1* expression is linked to enhanced oxidative metabolism. However, brown adipocyte specific *Nrf1* loss-of-function did neither affect *Ucp1* mRNA nor UCP1 protein levels, independent of housing temperature of mice (Goncalves *et al*, 2018). Taken together, the involvement of *Nrf1* in the control of *Ucp1* expression in the proliferating and highly glycolytic preadipocyte appeared to be rather counterintuitive, given its role in oxidative metabolism as opposed to glycolysis and in the absence of any experimental evidence linking it to the regulation of *Ucp1* transcription.

Hairy and enhancer of split 1 (*Hes1*) is a basic helix loop helix transcription factor and a well-known Notch signaling effector molecule (Ranganathan *et al*, 2011). During development *Hes1* induces cell proliferation of various cell types and keeps cells in the undifferentiated state (Kageyama *et al*, 2000). Activation of Notch signaling or overexpression of *Hes1* in 3T3-L1 preadipocyts suppresses adipogenesis (Ross *et al*, 2006). Notably, Notch signaling has also been shown to be inversely correlated to *Ucp1* expression during adaptive thermogenesis in mice (Bi *et al*, 2014). In summary, these data indicate that FGF8b induced *Ucp1* expression is predicated on the fact that the responsive cells are undifferentiated, further supporting that FGF8b acts on the preadipocyte fraction to upregulate *Ucp1* expression in cultured cells. However, no mechanistic link has been reported in the literature between *Hes1* and *Ucp1* so far, and more research is needed to experimentally validate the non-canonical transcriptional roles of both *Nrf1* and *Hes1* in *Ucp1* transcription in preadipocytes.

8. Conclusion

In conclusion, the present study experimentally established that FGF8b, a member of the paracrine FGF protein family, activated a FGFR1-MEK1/2-ERK1/2 axis to induce two metabolic pathways, i.e. the PGE_2 biosynthetic pathway and glycolysis to control *Ucp1* expression in preadipocytes. The coordinated induction of the prostaglandin metabolic pathway enabled a rapid surge in PGE_2 levels, which was a required event and to some extent sufficient to regulate *Ucp1* gene expression. In order to achieve a full-scale induction of *Ucp1* in preadipocytes, high glycolytic fluxes were necessary in the presence of elevated PGE_2 biosynthesis and a failure to enhance this flux, as in the case with FGF1, negatively affected the ability of paracrine FGFs to induce *Ucp1* expression. Importantly, the effectiveness to induce *Ucp1* gene expression in preadipocytes correlated with the mitogenic potential of the particular FGF. Thus, *Ucp1* gene expression was under the control of both PGE_2 and glucose metabolism in the undifferentiated, proliferating preadipocyte, a cell type formerly unrecognized as a site of *Ucp1* expression. Taken together, these data outlined a novel regulatory network, in control of *Ucp1* transcription, which was independent of adipogenesis, and provided some evidence in favor of a potentially redox regulatory function of *Ucp1* in the preadipocyte. Thus, the presented model offers the unique opportunity to identify novel non-canonical regulators of *Ucp1* expression by dissecting the transcriptional regulation of *Ucp1* without any obscuring overlay of the adipogenic or thermogenic transcriptional program.

REFERENCES

Alexandra G, Konstantina B, Dimitra K, Christos K, Efthimios S & Michael IK (2017) Thermogenic protein UCP1 and UCP3 expression in non-small cell lung cancer: relation with glycolysis and anaerobic metabolism. *Cancer Biol Med* 14: 396

Alnabulsi A, Cash B, Hu Y, Silina L, Alnabulsi A & Murray GI (2019) The expression of brown fat-associated proteins in colorectal cancer and the relationship of uncoupling protein 1 with prognosis. *Int J Cancer* 145: 1138–1147

Arch JRS (2002) β3-adrenoceptor agonists: Potential, pitfalls and progress. *Eur J Pharmacol* 440: 99–107

Bai Y, Shang Q, Zhao H, Pan Z, Guo C, Zhang L & Wang Q (2016) Pdcd4 restrains the self-renewal and white-to-beige transdifferentiation of adipose-derived stem cells. *Cell Death Dis* 7: e2169-11

Bartelt A, Bruns OT, Reimer R, Hohenberg H, Ittrich H, Peldschus K, Kaul MG, Tromsdorf UI, Weller H, Waurisch C, *et al* (2011a) Brown adipose tissue activity controls triglyceride clearance. *Nat Med* 17: 200–206

Bartelt A, Bruns OT, Reimer R, Hohenberg H, Ittrich H, Peldschus K, Kaul MG, Tromsdorf UI, Weller H, Waurisch C, *et al* (2011b) Brown adipose tissue activity controls triglyceride clearance. *Nat Med* 17: 200–206

Bartelt A & Heeren J (2014) Adipose tissue browning and metabolic health. *Nat Rev Endocrinol* 10: 24–36

Becher T, Palanisamy S, Kramer DJ, Eljalby M, Marx SJ, Wibmer AG, Butler SD, Jiang CS, Vaughan R, Schöder H, *et al* (2021) Brown adipose tissue is associated with cardiometabolic health. *Nat Med* 27: 58–65

Bi P, Shan T, Liu W, Yue F, Yang X, Liang XR, Wang J, Li J, Carlesso N, Liu X, *et al* (2014) Inhibition of Notch signaling promotes browning of white adipose tissue and ameliorates obesity. *Nat Med* 20: 911–918

Cannon B & Nedergaard J (2004) Brown Adipose Tissue: Function and Physiological Significance. *Physiol Rev* 84: 277–359

Cao W, Daniel KW, Robidoux J, Puigserver P, Medvedev A V., Bai X, Floering LM, Spiegelman BM & Collins S (2004) p38 Mitogen-Activated Protein Kinase Is the

Central Regulator of Cyclic AMP-Dependent Transcription of the Brown Fat Uncoupling Protein 1 Gene. *Mol Cell Biol* 24: 3057–3067

Cao Y & Prescott SM (2002) Many actions of cyclooxygenase-2 in cellular dynamics and in cancer. *J Cell Physiol* 190: 279–286

Carrière A, Jeanson Y, Berger-Müller S, André M, Chenouard V, Arnaud E, Barreau C, Walther R, Galinier A, Wdziekonski B, *et al* (2014) Browning of white adipose cells by intermediate metabolites: An adaptive mechanism to alleviate redox pressure. *Diabetes* 63: 3253–3265

Chan BS, Endo S, Kanai N & Schuster VL (2002) Identification of lactate as a driving force for prostanoid transport by prostaglandin transporter PGT. *Am J Physiol - Ren Physiol* 282: 1097–1102

Chartoumpekis D V., Habeos IG, Ziros PG, Psyrogiannis AI, Kyriazopoulou VE & Papavassiliou AG (2011) Brown adipose tissue responds to cold and adrenergic stimulation by induction of FGF21. *Mol Med* 17: 736–740

Chomczynski P & Sacchi N (1987) Single-step method of RNA isolation by acid guanidinium thiocyanate-phenol-chloroform extraction. *Anal Biochem* 162: 156–159

Crossley PH & Martin GR (1995) The mouse Fgf8 gene encodes a family of polypeptides and is expressed in regions that direct outgrowth and patterning in the developing embryo. *Development* 121: 439–451

Cypess AM, Weiner LS, Roberts-Toler C, Elía EF, Kessler SH, Kahn PA, English J, Chatman K, Trauger SA, Doria A, *et al* (2015) Activation of human brown adipose tissue by a β3-adrenergic receptor agonist. *Cell Metab* 21: 33–38

DeBerardinis RJ, Lum JJ, Hatzivassiliou G & Thompson CB (2008) The Biology of Cancer: Metabolic Reprogramming Fuels Cell Growth and Proliferation. *Cell Metab* 7: 11–20

Degirolamo C, Sabbà C & Moschetta A (2016) Therapeutic potential of the endocrine fibroblast growth factors FGF19, FGF21 and FGF23. *Nat Rev Drug Discov* 15: 51–69

Dieckmann S, Maurer S, Fromme T, Colson C, Virtanen KA, Amri EZ & Klingenspor M (2020) Fatty Acid Metabolite Profiling Reveals Oxylipins as Markers of Brown

but Not Brite Adipose Tissue. *Front Endocrinol (Lausanne)* 11: 73

Dutchak PA, Katafuchi T, Bookout AL, Choi JH, Yu RT, Mangelsdorf DJ & Kliewer SA (2012) Fibroblast growth factor-21 regulates PPARγ activity and the antidiabetic actions of thiazolidinediones. *Cell* 148: 556–567

Eli Y, Przedecki F, Levin G, Kariv N & Raz A (2001) Comparative effects of indomethacin on cell proliferation and cell cycle progression in tumor cells grown in vitro and in vivo. *Biochem Pharmacol* 61: 565–571

Emanuelli B, Vienberg SG, Smyth G, Cheng C, Stanford KI, Arumugam M, Michael MD, Adams AC, Kharitonenkov A & Kahn CR (2014) Interplay between FGF21 and insulin action in the liver regulates metabolism. *J Clin Invest* 124: 515–527

Fischer-Posovszky P, Newell FS, Wabitsch M & Tornqvist HE (2008) Human SGBS cells - A unique tool for studies of human fat cell biology. *Obes Facts* 1: 184–189

Fischer C, Seki T, Lim S, Nakamura M, Andersson P, Yang Y, Honek J, Wang Y, Gao Y, Chen F, *et al* (2017) A miR-327-FGF10-FGFR2-mediated autocrine signaling mechanism controls white fat browning. *Nat Commun* 8: 3–18

Fisher FF, Kleiner S, Douris N, Fox EC, Mepani RJ, Verdeguer F, Wu J, Kharitonenkov A, Flier JS, Maratos-Flier E, *et al* (2012) FGF21 regulates PGC-1α and browning of white adipose tissues in adaptive thermogenesis. *Genes Dev* 26: 271–281

García-Alonso V & Clária J (2014) Prostaglandin E 2 signals white-to-brown adipogenic differentiation. *Adipocyte* 3: 290–296

García-Alonso V, López-Vicario C, Titos E, Morán-Salvador E, González-Périz A, Rius B, Párrizas M, Werz O, Arroyo V & Clària J (2013) Coordinate functional regulation between microsomal prostaglandin e synthase-1 (mPGES-1) and peroxisome proliferator-activated receptor γ (PPARγ) in the conversion of white-to-brown adipocytes. *J Biol Chem* 288: 28230–28242

García-Alonso V, Titos E, Alcaraz-Quiles J, Rius B, Lopategi A, López-Vicario C, Jakobsson PJ, Delgado S, Lozano J & Clària J (2016) Prostaglandin E2 exerts multiple regulatory actions on human obese adipose tissue remodeling, inflammation, adaptive thermogenesis and lipolysis. *PLoS One* 11: 1–17

Garcia B, Martinez-De-Mena R & Obregon MJ (2012) Arachidonic acid stimulates

DNA synthesis in brown preadipocytes through the activation of protein kinase C and MAPK. *Biochim Biophys Acta - Mol Cell Biol Lipids* 1821: 1309–1315

García B & Obregón MJ (2002) Growth factor regulation of uncoupling protein-1 mRNA expression in brown adipocytes. *Am J Physiol - Cell Physiol* 282: 105–112

Gemel J, Gorry M, Ehrlich GD & MacArthur CA (1996) Structure and Sequence of Human FGF8. *Genomics* 35: 253–257

Ghosh K, Shankar DB, Shackleford M, Wu K & Miller GJ (1996) Molecular Cloning and Characterization of Human FGF8 Alternative Messenger RNA Forms. *Cell growth Differ* 7: 1425–1434

Goncalves LS, Eguchi K, Fischer AW, Parlakgül G & Nicole A (2018) Brown adipose tissue thermogenic adaptation requires Nrf1- mediated proteasomal activity. *Nat Med* 24: 292–303

Hanna VS & Hafez EAA (2018) Synopsis of arachidonic acid metabolism: A review. *J Adv Res* 11: 23–32

Herman CA, Zenser T V, Davis BB & Louis S (1977) Prostaglandin E2 production by renal inner medullary tissue slices: effect of metabolic inhibitors. *Prostaglandins* 14: 679–687

Hondares E, Iglesias R, Giralt A, Gonzalez FJ, Giralt M, Mampel T & Villarroya F (2011) Thermogenic activation induces FGF21 expression and release in brown adipose tissue. *J Biol Chem* 286: 12983–12990

Hondares E, Rosell M, Gonzalez FJ, Giralt M, Iglesias R & Villarroya F (2010) Hepatic FGF21 Expression Is Induced at Birth via PPARα in Response to Milk Intake and Contributes to Thermogenic Activation of Neonatal Brown Fat. *Cell Metab* 11: 206–212

Itoh N & Ornitz DM (2011) Fibroblast growth factors: from molecular evolution to roles in development, metabolism and disease. *J Biochem* 149: 121–30

Jeanson Y, Carrière A & Casteilla L (2015) A new role for browning as a redox and stress adaptive mechanism? *Front Endocrinol (Lausanne)* 6: 1–11

Jeong JH, Chang JS & Jo YH (2018) Intracellular glycolysis in brown adipose tissue is essential for optogenetically induced nonshivering thermogenesis in mice. *Sci*

Rep 8: 1–14

de Jong JMA, Larsson O, Cannon B & Nedergaard J (2015) A stringent validation of mouse adipose tissue identity markers. *Am J Physiol - Endocrinol Metab* 308: E1085–E1105

Kageyama R, Ohtsuka T & Tomita K (2000) The bHLH gene Hes1 regulates differentiation of multiple cell types. *Mol Cells* 10: 1–7

Kaisanlahti A & Glumoff T (2019) Browning of white fat: agents and implications for beige adipose tissue to type 2 diabetes. *J Physiol Biochem* 75: 1–10

Kalinovich A V., de Jong JMA, Cannon B & Nedergaard J (2017) UCP1 in adipose tissues: two steps to full browning. *Biochimie* 134: 127–137

Keeley T, Kirov A, Koh WY, Demambro V, Bergquist I, Cotter J, Caradonna P, Siviski ME, Best B, Henderson T, *et al* (2019) Resistance to visceral obesity is associated with increased locomotion in mice expressing an endothelial cell-specific fibroblast growth factor 1 transgene. *Physiol Rep* 7: 1–16

Kim HM, Han JW & Chan JY (2016) Nuclear Factor Erythroid-2 Like 1 (NFE2L1): Structure, function and regulation. *Gene* 584: 17–25

Kim KH, Jeong YT, Oh H, Kim SH, Cho JM, Kim Y-N, Kim SS, Kim DH, Hur KY, Kim HK, *et al* (2013) Autophagy deficiency leads to protection from obesity and insulin resistance by inducing Fgf21 as a mitokine. *Nat Med* 19: 83–92

Kim N, Nam M, Kang MS, Lee JO, Lee YW, Hwang GS & Kim HS (2017) Piperine regulates UCP1 through the AMPK pathway by generating intracellular lactate production in muscle cells. *Sci Rep* 7: 1–13

Lagarde D, Jeanson Y, Barreau C, Moro C, Peyriga L, Guissard C, Arnaud E, Galinier A, Pellerin L, Chouchani ET, *et al* (2021) Lactate fluxes mediated by the monocarboxylate transporter-1 are key determinants of the metabolic activity of beige adipocytes. *J Biol Chem* 296: 1–14

Leahy KM, Ornberg RL, Wang Y, Zweifel BS, Koki AT & Masferrer JL (2002) Cyclooxygenase-2 inhibition by celecoxib reduces proliferation and induces apoptosis in angiogenic endothelial cells in vivo. *Cancer Res* 62: 625–631

Li Y, Bolze F, Fromme T & Klingenspor M (2014) Intrinsic differences in BRITE adipogenesis of primary adipocytes from two different mouse strains. *Biochim*

Biophys Acta - Mol Cell Biol Lipids 1841: 1345–1352

Li Y, Schwalie PC, Bast-Habersbrunner A, Mocek S, Russeil J, Fromme T, Deplancke B & Klingenspor M (2019) Systems-Genetics-Based Inference of a Core Regulatory Network Underlying White Fat Browning. *Cell Rep* 29: 4099-4113.e5

Lin CS & Klingenberg M (1980) Isolation of the uncoupling protein from brown adipose tissue mitochondria. *FEBS Lett* 113: 299–303

Liu X, Zheng Z, Zhu X, Meng M, Li L, Shen Y, Chi Q, Wang D, Zhang Z, Li C, *et al* (2013) Brown adipose tissue transplantation improves whole-body energy metabolism. *Cell Res* 23: 851–854

Lo KA & Sun L (2013) Turning WAT into BAT: A review on regulators controlling the browning of white adipocytes. *Biosci Rep* 33: 711–719

Love MI, Huber W & Anders S (2014) Moderated estimation of fold change and dispersion for RNA-seq data with DESeq2. *Genome Biol* 15: 1–21

MacArthur C a, Lawshé a, Shankar DB, Heikinheimo M & Shackleford GM (1995a) FGF-8 isoforms differ in NIH3T3 cell transforming potential. *Cell Growth Differ* 6: 817–25

MacArthur CA, Lawshe A, Xu J, Santos-Ocampo S, Heikinheimo M, Chellaiah AT & Ornitz DM (1995b) FGF-8 isoforms activate receptor splice forms that are expressed in mesenchymal regions of mouse development. *Development* 121: 3603–3613

Maddaluno L, Urwyler C & Werner S (2017) Fibroblast growth factors: key players in regeneration and tissue repair. *Development* 144: 4047–4060

Madsen L, Pedersen LM, Lillefosse HH, Fjære E, Bronstad I, Hao Q, Petersen RK, Hallenborg P, Ma T, de Matteis R, *et al* (2010) UCP1 induction during recruitment of brown adipocytes in white adipose tissue is dependent on cyclooxygenase activity. *PLoS One* 5: e11391

Mattila MM & Härkönen PL (2007) Role of fibroblast growth factor 8 in growth and progression of hormonal cancer. *Cytokine Growth Factor Rev* 18: 257–266

Maurer S, Harms M & Boucher J (2020) The colorful versatility of adipocytes: white-to-brown transdifferentiation and its therapeutic potential in man. *FEBS J*: 1–19

Meyersl EN, Lewandoskp M & Martin GR (1998) An FgfB mutant allelic series generated by Cre- and Flp-mediated recombination. *Nat Genet* 18: 1–6

Mookerjee SA & Brand MD (2015) Measurement and Analysis of Extracellular Acid Production to Determine Glycolytic Rate. *J Vis Exp* 2: 1–9

Mookerjee SA, Nicholls DG & Brand MD (2016) Determining Maximum Glycolytic Capacity Using Extracellular Flux Measurements. *PLoS One* 11: e0152016

Nedergaard J & Cannon B (2013) UCP1 mRNA does not produce heat. *Biochim Biophys Acta - Mol Cell Biol Lipids* 1831: 943–949

Ornitz DM & Itoh N (2015) The fibroblast growth factor signaling pathway. *Wiley Interdiscip Rev Dev Biol* 4: 215–266

Otsuka T, Mengsteab PY & Laurencin CT (2021) Control of mesenchymal cell fate via application of FGF-8b in vitro. *Stem Cell Res* 51: 102155

Pellegrinelli V, Carobbio S & Vidal-Puig A (2016) Adipose tissue plasticity: how fat depots respond differently to pathophysiological cues. *Diabetologia* 59: 1075–1088

Perdikari A, Leparc GG, Balaz M, Pires ND, Lidell ME, Sun W, Fernandez-Albert F, Müller S, Akchiche N, Dong H, *et al* (2018) BATLAS: Deconvoluting Brown Adipose Tissue. *Cell Rep* 25: 784-797.e4

Pisani DF, Ghandour RA, Beranger GE, Le Faouder P, Chambard JC, Giroud M, Vegiopoulos A, Djedaini M, Bertrand-Michel J, Tauc M, *et al* (2014) The ω6-fatty acid, arachidonic acid, regulates the conversion of white to brite adipocyte through a prostaglandin/calcium mediated pathway. *Mol Metab* 3: 834–847

Ranganathan P, Weaver KL & Capobianco AJ (2011) Notch signalling in solid tumours: A little bit of everything but not all the time. *Nat Rev Cancer* 11: 338–351

Rosen ED, Walkey CJ, Puigserver P & Spiegelman BM (2000) Transcriptional regulation of adipogenesis. *Genes Dev* 14: 1293–1307

Ross DA, Hannenhalli S, Tobias JW, Cooch N, Shiekhattar R & Kadesch T (2006) Functional analysis of Hes-1 in preadipocytes. *Mol Endocrinol* 20: 698–705

Rulifson IC, Collins P, Miao L, Nojima D, Lee KJ, Hardy M, Gupte J, Hensley K,

Samayoa K, Cam C, *et al* (2017) In vitro and in vivo analyses reveal profound effects of fibroblast growth factor 16 as a metabolic regulator. *J Biol Chem* 292: 1951–1969

Samms RJ, Smith DP, Cheng CC, Antonellis PP, Perfield JW, Kharitonenkov A, Gimeno RE & Adams AC (2015) Discrete Aspects of FGF21 In Vivo Pharmacology Do Not Require UCP1. *Cell Rep* 11: 991–999

Shamsi F, Xue R, Huang TL, Lundh M, Liu Y, Leiria LO, Lynes MD, Kempf E, Wang CH, Sugimoto S, *et al* (2020) FGF6 and FGF9 regulate UCP1 expression independent of brown adipogenesis. *Nat Commun* 11

Si Y, Palani S, Jayaraman A & Lee K (2007) Effects of forced uncoupling protein 1 expression in 3T3-L1 cells on mitochondrial function and lipid metabolism. *J Lipid Res* 48: 826–836

Si Y, Shi H & Lee K (2009) Metabolic flux analysis of mitochondrial uncoupling in 3T3-L1 adipocytes. *PLoS One* 4: 1–8

Singh R, Parveen M, Basgen JM, Fazel S, Meshesha MF, Thames EC, Moore B, Martinez L, Howard CB, Vergnes L, *et al* (2016) Increased expression of beige/brown adipose markers from host and breast cancer cells influence xenograft formation in mice. *Mol Cancer Res* 14: 78–92

Stanford KI, Middelbeek RJW, Townsend KL, An D, Nygaard EB, Hitchcox KM, Markan KR, Nakano K, Hirshman MF, Tseng YH, *et al* (2013) Brown adipose tissue regulates glucose homeostasis and insulin sensitivity. *J Clin Invest* 123: 215–223

Sun Y, Wang R, Zhao S, Li W, Liu W, Tang L, Wang Z, Wang W, Liu R, Ning G, *et al* (2019) FGF9 inhibits browning program of white adipocytes and associates with human obesity. *J Mol Endocrinol* 62: 79–90

Sunmonu NA, Li K & Li JYH (2011) Numerous isoforms of Fgf8 reflect its multiple roles in the developing brain. *J Cell Physiol* 226: 1722–1726

Tanaka A, Miyamoto K, Minamino N, Takeda M, Sato B, Matsuo H & Matsumoto K (1992) Cloning and characterization of an androgen-induced growth factor essential for the androgen-dependent growth of mouse mammary carcinoma cells. *Proc Natl Acad Sci U S A* 89: 8928–8932

Tews D, Pula T, Funcke JB, Jastroch M, Keuper M, Debatin KM, Wabitsch M & Fischer-Posovszky P (2019) Elevated UCP1 levels are sufficient to improve glucose uptake in human white adipocytes. *Redox Biol* 26: 101286

Uchii M, Tamura T, Suda T, Kakuni M, Tanaka A & Miki I (2008) Role of fibroblast growth factor 8 (FGF8) in animal models of osteoarthritis. *Arthritis Res Ther* 10: 1–10

Vegiopoulos A, Müller-Decker K, Strzoda D, Schmitt I, Chichelnitskiy E, Ostertag A, Diaz MB, Rozman J, De Angelis MH, Nüsing RM, *et al* (2010) Cyclooxygenase-2 controls energy homeostasis in mice by de novo recruitment of brown adipocytes. *Science (80-)* 328: 1158–1161

Véniant MM, Sivits G, Helmering J, Komorowski R, Lee J, Fan W, Moyer C & Lloyd DJ (2015) Pharmacologic Effects of FGF21 Are Independent of the "Browning" of White Adipose Tissue. *Cell Metab* 21: 731–738

Villarroya F, Cereijo R, Villarroya J & Giralt M (2017a) Brown adipose tissue as a secretory organ. *Nat Rev Endocrinol* 13: 26–35

Villarroya F, Peyrou M & Giralt M (2017b) Transcriptional regulation of the uncoupling protein-1 gene. *Biochimie* 134: 86–92

Virtue S, Feldmann H, Christian M, Tan CY, Masoodi M, Dale M, Lelliott C, Burling K, Campbell M, Eguchi N, *et al* (2012) A new role for lipocalin prostaglandin D synthase in the regulation of brown adipose tissue substrate utilization. *Diabetes* 61: 3139–3147

Waldén TB, Hansen IR, Timmons JA, Cannon B & Nedergaard J (2012) Recruited vs. nonrecruited molecular signatures of brown, 'brite,' and white adipose tissues. *Am J Physiol - Endocrinol Metab* 302: 19–31

Wang D & Dubois RN (2006) Prostaglandins and cancer. *Gut* 55: 115–122

Wang H, Willershäuser M, Karlas A, Gorpas D, Reber J, Ntziachristos V, Maurer S, Fromme T, Li Y & Klingenspor M (2019) A dual Ucp1 reporter mouse model for imaging and quantitation of brown and brite fat recruitment. *Mol Metab* 20: 14–27

Wang W & Seale P (2016) Control of brown and beige fat development. *Nat Rev Mol Cell Biol* 17: 691–702

Weitzel JM, Iwen KAH & Seitz HJ (2003) Special Review Series – Biogenesis and Physiological Adaptation of Mitochondria Regulation of mitochondrial biogenesis by thyroid hormone Experimental Physiology : *Exp Physiol*: 121–128

Westphal S, Gantert T, Kless C, Hüttinger K, Klingenspor M & Fromme T (2019) Fibroblast growth factor 8b induces uncoupling protein 1 expression in epididymal white preadipocytes. *Sci Rep* 9: 1–11

Wu et al. Z (1999) Mechanisms Controlling Mitochondrial Biogenesis and Respiration through the Thermogenic Coactivator PGC-1. *Cell* 98: 115–124

Wu J, Boström P, Sparks LM, Ye L, Choi JH, Giang AH, Khandekar M, Virtanen KA, Nuutila P, Schaart G, *et al* (2012a) Beige adipocytes are a distinct type of thermogenic fat cell in mouse and human. *Cell* 150: 366–376

Wu J, Khandekar M, Nuutila P, Schaart G, Huang K, Tu H & Van WD (2012b) Beige Adipocytes are a Distinct Type of Thermogenic Fat Cell in Mouse and Human. *Cell* 150: 366–376

Xue B, Coulter A, Rim JS, Koza R a & Kozak LP (2005) Transcriptional Synergy and the Regulation of Ucp1 during Brown Adipocyte Induction in White Fat Depots. *Society* 25: 8311–8322

Zhao Y, Hu Q, Cheng F, Su N, Wang A, Zou Y, Hu H, Chen X, Zhou HM, Huang X, *et al* (2015) SoNar, a Highly Responsive NAD+/NADH Sensor, Allows High-Throughput Metabolic Screening of Anti-tumor Agents. *Cell Metab* 21: 777–789

APPENDIX

Table 6. Oxylipin limit of detection (LOD) and lower limit of quantitation (LLOQ)

Metabolite	Mean [DMEM+ 10% FCS]	STD [DMEM+ 10% FCS]	LOD concentration	LLOQ concentration
TXB2	0,653	0,024	3,395	11,311
RvE1	0,001	0	0,007	0,009
RvD2	0,005	0,001	0,013	0,021
RvD1	0,023	0,004	0,088	0,236
PGF2alpha	0,031	0,007	0,132	0,407
PGE2	0,029	0,008	0,053	0,175
PGD2	0,017	0,008	0,086	0,276
PDX	0,001	0	0,002	0,006
MAR1	0,002	0,002	0,004	0,007
LXA4	0,012	0,003	0,04	0,129
LTE4	0,001	0	0,004	0,005
LTD4	0,001	0	0,001	0,002
LTC4	NA	NA	NA	NA
LTB4	0,003	0,001	0,011	0,024
EPA	6,171	0,099	0,672	2,217
DHA	310,06	19,542	960,762	3200,972
DGLA	4,312	0,513	0,443	1,476
ALA	0,252	0,009	0,033	0,04
AA	39,071	2,962	9,418	31,31
9-HODE	0,71	0,024	3,051	8,708
9-HETE	0,231	0,055	0,61	1,991
9,10-DiHOME	0,639	0,087	2,983	9,866
8-iso-PGF2alpha	0,006	0,002	0,019	0,035
8,9-EET	0,038	0,013	0,058	0,162
8,9-DHET	0,028	0,008	0,094	0,303
6-keto-PGF1alpha	0,001	0,001	0,009	0,014
5-oxoETE	0,029	0,006	0,047	0,138
5-HETE	0,452	0,02	3,187	10,601
5-HEPE	0,035	0,006	0,128	0,407
5,6-EET	NA	NA	NA	NA
5,6-DHET	0,028	0,004	0,165	0,527
4-HDHA	0,764	0,041	4,068	13,521
20-HETE	0,014	0,003	0,015	0,045
18-HEPE	0,036	0,004	0,087	0,28
17-HDHA	0,069	0,006	0,051	0,157
15-oxoETE	0,187	0,03	1,674	5,469
15-HpETE	NA	NA	NA	NA
15-HETrE	0,24	0,01	2,378	7,748
15-HETE	0,175	0,012	0,672	2,226
15-HEPE	0,064	0,004	0,178	0,572
14,15-EET	0,069	0,035	0,818	2,674
13-HODE	0,732	0,051	3,075	9,072
13-HDHA	0,067	0,013	0,237	0,781
12-oxoETE	NA	NA	NA	NA
12-HETE	6,63	0,233	28,266	94,092
12-HEPE	0,497	0,052	0,778	2,569
12,13-DiHOME	0,56	0,032	2,084	6,899
11-HETE	0,75	0,043	10,404	34,589
11-HDHA	0,13	0,038	0,465	1,516
11,12-EET	0,002	0	0,015	0,024
11,12-DHET	0,074	0,006	0,247	0,818

ACKNOWLEDGEMENTS

- *Worte können den Grad meiner Dankbarkeit nicht ausdrücken, für all jene Menschen, die mich auf diesem langjährigen Weg begleitet und unterstützt haben. Auch wenn ihr individueller Anteil noch so klein gewesen sein mag, so wäre meine Arbeit ohne sie im Ganzen doch nie zustande gekommen. -*

TG (2021)

STATEMENT OF AUTHORSHIP

Eidesstattliche Erklärung

Ich erkläre an Eides statt, dass ich die bei der promotionsführenden Einrichtung der TUM School of Life Sciences Weihenstephan der TUM zur Promotionsprüfung vorgelegte Arbeit mit dem Titel:

Recruitment of brown adipocytes in visceral white adipose tissue by fibroblast growth factor 8b

am Lehrstuhl für Molekulare Ernährungsmedizin

unter der Anleitung und Betreuung durch: Prof. Dr. Martin Klingenspor ohne sonstige Hilfe erstellt und bei der Abfassung nur die gemäß § 6 Ab. 6 und 7 Satz 2 angebotenen Hilfsmittel benutzt habe.

Ich habe keine Organisation eingeschaltet, die gegen Entgelt Betreuerinnen und Betreuer für die Anfertigung von Dissertationen sucht, oder die mir obliegenden Pflichten hinsichtlich der Prüfungsleistungen für mich ganz oder teilweise erledigt.

Ich habe die Dissertation in dieser oder ähnlicher Form in keinem anderen Prüfungsverfahren als Prüfungsleistung vorgelegt.

Die vollständige Dissertation wurde noch nicht veröffentlicht.

Ich habe den angestrebten Doktorgrad noch nicht erworben und bin nicht in einem früheren Promotionsverfahren für den angestrebten Doktorgrad endgültig gescheitert.

Die öffentlich zugängliche Promotionsordnung der TUM ist mir bekannt, insbesondere habe ich die Bedeutung von § 28 (Nichtigkeit der Promotion) und § 29 (Entzug des Doktorgrades) zur Kenntnis genommen. Ich bin mir der Konsequenzen einer falschen Eidesstattlichen Erklärung bewusst.

Mit der Aufnahme meiner personenbezogenen Daten in die Alumni-Datei bei der TUM bin ich einverstanden.

_____

Freising, 20.01.2021

PUBLICATIONS

- **Fibroblast growth factor induced Uncoupling protein 1 expression in preadipocytes requires prostaglandin E2 production and glycolytic flux. T. Gantert**, F. Henkel, C. Wurmser, J. Oeckl, L. Fischer, M. Haid, J. Adamski, J. Esser-von Bieren, M. Klingenspor, T. Fromme. (2021). (*in review*)

- **High-protein diet more effectively reduces hepatic fat than low-protein diet despite lower autophagy and FGF21 levels.** C. Xu, M. Markova, N. Seebeck, A. Loft, S. Hornemann, **T. Gantert**, S. Kabisch, K. Herz, J. Loske, M. Ost, V. Coleman, F. Klauschen, A. Rosenthal, V. Lange, J. Machann, S. Klaus, T. Grune, S. Herzig, O. Pivovarova-Ramich, A. F. H. Pfeiffer, Liver Int. 2982–2997 (2020).

- **Fibroblast growth factor 8b induces uncoupling protein 1 expression in epididymal white preadipocytes.** S. Westphal, **T. Gantert**, C. Kless, K. Hüttinger, M. Klingenspor, T. Fromme, Scientific Reports volume 9, 8470 (2019). [**Prepublication of parts of the PhD-thesis**]

- **Bile acid supplementation decreases body mass gain in C57BL/6J but not 129S6/SvEvTac mice without increasing energy expenditure.** T. Fromme, K. Hüttinger, S. Maurer, Y. Li, **T. Gantert**, J. Fiamoncini, H. Daniel, S. Westphal & M. Klingenspor, Scientific Reports volume 9, 131 (2019).

- **A liver stress-endocrine nexus promotes metabolic integrity during dietary protein dilution.** A. Maida, A. Zota, K. A. Sjøberg, J. Schumacher, T. P. Sijmonsma, A. Pfenninger, M. M. Christensen, **T. Gantert**, J. Fuhrmeister, U. Rothermel, D. Schmoll, M. Heikenwälder, J. L. Iovanna, K. Stemmer, B. Kiens, S. Herzig, and A. J. Rose, J Clin Invest. 126(9):3263–3278 (2016).

_____

Freising, 20.01.2021